The Ediacarian-Cambrian tectonic evolution of western Dronning Maud Land : New ^{40}Ar-^{39}Ar and Sr/Nd data from Sverdrupfjella and Kirwanveggan, the source of the Urfjell Group and Implications for the Kuunga Orogeny and Gondwana amalgamation .

Geoffrey H. Grantham[1], Jan D. Kramers[1] , Bruce Eglington[2]and Erasmus P. Burger[3]

[1] Department of Geology, University of Johannesburg, P.O. Box 524, Auckland Park, 2006, South Africa.

[2] Saskatchewan Isotope Laboratory, Department of Geological Sciences, University of Saskatchewan, Saskatoon, Saskatchewan, Canada.

[3] Department of Geology, University of Pretoria, Pretoria, South Africa 0001.

Abstract

Biotite $^{40}Ar/^{39}Ar$ ages from Mesoproterozoic gneisses from Kirwanveggan and Sverdrupfjella vary between 868-497 Ma and 547-326 Ma respectively. Hornblende ages from Kirwanveggan and Sverdrupfjella gneisses vary between 1067-480Ma and 550-450Ma respectively. The similar ages for hornblende and biotite from Sverdrupfjella are consistent with rapid uplift. The age differences between biotite and hornblende imply differential cooling southwards and heating over northern Kirwanveggan at ~500Ma with southern Kirwanveggan preserving Mesoproterozoic $^{40}Ar/^{39}Ar$ ages in hornblende. The heating is inferred to result from burial in a nappe footwall.

Biotite ages throughout Sverdrupfjella and Kirwanveggan are similar to deposition ages of Urfjell Group clastic sediments which define the southern uplift and deposition limits at ~530Ma. Radiogenic Nd/Sr isotope characteristics of the Urfjell Group are similar to basement

gneisses from nearby Kirwanveggan, eastern Sverdrupfjella, Gjelsvikfjella and central Dronning Maud Land (CDML) but dissimilar to western Sverdrupfjella. Contrastingly, Urfjell Group detrital zircon patterns suggest derivation from a source similar to CDML, ~500km away.

Tectonic analysis of Dronning Maud Land (DML), using Sr/Nd radiogenic isotope, $^{40}Ar/^{39}Ar$ and SHRIMP U/Pb zircon data, P-T-t estimates and structural analysis allow an interpretation that eastern Sverdrupfjella, Gjelsvikfjella and CDML comprise a nappe complex, emplaced southeastwards over western Sverdrupfjella at ~500-480Ma. The timing of nappe emplacement is constrained by 510-490Ma syn-D3 granitic intrusions and rapid uplift reflected by $^{40}Ar/^{39}Ar$ data in Sverdrupfjella. Earlier top-to-the-NW D1-D2 folds and thrust faults preserved in the nappe complex predate the D3 nappe implacement. Emplacement of the nappe complex would position the Urfjell Group source closer to its basin depository. The Kuunga Orogeny extent in DML is limited to central Kirwanveggan, with its southern limit being the Urfjell Group basin at ca. 530Ma. Planar fabrics defined by hornblende and biotite, with ages up to ~1100Ma in southern Kirwanveggan, imply Mesoproterozoic deformation there with partial resetting of $^{40}Ar/^{39}Ar$ ages in northern Kirwanveggan. In contrast, D3 deformation in Sverdrupfjella is Cambrian in age.

Integration of geochronological, geochemical, aeromagnetic and aerogravity data from WDML support the structural differences observed between Kirwanveggan and Sverdrupfjella and support a depth/heating gradient at ~530Ma between N. Sverdrupfjella and S. Kirwanveggan.

Keywords: Ar/Ar and Sr/Nd data; Cambrian uplift, Dronning Maud Land, Antarctica; Kuunga Orogeny; Gondwana amalgamation.

INTRODUCTION

Reconstructions of Gondwana place Dronning Maud Land (DML), Antarctica adjacent to northern Mozambique and South Africa (Grantham et al., 1988; Groenewald et al., 1991). The placement of DML adjacent to N. Mozambique is supported by rocks with similar Mesoproterozoic to Cambrian crystallisation and metamorphic ages in both areas (Grantham et al., 2008). However debate exists as to the distribution and timing of orogenic events in the area concerning the extents and relationships between the geology of the East African and Kuunga Orogenies (Meert, 2003) which overlap in the broad area between WDML and southern Africa (Figure 1) in Gondwana.

The East African Orogeny (EAO) was initially defined by Stern (1994) as involving the closure of the Neoproterozoic-age Mozambique Ocean between ~900–650 Ma during which an accretionary collage of arc and micro continental terranes accreted and sutured East and West Gondwana along a N-S oriented orogenic belt. Stern (2002) demonstrated that significant juvenile magmatism within this age range characterised this orogeny and indicated the extent of the EAO as stretching from Arabia to N. Mozambique. A southern continuation of the EAO, from Mozambique to Heimefrontfjella, Antarctica, was proposed by Jacobs et al., (1998) and Jacobs and Thomas (1994). This is questioned by Collins and Pisarevsky (2005) and Grantham et al. (2008). Collins and Pisarevsky (2005) reflect the termination of the EAO rocks along the ENE-

SW oriented Lurio Belt which transects N. Mozambique, supported by Grantham et al., (2008) who infer a major crustal boundary along the Lurio Belt of N. Mozambique. The crustal boundary is correlatable with that separating the Highlands and Vijayan Complexes in Sri Lanka, located to the east in a reconstructed Gondwana (Grantham et al., 2008). The crustal boundary is evident from available geochronological data which show that the rocks north of the Lurio Belt discontinuity comprise an accretionary nappe complex with crystallisation ages typical of the EAO, between ~600 and 900 Ma (Stern, 1994; Bingen et al., 2009; Grantham et al., 2008). In contrast the rocks south of it in the Nampula Terrane, have ages which pre-date the EAO with ages of ~1000-1140 Ma (Hokada et al., 2019), intruded by granitic plutons and veins with ages of ~480-500 Ma (Macey et al., 2010, Grantham et al., 2008). The Nampula Terrane has with no recognised crystallisation ages typical of the EAO between ca.600 and ca.900 Ma. In Antarctica, rocks underlying CDML have zircon age distribution patterns similar to rocks from N of the Lurio Belt in Mozambique with significant ages between ca. 600-900 Ma (Grantham et al., 2008), dissimilar to the adjacent Nampula Terrane in reconstructed Gondwana. The EAO in N. Mozambique is separated from similar-aged rocks in CDML by the older, continuous ~1100 Ma Maud-Nampula belt (Hokada et al., 2019).

The Kuunga Orogeny was defined by Meert (2003), who recognised a younger event geochronologically, the associated rocks of which define an E-W oriented belt cross-cutting the EAO and extending westwards through the Zambezi Belt to the Damara Belt of Namibia and eastwards through Dronning Maud Land, Antarctica into Sri Lanka. Further extensions of the Kuunga Orogeny are recognised in the Prince Charles Mountains and Prydz Bay area (Boger,

2011), the Denman Glacier area of Antarctica (Daczko et al., 2018) and beyond into China (Li et al., 2017). Age contrasts between the EAO and KO are 900-650 Ma and 570-530 Ma, recognised by Stern (1994) and Meert (2003) respectively. Bingen et al., (2009) have also recognised overprinting of the EAO lithologies by the KO as one progresses southwards toward the Lurio Belt in N. Mozambique. KO overprinting is also recognised in CDML as well as the intervening ~1100 Ma Nampula Terrane in northern Mozambique (Grantham et al., 2008). No direct continuous geographical link between the EAO north of the Lurio Belt and CDML is seen. Grantham et al., (2008) inferred a tectonic-related link between the two areas via the erosional klippen (Monapo and Mugeba, Grantham et al., 2013 and Roberts et al., 2005 respectively) which overly the Nampula Terrane.

This study focuses on the timing and extent of post-orogenic inversion in the Sverdrupfjella and Kirwanveggan areas of WDML, Antarctica (Figure 1 study area), particularly focussing on the late Neoproterozoic to Cambrian period. The approach of the study involves an $^{40}Ar/^{39}Ar$ study of biotite and hornblende from Sverdrupfjella and Kirwanveggan (Figure 2), recognising that these minerals are described as having closure or blocking temperatures of ~300^{o}C and ~500^{o}C respectively (Spear, 1995, p. 719). The samples selected were all collected from basement gneisses in Sverdrupfjella and Kirwanveggan where typical ages for these gneisses vary between ~1000 Ma to ~1150 Ma (Board et al, 2005; Grantham et al., 2011; Harris, 1999). In addition, the southern extent of the ~550-500 Ma orogenesis in WDML is also defined by the Urfjell Group in southern Kirwanveggan (Figure 2). The Urfjell Group comprises sandstones, grits and minor conglomerates, whose age of deposition has been constrained as being ~530

Ma, based on a Rb/Sr study (Moyes et al., 1997) and a detrital zircon study by Croaker (1999), reported in Kleinschmidt et al., (2000). The Urfjell Group clastic sedimentary rocks have been subjected to brittle faulting in a strike-slip setting (Croaker, 1999, Moyes et al., 1997). Primary sedimentary bedding and cross bedding are well preserved and reflect sedimentary depositional transport from the NE (Croaker, 1999) (Figure 3). In contrast, a well constrained P-T path from northern Sverdrupfjella by Pauly et al., (2016) infers a depth of ca. 6kbar at the same time indicating a crustal gradient from NE Sverdrupfjella to SW Kirwanveggan of ca.6kb to surface, along the Sverdrupfjella-Kirwanveggan mountain ranges (Figure 2).

Grantham et al., (2008) proposed a mega-nappe structure emplaced during the Kuunga Orogeny in which part of northern Gondwana, comprising rocks of EAO genesis, were thrust ~600 km over southern Gondwana during the amalgamation of the Gondwana supercontinent. The timing of the nappe emplacement was inferred to be between 590 and 550 Ma. The model was postulated in order to explain geochronological age disparities between the geology of CDML and the Nampula Complex of N. Mozambique which are juxtaposed in reconstructed Gondwana. It was inferred that the rocks underlying CDML are lithologically and geochronologically correlatable with those exposed in the Namuno Terrane in Mozambique (north of the Lurio Belt discontinuity). The nature and partial extent of the nappe structure are supported by the presence of klippen in the Monapo and Mugeba areas of N. Mozambique described by Roberts et al., (2005) and Grantham et al., (2013) respectively. The Monapo Complex has granulite assemblages with ages comparable to those recorded in Sor Rondane, CDML, Antarctica (Grantham et al., 2013). The correlation of rocks from the Cabo Delgado

Complex of N. Mozambique is also supported by Ravikant et al., (2018) who have correlated rocks from the Schirmacher Oasis area in CDML, with rocks of the Montepuez Complex of northern Mozambique. In Kirwanveggan, the extent of the nappe was inferred to be reflected by the decreasing grade of metamorphism southward in mineral assemblages in Kirwanveggan, the absence of Cambrian-age granitic and pegmatite veins in Kirwanveggan and the ~530 Ma Urfjell Group sedimentary rocks (Grantham et al.,2008).

In order to examine the uplift history of Sverdrupfjella and Kirwanveggan, samples from Sverdrupfjella were collected for this $^{40}Ar/^{39}Ar$ study during the 2013/2014 and 2014/2015 Antarctic field seasons whereas samples from Kirwanveggan were collected in 1992/1993 and 1993/1994 field seasons. The localities of the various samples are shown in Figure 2. The data derived from these samples will be compared with similar data from Jacobs et al., (1995; 1999) from Heimefrontfjella, as well as unpublished data from Sverdrupfjella from Board, (2001) and from Kirwanveggan from Harris (1999).

SAMPLE PREPARATION AND ANALYTICAL PROCEDURES

$^{40}Ar/^{39}Ar$ samples

Amphibole and mica were separated from samples for $^{40}Ar/^{39}Ar$ dating. The minerals were separated from the fine fraction of the coarse crush. Filter paper, a binocular microscope and steel tweezers were used to separate mica. A binocular microscope, steel tweezers and a sterile plastic petri dish were used to separate amphibole (identified using colour and cleavage) from

material in ethanol (just enough to submerge material), after the sample was run over paper to remove dust which was too fine for separation by hand.

Handpicked ca. 0.2 mg grains for each sample were wrapped in single aluminium foils, and vacuum sealed in a silica glass tube along with standards at the top and bottom of the package. Samples were irradiated at the NTP radioisotopes SAFARI1 nuclear reactor at Pelindaba, South Africa, for 20 h in position B2W while the reactor was running at 20 MW. For each sample two or three grains were analysed by stepwise heating at the University of Johannesburg's SPECTRUM analytical facility. The analyses were done using a defocused beam from a continuous Nd-YAG 1064 nm wavelength laser, with the sample port connected to a MAP 215-50 noble gas mass spectrometer. A Johnston focused-flow electron multiplier operated in analogue mode was used. Routine blank measurements (for correction) were interspersed before sessions and at 4 step intervals. Both the Fish Canyon Sanidine standard and amphiboles from McClure Mountains and Hb3GR were used as monitors, yielding identical *J*-values within uncertainty limits. Measurement control and data reduction were done using in-house software, which includes full error propagation, using Monte Carlo procedures. The data was produced using ^{40}Ar decay parameters of Renne *et al.* (2010). Step heating profiles were prepared using the Isoplot Excel macro prepared by Ludwig (2001),

Rb/Sr and Sm/Nd whole rock analyses from Kirwanveggan

Whole rock samples of granitoids from Kirwanveggan were analysed for Rb/Sr and Sm/Nd chemistry at the National Physical Research Laboratory at CSIR, Pretoria. The analytical procedures for Rb/Sr applied

are described in Harmer et al., (1998). Sr isotope compositions were normalized to $^{86}Sr/^{88}Sr = 0.1194$ and are reported relative to a value of 0.710250 for NIST 987. One sigma analytical uncertainties are 0.8% for $^{87}Rb/^{86}Sr$ and 0.01% for $^{87}Sr/^{86}Sr$ with no error correlation.

Samples for Sm/Nd isotope analysis were spiked with a mixed ^{149}Sm-^{150}Nd tracer solution, followed by dissolution in Parr™ Teflon microwave pressure vessels using HF and HNO_3 acid. Sm and Nd were purified using standard cation (AG50Wx12) and Ln resin ion exchange techniques. Nd isotope compositions were normalized to a value of 0.7219 for $^{146}Nd/^{144}Nd$ using an exponential fractionation correction. One sigma analytical uncertainties are 0.6% for $^{147}Sm/^{144}Nd$ and 0.005% for $^{143}Nd/^{144}Nd$. $^{143}Nd/^{144}Nd$ for an in-house Ames standard is 0.512129 +/- 9 (1σ on 26 replicates) and 0.511854 +/- 7 for La Jolla Nd standard (1σ on 6 replicates).Rb/Sr and Sm/Nd data were reduced using the program GEODATE , compiled by Eglington and Harmer (1999).

PETROGRAPHY OF THE SAMPLES

Sverdrupfjella

Rock units sampled in Sverdrupfjella were typically intermediate to basic gneisses to ensure the presence of both biotite and hornblende.

Sample 008bD (Figure 4a): The medium-grained sample contains khaki biotite (~40%), pale blue-green amphibole (~45%), plagioclase (~8%), opaques (~5%) and subordinate quartz. The biotite and ampibole define a strong planar foliation. The sample is predominantly composed of amphibole and mica. Opaques occur in fractures along grain boundaries. Small rounded grains of quartz are included in amphibole. The rock shows a granoblastic texture consistent with equilibrium. Neither biotite nor hornblende show noticeable alteration.

Sample 012cG (Figure 4b): The medium-grained sample contains fox-red biotite (~35%), pale blue-green amphibole (~25%), plagioclase (~30%), quartz (~10%), zircon and opaques (~<5%). A strong planar fabric is defined by biotite and amphibole. Biotite and amphibole have no noticeable alteration.

Sample 017bD (Figure 4c) : The fine-grained sample contains khaki biotite (~15%), blue-green amphibole (~30%), quartz (~10%), plagioclase (~40%), zircon and opaques (~5%). The rock is granoblastic with no obvious foliation. Zircon is included in biotite. Small rounded quartz grains are included in most other minerals. Amphibole and biotite show no obvious alteration.

Sample 032bC (Figure 4d):The medium-grained sample contains amphibole (~45%), plagioclase (~40%), quartz (~10%), epidote and opaques with no mica observed in thin section. The texture is granoblastic equigranular with no obvious foliation observed. No visible alteration of amphibole is seen. Plagioclase is subhedral and no alteration was noticed.

Sample 036bD (Figure 4e): The medium-grained sample contains biotite (~20%), amphibole (~25%), clinopyroxene (~15%), plagioclase (~30%), quartz (~5%), titanite and opaques. The texture is equigranular granoblastic indicating equilibrium between the grains. Biotite and amphibole show no obvious alteration.

Sample 038bA (Figure 4f): The medium grained equigranular granoblastic sample contains biotite (~15%), amphibole (~30%), quartz (~10%), plagioclase (~45%), zircon and opaques. The sample is dominated by large grains of plagioclase, which is locally altered. A planar fabric defined by concentrations of amphibole and biotite is seen. Amphibole and biotite do not show visible alteration.

Kirwanveggan

All samples in Kirwanveggan were collected from the Kirwanveggan Megacrystic granitic orthogneiss (Grantham et al., 1995) unit which typically contains both biotite and hornblende and is also exposed at all major nunataks in Kirwanveggan.

Sample 92/14 (Figure 5a): The medium grained porphyroclastic inequigranular sample contains khaki biotite (~25%), amphibole (~25%), quartz (~25%), plagioclase (~10%), K-feldspar (~10%), opaque's and zircon. There is a planar foliation defined by biotite and hornblende. Feldspar varies greatly in grain size defining a porphyroclastic texture typical of the Kirwanveggan Megacrystic Orthogneiss (Grantham et al., 1995). Coarse K-feldspar grains display some perthitic exsolution whereas plagioclase grains are commonly altered. Biotite and amphibole do not show noticable alteration.

Sample 92/35 (Figure 5b): The sample contains dark brown biotite (~15%), olive green hornblende (~10%), quartz (~25%), plagioclase (~20%), K-feldspar (~25%), garnet, zircon and opaque's. Biotite and hornblende define a planar fabric. The feldspars define a porphyroclastic texture. Quartz grains show undulatory extinction typical of strain. Plagioclase displays some partial sauseritisation. Biotite and hornblende do not display noticeable alteration.

Sample 92/41 (Figure 5c): The sample comprises khaki biotite mica (~10%), olive green hornblende (~5%), quartz (~30%), plagioclase (~25%), K-feldspar (~20%), epidote, titanite and opaques. The rock has a relict porphyroclastic texture with coarse rounded feldspar grains in a matrix of strained recrystalised quartz and aligned biotite and hornblende grains. The relict porphyroclastic feldspar grains have been recrystallised, now defining aggregates preserving

the porphyroclastic grain shape. Biotite and hornblende do not show visible alteration. The presence of epidote suggests a lower grade assemblage compared to other samples.

Sample 92/61 (Figure 5d): The sample contains fox red to khaki zoned biotite (~10%), pale blue green hornblende (~20%), quartz (~25%), plagioclase (~20%), K-feldspar (~15%), clinopyroxene (5%), chlorite and opaques. Clinopyroxene locally forms relict cores to hornblende grains Biotite grains are aligned locally and are weakly folded demonstrating their pretectonic genesis. Most minerals form mortar textures, typical of recrystallisation under strain. Some grains of amphibole preserve symplectitic textures with intergrowths of hornblende and quartz, typical of retrograde clinopyroxene hydration. Biotite locally has needles of rutile forming a saginitic texture, typical of retrograde exsolution of TiO_2 from higher grade Ti-rich biotite.

Sample 92/77 (Figure 5e): The sample comprises biotite (~10%), amphibole (~5%), quartz (~35%), plagioclase (~20%), K-feldspar (~20%), epidote, chlorite and opaques. The ferromagnesian minerals define a strong planar fabric in between coarse porphyroclastic feldspar grains. Quartz is highly strained. Plagioclase is locally sausseritised. Coarse K-feldspar grains are perthitic. Amphibole, biotite and chlorite form clusters along fractures in the rock. The planar fabric is defined by low grade mineralogy of chlorite and biotite which is bent around pretectonic amphibole.

Sample 92/84 (Figure 5f): The sample contains khaki biotite (~10%), olive green hornblende (~20%), quartz (~25%), plagioclase (~25%), K-feldspar (~15%) and titanite and opaques (~5%). The rock has a porphyroclastic texture defined by coarse feldspar grains with the ferromagnesian minerals and quartz being interstitial to the coarse feldspars. The planar fabric present in this rock, defined by biotite and hornblende, is weak in comparison to other samples

from Kirwanveggan. Plagioclase is locally sausseritised. Opaque minerals, presumably ilmenite, with reaction rims of titanite are present. Medium grained hornblende grains have crude rims of biotite.

Sample 92/89 (Figure 5g): The sample comprises khaki biotite (~15%), olive green amphibole (~20%), quartz (~20%), plagioclase (~20%), K-feldspar (~15%) and titanite, garnet and opaques (~10%). Biotite and hornblende define a weak planar fabric. The rock is fine grained with banding that is defined by the concentration of mica (localized alignment) and amphibole. Biotite and hornblende do not show obvious alteration.

Conclusions

The mineralogy of the samples is summarised in Table 1 from which it apparent all samples have assemblages typical of medium grade amphibolites facies metamorphism, with only the two most southerly samples from southern Kirwanveggan containing subordinate quantities of minerals typical of low grade metamorphism i.e. chlorite and epidote.

^{40}AR-^{39}AR GEOCHRONOLOGY

Introduction

Step heating of biotite and hornblende pairs on 13 samples were completed at the University of Johannesburg. Six samples from Sverdrupfjella were analysed and seven from Kirwanveggan. The sample localities are shown in Figure 2. The data tables are presented in Grantham et al., (2019) and summarised in Table 2. Figures were prepared using the Excel Macro Isoplot, programmed by Ludwig, (2001).

Sverdrupfjella

Sample 008bD (Figure 6a and b): The step heating profile for hornblende yields a well-defined plateau age of 509.8 ± 3.5 Ma including 97.6% of the gas released with a Ca/K ratio of 37.18, consistent with amphibole. The biotite profile is marginally less well defined yielding a weighted average age of 492.2 ± 2.13 Ma and a Ca/K ratio of 0.0039, consistent with biotite.

Sample 012cG (Figure 6c and d): The step heating profile for hornblende yields a weighted average age of 552.6 ± 2.4 Ma (Ca/K ratio of 6.08) whereas the biotite yields a weighted average age of 547.1 ± 2.3 Ma (Ca/K ratio of 0.052), reflecting an age difference between the two of ~5 Ma.

Sample 017bD (Figure 6e and f): The step heating profile for hornblende yields a weighted average age of 502.6 ± 4.2 Ma (Ca/K=19.4) whereas biotite yields a weighted average age of 463.1 ± 1.2 Ma (Ca/K ratio=.009, reflecting a difference between the two of ~40 Ma.

Sample 032bC (Figure 6g and h): The step heating profile for hornblende yields a plateau age of 468.3 ± 1.5 Ma (Ca/K=7.14) whereas the biotite yields a poorly constrained weighted average age of 326.1 ± 9.1 Ma (Ca/K=0.036).

Sample 036bD(Figure 7and b): Step heating profile for two biotite samples yield weighted average ages of 499.4 ± 2.73 Ma (Ca/K= 0.035) (not shown) and 479.6 ± 1.9 Ma (Ca/K=0.15) respectively whereas a hornblende sample yielded an age of 452.7 ± 2.34 Ma (Ca/K=8.24).

Sample 038bA (Figure 7c and d): The step heating profile for hornblende yields a weighted average age of 508.6 ± 2.4 Ma (Ca/K= 19.7) whereas biotite yields a weighted average age of 463.1 ± 1.2 Ma (Ca/K=0.006, reflecting a difference between the two of ~45 Ma.

Kirwanveggan

*Sample 92/*14 (Figure 7e and f): The step heating profile for hornblende yields a weighted average age of 480.6 ± 2.1 Ma (Ca/K ratio of 4.13) whereas the biotite yields a weighted average age of 506.3 ± 2.2 Ma (Ca/K ratio of 0.052).

Sample 92/35 (Figure 7g and h): The step heating profile for hornblende yields weighted average age of 508 ± 2.7 Ma (Ca/K=5.38) whereas the biotite yields plateau age of 504.56 ± 0.95 Ma (Ca/K=0.046), reflecting a difference between the two of ~3 Ma.

Sample 93/41 (Figure 8a and b): The step heating profile for hornblende yields weighted average age of 527 ± 3.6 Ma (Ca/K= 4.91) whereas the biotite yields plateau age of 498.2 ± 1.9 Ma (Ca/K=.008), reflecting a difference between the two of ~30 Ma.

Sample 93/61 (Figure 8c and d): No biotite was successfully separated from this sample. Two step heating profiles for two hornblende samples yield weighted average ages of 1265.56 ± 5.8 Ma (Ca/K =24.97) and 1076.5 ± 4.5 Ma (Ca/K= 15.45) respectively. These ages are of similar order to the zircon U/Pb SHRIMP ages from Kirwanveggan, implying that these rocks have not been heated >~500^{o}C since that time.

Sample 93/77 (Figure 8e and f): The step heating profile for hornblende yields weighted average age of 840.4 ± 3.5 Ma (Ca/K= 3.38) whereas the biotite yields a weighted average age of 503.7 ± 2.2 Ma (Ca/K= 0.53), reflecting a difference between the two of ~340 Ma.

Sample 93/84 (Figure 8g and h): The step heating profile for hornblende yields weighted average age of 817.7 ± 4.7 Ma (Ca/K=4.13) whereas the biotite yields a weighted average age of 503.7 ± 2.2 Ma (Ca/K=0.031), reflecting a difference between the two of ~340 Ma.

Sample 92/89 (Figure 8i and j): The step heating profile for hornblende yields a weighted average age of 526.5 ± 2.2 Ma (Ca/K=4.13) whereas the biotite yields a weighted average age of 529.1 ± 2.3 Ma (Ca/K= 0.016).

DISCUSSION AND CONCLUSIONS

DISCUSSION OF $^{40}Ar/^{39}Ar$ DATA FROM SVERDRUPFJELLA, KIRWANVEGGAN AND HEIMEFRONTFJELLA

The differences in ages between hornblende and biotite for each sample are summarised in Table 3. From these data inferred cooling rates and erosion rate equivalents can be calculated assuming closure temperatures of 500°C and 300°C for hornblende and biotite respectively (Spear 1995, p. 719). Typically those samples where the age of hornblende is older than biotite, as most samples are (Table 3), are consistent with closure temperature studies but assume that no other variables are involved. No logical explanation can be provided for samples where within sample ages of hornblende are less than those of biotite (e.g. samples 036bD, 92/14, 93/84 and 93/89 from Kirwanveggan). A variable which could affect sample pairs in Sverdrupfjella is that granite veins with ages of ~480-500 Ma are distributed throughout Sverdrupfjella and could have resulted in localised heating affecting biotite differential sooner and longer than hornblende, if at all. Consequently, no definitive or reliable cooling or uplift rates at specific localities can be inferred. Differences between biotite and hornblende ages spatially in Sverdrupfjella and Kirwanveggan are apparent and are discussed below. The consistant pattern of hornblende ages being greater than biotite ages and the similarity in ages between hornblende-biotite pairs in Sverdru[fjella, is probably related to the near synchronous granite sheet emplacement at ca. 500 Ma (see below). Localised ductile shearing

which affects some granite sheets, indicates localised planar fabric development. However, most contacts between granite sheets and their hosts are angular, locally discordant and sharp, typical of brittle emplacement. Whereas localised ductile shear could have induced planar fabrics defined by hornblende and biotite at ca. 500Ma, the ages of ca. 550-490 Ma in hornblende and biotite in Sverdrupfjella are thought to result from heating from granite emplacement combined with depths up to to ca. 12km which would equate to an ambient background temperature of 300^{o}C with a geothermal gradient of 25^{o}C/km. In Kirwanveggan, no granite sheets are seen. Consequently the reset ages in Kirwanveggan can only be related to heating related to burial without any thermal input fron granite intrusions.

Previously completed $^{40}Ar/^{39}Ar$ studies in Sverdrupfjella, Kirwanveggan and Heimefrontfjella are summarised in Table 4 in Grantham et al., (2019). The data from this study are shown in Figures 9 and 10. Figure 9 shows the $^{40}Ar/^{39}Ar$ data for biotite ages through Sverdrupfjella and Kirwanveggan from which it is apparent that most of the ages in Sverdrupfjella are between 450 Ma and 500 Ma with one sample <400 Ma and one marginally greater than 500 Ma. The data from Kirwanveggan vary with one age marginally less than 500, three ages between 500 and 600 and one age >800 Ma. No obvious gradient is evident from the biotite data but it is apparent that the Kirwanveggan ages are higher on average than Sverdrupfjella by ca. 50 Ma. Figure 9 also shows the locality of an $^{40}Ar/^{39}Ar$ age from detrital muscovite from the Urfjell Group of 579 Ma (Croaker, 1999) confirming the sedimentary rock age of deposition < 579 Ma. In addition, Kleinschmidt et al., (2000) report six $^{40}Ar/^{39}Ar$ ages on detrital muscovite from the Urfjell Group with ages ranging between 563 Ma to 583 Ma. Figure 5f shows a thin section

photograph of an arenite from Urfjell, from which it is apparent that the rock is immature, undeformed, with weakly rounded, and reasonably well sorted, grains. The sample is typical of a proximal sandstone which has not been transported extensive distances, containing a significant feldspar content. The photomicrograph also displays an incipient fine grained, intergranular growth of white mica. Kleinschmidt et al. (2000) report ages of ca. 450 Ma to 468 Ma from very fine fractions of sericite from the Urfjell Group which presumably represent the age of the intergranular white mice shown in Figure 5f and probably constrain the age of low grade metamorphism at that time.

Figure 10 shows the $^{40}Ar/^{39}Ar$ data for hornblende ages through Sverdrupfjella and Kirwanveggan from which it is apparent that most of the ages in Sverdrupfjella are between ca.500 and ca. 550 Ma with 3 samples marginally <500 Ma. It may be significant that those samples with marginally younger ages are from lower altitudes possible implying younger uplift/deeper erosion histories. The data from Kirwanveggan vary considerable and suggest a gradient of ca. 500 Ma in the north to ca. 1100 Ma in the most southerly exposure of gneisses at Skappelnabben. The basement gneisses in Kirwanveggan have SHRIMP U/Pb zircon ages of between ca. 950 Ma and ca. 1150 Ma (Jackson, 1999, Harris 1999). Consequently the $^{40}Ar/^{39}Ar$ ages of hornblende and biotite from the gneisses of central Kirwanveggan suggest that the rocks have been heated to >~300^{o}C, resulting in partial to complete reset biotite ages of ~500-860 Ma, but did not reach temperatures of ~500^{o}C, resulting in older hornblende ages being preserved at Skappelknabben and consequently implying a decreasing crustal thickness southwards. The preservation of older ages in hornblende, which, along with biotite, define the

pervasive planar fabric in these rocks, indicates that the fabric is also old and ca. 1000 Ma in age. This older age from amphibole is consistent with similar ages of 876±7 Ma and 1058±7 Ma from the SSW dipping mylonitic gneisses of the Polaris Formation exposed in an inlier from southern Kirwanveggan described by Kleinschmidt et al., (1996), the ages presumably defining minimum ages for the fabrics preserved in the rocks.

The decreasing crustal thickness southwards is consistent with the presence of Urfjell Group quartz arenites and grits at Drapane, ca. 15 km further southwest from Skappelnabben with the age of the sedimentary rocks being ca. 530 Ma (Moyes et al., 1997), supported by a detrital zircon study from the Urfjell Group indicating a maximum depositional age of ca. 530 Ma (Croaker, 1999) (Figure 11, top left), the age of the youngest detrital zircon recorded.

DISCUSSION OF THE URFJELL GROUP PROVENANCE

Croaker (1999) and Moyes et al. (1997) report Rb/Sr and Sm/Nd data from the Urfjell Group. This data is compared with whole rock data from basement gneisses in Kirwanveggan (Table 5), Sverdrupfjella, Gjelsvikfjella, Central Dronning Maud Land and Sor Rondane (Figure 12, top). The data from Urfjell Group are comparatively juvenile and are most similar to gneisses from Kirwanveggan, albeit it more evolved from a $Sr_{i@530\ Ma}$ perspective. Recognising the relative immaturity of the sedimentary rocks of the Urfjell Group, transport directions from the NE (Croaker, 1999; Moyes et al., 1997) and the proximity of Maud Belt gneisses, in Kirwanveggan and Sverdrupfjella, to the Urfjell Group, a source similar to Kirwanveggan could be anticipated. However, comparison of the zircon profile from Kirwanveggan (Figure 11, top right) with that

from the Urfjell Group (Figure 11, top left) indicates that it is an unlikely source, having zircons which are almost exclusively Mesoproterozoic in age.

Progressing further northeastwards, comparison of the zircon data from Sverdrupfjella and Gjelsvikfjella with that from the Urfjell Group, shows that they are also unlikely sources for the sedimentary rocks, both having significant zircon populations in the ranges ca. 400 Ma -<600 Ma and ca. 950 Ma- 1150 Ma but with no zircons with ages between ca. 600 Ma – ca. 950 Ma (Figure 11 top left, center left and center right). Similarly, comparison of the $Sr_{i@530Ma}/Nd_{i@530Ma}$ data from Sverdrupfjella and Gjelsvikfjella are dissimilar to that from the Urfjell Group (Figure 12 top), particularly the data from west Sverdrupfjella, which reflects the basement gneisses there are characterised by highly evolved $Sr_{i@530Ma}/Nd_{i@530Ma}$ signatures, implying involvement of older crust in their genesis. Grantham et al., (2011) has suggested that these data suggest continuation of the Archaean-age Kalahari(Grunehogna) Craton beneath the Maud Belt at depth, a conclusion which has also been made by Marschall et al., (2013).

Comparison of the detrital zircon profile of the Urfjell Group with those of CDML and Sor Rondane show that they have zircon profiles more comparable to the Urfjell Group with considerable zircon grains with ages between ca. 600 Ma and 950 Ma (Figure 11 bottom left and bottom right). Similarly the $Sr_{i@530Ma}/Nd_{i@530Ma}$ data from those areas are also juvenile with the $Sr_{i@530Ma}$ data reflecting a less evolved source to the Urfjell Group rocks (Figure 12, top). Consequently, the source area with the closest zircon-age characteristics to the Urfjell Group rocks are from western CDML, with the closest area with rocks with zircons of ages >600 Ma

being at Hochlinfjellet, some ca. 370km away to the NE, ca. 100kms E of Gjelsvikfjella, reported by Baba et al., (2015) from the western end of Central Dronning Maud Land (Figure 13).

The $^{40}Ar/^{39}Ar$ data presented here demonstrate that Kirwanveggan has not experienced significant uplift as a potential erosional sediment source for the Urfjell Group (Figures 9 and 10), a conclusion supported by the zircon age profiles of Kirwanveggan and Urfjell (Figure 11 top left and right). In contrast, P-T-t data from eastern Sverdrupfjella, Gjelsvikfjella and western CDML all show isothermal decompression paths with pressures in excess of 10kb down to ca.4-6kb (Groenewald and Hunter, 1991; Grantham et al., 1995; Engvik et al., 2004; Board et al., 2005, Pauly et al., 2016; Baba et al., 2008) implying significant loss of material due to erosion and uplift. In addition, Pauly et al., (2016) demonstrate the timing of decompression between ca. 570 Ma to ca. 520 Ma. Western Sverdrupfjella, however has P-T estimates <9kb (Grantham et al., 1995, Grosch et al., 2015) with Grantham et al., (1995) suggesting a heating path consistent with tectonic loading in a footwall setting.

With the broad structure of Sverdrupfjella, dipping ESE (Grantham et al., 1995), the differing P-T determinations between east and west Sverdrupfjella, imply an inverted P-T gradient. In addition, notice needs to be taken of the recognition that eastern Sverdrupfjella is characterised by numerous D1-D2 NW directed thrust faults (Grantham et al., 1995), which have emplaced rocks with higher P-T estimates over rocks with lower P-T estimates, resulting in the apparent inverted P-T gradient.

A factor in supporting differences between east and west Sverdrupfjella is demonstrated in Figure 12 (centre and bottom) which show significant differences in the $\varepsilon Sr_{@490Ma}/\varepsilon Nd_{@490Ma}$ signatures in the basement gneisses. Data from western Sverdrupfjella imply significant involvement of older crust in the genesis of the basement gneisses in contrast to data from the eastern Sverdrupfjella basement gneisses which have relatively juvenile characteristics. Figure 12 (bottom) demonstrates that the ca. 490 Ma granites are unlikely to have been generated by partial melting of the Mesoproterozoic gneisses underlying eastern Sverdrupfjella and Gjelsvikfjella, which they intrude but are probable partial melts of gneisses similar to those exposed in western Sverdrupfjella.

Integrating the $^{40}Ar/^{39}Ar$ data from this study with that published from Heimefrontfjella (Jacobs et al., 2005; 2009) (Figures 13 and 14) shows that the Maud Belt exposures in Kirwanveggan are separated from Heimefrontfjella by younger Urfjell Group and Karoo-age sedimentary rocks with hornblende $^{40}Ar/^{39}Ar$ ages showing a decreasing age gradient from NE Sverdrupfjella to SW Heimefrontfjella (Figure 14). Mica ages in Kirwanveggan and eastern Heimefrontfjella are similar (ca. 490-510 Ma), whereas those from western Heimefrontfjella are significantly older (ca. 970 Ma). The presence of relatively undeformed Urfjell Group arenites in Urfjell in particular, along with Karoo-age sedimentary rocks and basaltic lavas, extending from southern Kirwanveggan and N. Heimefrontfjella westwards to Vestfjella suggest that the EAO and KO do not extend as far as Heimefrontfjella, at least along the Grunehogna craton margin.

DISCUSSION OF THE ROLE OF CAMBRIAN-AGE GRANITE INTRUSIONS IN SVERDRUPFJELLA , GJELSVIKFJELLA AND CDML.

Post-dating deposition of the immature ca. <530 Ma Urfjell Group clastic sediments at surface, ca. 480-500 Ma granites were being generated and intruded in Sverdrupfjella, Gjelsvikfjella and CDML with the nearest exposures of granitic veins to Urfjell being in the most southerly nunataks in Sverdrupfjella at Nupskapa, ca.200km to the ENE (Figure 13). In Sverdrupfjella, the ca. 470-490 Ma old Dalmatian Granite (Grantham et al., 1991; Krynauw and Jackson, 1995) is seen as granitic sheets up to ca. 10m thick, distributed throughout Sverdrupfjella, intruding both east and western domains. Other intrusions of similar age include the Brattskarvet Granite at the northern end of Sverdrupfjella, with reported ages of 491 ± 4 Ma (Pauly et al., 2016) and 474 ± 10 Ma (Krynauw and Jackson, 1995) and aplite and granitic veins in southern Sverdrupfjella and Gjelsvikfjella with ages of 480±10 Ma (Board et al., 2006, Sverdrupfjella), 497 ± 5 Ma (Bisnath et al., 2006, Gjelsvikfjella), 485-506 Ma (Paulson and Austrheim, 2003, Gjelsvikfjella) and 487 ± 4 Ma (Jacobs et al., 2003a, Gjelsvikfjella). These granites and veins, which intrude both eastern and western domains in Sverdrupfjella, have $\varepsilon Sr_{@490Ma}/\varepsilon Nd_{@490Ma}$ characteristics comparable to the basement gneisses exposed in western Sverdrupfjella (Figure 12 center), suggesting their genesis by partial melting of gneisses at depth in the footwall of, and intruded into, the eastern Sverdrupfjella hanging wall of the accretionary complex. Grantham et al., (1991) and Grantham (1992) inferred the emplacement of the Dalmatian Granite veins at Salknappen and Kvitkjolen (ca. 5kms south of Salknappen, Figures 15 and 16) as syntectonic with a top-to-the-S-SE sense of shear. Whereas the early deformation history (D1 and D2) of Sverdrupfjella has been reported as involving top-to-the-NW folding and thrust

faulting (Grantham et al., 1995, Board et al., 2006), no clear age constraints are available on the early D1 and D2 deformation events. In contrast, analysis of the displacement of pre-Dalmatian Granite structures, along the Dalmatian Granite sheets at Salknappen (Byrnes, 2015) and Skarsnuten (Figure 15), supports a top-to-the-S-SE sense of shear during the syntectonic emplacement of the Dalmatian Granite veins at ca. 490 Ma (Figure 15). The top-to-the-SE sense of shear is inferred to be related to and co-eval with the top-to-the-SE D3 folding recognised in the footwall domain in western Sverdrupfjella (Grantham, 1992; Grantham et al., 1995, Bumby et al., 2019). Consequently, it is concluded that top-to-the-SE deformation with syntectonic granite emplacement at ca.490-500 Ma occurring synchronously with deposition of the Urfjell Group sediments to the SW and that the earlier NW-directed D1 and D2 deformation in Sverdrupfjella, preserve an earlier, unrelated deformation history. Significantly, no top to the SE deformation has been recognised in Kirwanveggan (Grantham et al., 1995; Grantham et al., 2008, Harris, 1995; Ferrar, 1994)

DISCUSSION OF THE TECTONICS OF WESTERN DRONNING MAUD LAND.

Jacobs et al., (2003a,b) and Baba et al., (2015) describe a WNW-ESE oriented thrust fault with top-to-the-S sense of displacement in Gjelsvikfjella, with Baba et al., (2015) extending it southeastwards toward Hochlinfjellet (Figures 13 and 14). In addition, Baba et al., (2015) report granulites at Hochlinfjellet with U/Pb SHRIMP zircon ages of ca. 590-600 Ma, in the hanging wall of the thrusted block. These data demonstrate the southward emplacement of younger Neoproterozoic-age granulites over older Mesoproterozoic gneisses after ca. 590 Ma in Gjelsvikfjella and Hochlinfjellet.

Consequently it is apparent that eastern Sverdrupfjella, Gjelsvikfjella and CDML comprise a relatively juvenile accretionary thrust belt complex with relatively high P-T estimates, preserving an early top-the-NW directed tectonic history, which has subsequently been juxtaposed over western Sverdrupfjella at ca. 490 Ma, involving top-to-the-S-SE transport of eastern Sverdrupfjella over western Sverdrupfjella, with western Sverdrupfjella being characterised by gneisses with relatively low P-T estimates and strongly negative, evolved εNd isotopic signatures (Figure 12). In addition, it is possible that the top-to-the-SE deformation at ca. 490-500 Ma is not a local event but is potentially applicable eastwards to Sor Rondane where Tsukada et al., (2017) describe top-to-the-S thrust faulting with an age <ca. 530 Ma. Similarly top-to-the SE deformation at ca. 550Ma is recognised in NE Straumsnutane (Figure 13), west of Sverdrupfjella, located on the edge of the Grunehogna Craton (Bumby et al., 2019), An implication of its westward extent is that western Sverdrupfjella through to NE Straumsnutane were located in the footwall of a contiguous nappe structure described below.

Grantham et al., (2008; 2013) proposed a mega-nappe structure involving the emplacement of Namuno Terrane rocks from northern Mozambique, over the Nampula Terrane, with the Namuno Terrane rocks being correlatable with rocks from CDML to Sor Rondane in the east, the correlation being supported by comparable geochronological age distributions between the Namuno Terrane, Mozambique and CDML and Sor Rondane. The recognition of rocks of similar age and composition by Baba et al., (2015) in western CDML to those further east (including Schirmacher Oasis, Ravikant et al., 2018) and Sor Rondane areas suggests that the distribution of the mega-nappe complex can be extended, westward and southward from the limits

proposed in Grantham et al., (2008), to include the gneisses and granulites exposed in western CDML, Gjelsvikfjella and Straumsnutane and also include the gneisses of eastern Sverdrupfjella, recognising the comparable εNd/εSr characteristics of east Sverdrupfjella, Gjelsvikfjella, Schirmacher Oasis and Sorrondane (Figure 12). In contrast, the gneisses of western Sverdrupfjella, are correlatable with the Barue Complex and Nampula Terranes of northern Mozambique (Grantham et al., 2008, 2011), but were located in the footwall of the nappe..

An implication of widening the extent of the Kuunga Orogeny mega-nappe complex to include eastern Sverdrupfjella and western CDML, facilitates a far closer potential proximal source for the Urfjell Group sediments to its depository ca. 200km away. Comparison of the tectonic structure of Dronning Maud Land in Figures 13 and 14, with available aeromagnetic and aerogravity data (Riedel et al., 2012, 2013), is consistent with the interpretations above (Figures 16a and b).

From Figure 16a, it is apparent that the major thrust shear zones inferred in Figures 13 and 14 are coincident with strong positive aeromagnetic anomalies (Figure 16a), including the shear zone separating the Grunehogna cratonic domain from the Maud Belt, the shear zone separating east and west Sverdrupfjella and the shear zone separating western CDML from Gjelsvikfjella. Similarly the Forster Magnetic anomaly, stretching from Heimefrontfjella to eastern CDML (Figure 16a) appears to continue into the Orvinfjella Shear Zone described by Bauer et al., (2003) as having a sinistral sense of shear, suggesting that the Forster Magnetic anomaly is underlain by a sinistral shear zone. In a reconstructed Gondwana, the Orvinfjella

Shear zone appears to be similarly oriented and positioned to the Namama shear zone which cuts the Nampula Terrane in Mozambique (Cadoppi et al., 1987).

From a comparison of the tectonic structure of Dronning Maud Land in Figure 16a with the crustal thickness image in Figure 16b, it can be seen that CDML and eastern Sverdrupfjella are characterised by thicker crust, consistent with structural stack thickening, in contrast to the markedly thinner crust underlying western Sverdrupfjella. A crustal thickening gradient is also apparent extending from western N. Sverdrupfjella, through Kirwanveggan and Urfjell, to north of Heimefrontfjella, consistent with thickening southward and ending in an area of thick crust, coincident with an east-west zone along which the Urfjell Group and Permian to Jurassic age Karoo sediments and volcanic rocks are preserved (Figure 16b), possibly forming a synformal mega-crustal downwarp probably of Cambrian to Jurassic age.

The tectonic/geological units of reconstructed Gondwana (Figure 17) facilitate an inferred cross section from N. Mozambique to Heimefrontfjella (Figure 18). The cross section in Figure 18 is modified after a similar cross section in Grantham et al., (2008). The cross section depicts a mega-nappe structure at ca. ~550 Ma with present day erosion levels for Africa and Antarctica, recognising that erosion in Antarctica has not been as intensive compared to Africa due to slower erosion rates in glacial settings as well as depression of Antarctica due to the weight of the ice cap. The cross section reflects the Cabo Delgado Nappe Complex (Viola et al., 2008; Bingen et al., 2009a) of the Namuno Terrane, N. Mozambique, comprising interleaved Mesoproterozoic and Neoproterozoic slices, emplaced over the Nampula Terrane with

preservation of the Neoproterozoic klippen of Mugeba and Monapo (Grantham et al., 2008, 2013) as well as the thrust fault relationships described by Jacobs et al. (2003a,b) and Baba et al., (2015) in Gjelsvikfjella and Hochlinfjellet. The cross section also reflects the sedimentary basin to the south in which the Cambrian age Urfjell Group as well as the younger Permian - Jurassic Karoo sediments and lavas were deposited in southern Kirwanveggan, Heimefrontfjella and Vestfjella. Erosion of the mega-nappe complex would have provided sediment with age characteristics typical of the hanging wall complex into the Urfjell Group and Karoo depositories, the deposition of the Urfjell Group sediments occurring synchronously with southward directed deformation and syntectonic granite emplacement in Sverdrupfjella. A detrital zircon profile from the Amelang Formation, the Karoo-age rock unit exposed in southern Kirwanveggan (Veevers and Saeed, 2007), is similar to the profiles for CDML and Sor Rondane described here.

CONCLUSIONS

$^{40}Ar/^{39}Ar$ laser step heating data from Mesoproterozoic basement gneisses from Kirwanveggan reveal significantly different ages for biotite and hornblende with ages varying between 497 Ma and 868 Ma and 480 Ma and 1067 Ma respectively, with the hornblende data reflecting increasing ages from NE to southwest. These data confirm a crustal thickness/heating gradient from NE Sverdrupfjella to SW Kirwanveggan, along with gravity data from N Sverdrupfjella to Heimefrontfjella. The crustal thickness gradient of ca. 12 km, seen today, in the NE to surface in the SW at ca. 500Ma is inferred to have involved preferential erosion in the north, related to

isostatic rebound after the nappe emplacement with nappe never reaching Drapane, in southern Kirwanveggan.

The relatively old ages from Kirwanveggan, derived from minerals which define the planar fabric, indicate that the SE dipping planar fabrics were formed during the Mesoproterozoic. In contrast, the SE dipping, layer parallel D1-D2 planar fabrics in Sverdrupfjella, particularly in eastern Sverdrupfjella, are inferred to be Neoproterozoic in age. Metacarbonates interlayered with calc-silicate and quartzofeldspathic gneisses at Fuglefjellet, in central eastern Sverdrupfjella, yield Sr ages of ~850 Ma (Grantham, unpubl. data) and are truncated by layer parallel D1-D2 thrust faults. In addition, a strong aeromagnetic anomaly is oriented parallel to the thrust-fault belt of Eastern Sverdrupfjella, but swings eastward in southern Sverdrupfjella and is discontinuous with the aeromagnetic anomaly which underlies Kirwanveggan.

Biotite ages throughout Sverdrupfjella and Kirwanveggan are similar to, and younger than, reported ages of deposition of the Urfjell Group clastic sediments, with the Urfjell constraining the southern limit of uplift, erosion and deposition at ~530 Ma. Radiogenic isotope characteristics of the Urfjell sedimentary rocks are similar to basement gneisses from Kirwanveggan, eastern Sverdrupfjella, Gjelsvikfjella and eastern Dronning Maud Land. In contrast detrital zircon patterns of the Urfjell Formation clastic sediments suggest derivation from a source similar to lithologies from central to eastern Dronning Maud Land, ca. 500km away.

Radiogenic isotope data from Sverdrupfjella basement gneisses show that significant differences between east and west Sverdrupfjella are evident with west Sverdrupfjella being characterised by T_{Dm} ages of ca. >2000 Ma in contrast to east Sverdrupfjella with T_{Dm} ages of <2000 Ma. Tectonic analysis of Dronning Maud Land, using the Sr/Nd radiogenic isotope data, along with SHRIMP U/Pb zircon data, P-T-t estimates and structural analysis allow the interpretation that eastern Sverdrupfjella, Gjelsvikfjella and CDML comprise a nappe complex which has been emplaced over western Sverdrupfjella toward S-SE at ca. 500-480 Ma, the timing being constrained by the age of 490 Ma syntectonic granitic intrusions and rapid uplift reflected by the $^{40}Ar/^{39}Ar$ data. The emplacement of this nappe complex would place a potential source for the Urfjell Group sediments significantly closer to the Urfjell Group basin depository. The reach of the Kuunga Orogeny in Dronning Maud Land is limited to central Kirwanveggan, with its southern limit represented by the Urfjell Group sedimentary basin at ca. 530 Ma.

The absence of significant Neoproterozoic deformation in Kirwanveggan along with the relatively undeformed nature of the ca. 530 Ma Urfjell Group clastic sedimentary rocks and Triassic-Jurassic-age cover rocks, extending from southern Kirwanveggan to Vestfjella, indicate the Kuunga Orogeny aerial extent is limited to Sverdrupfjella and possibly N. Kirwanveggan and also indicate that the EAO does not extend to Heimefrontfjella, at least along the eastern edge of the Grunehogna Craton.

ACKNOWLEDGEMENTS

The National Research Foundation is thanked for research grants 93079 and 110739 for research under the auspices of the South African National Antarctic Program. The Department of Environmental Affairs and Starlite Aviation are acknowledged for logistical support in the field and on the SA. Aghulhas II. Constructive reviews by Rudolph Trouw and an anonymous reviewer are similarly acknowledged. Mr. E. P. Burger, responsible for biotite and hornblende separations, questions the veracity of the nappe model.

REFERENCES

Adachi T., Osanai Y., Hokada T., Nakano N., Baba S., Toyoshima T. (2013) Timing of metamorphism in the central Sør Rondane Mountains, eastern Dronning Maud Land, East Antarctica: Constrains from SHRIMP zircon and EPMA monazite dating. *Precambrian Research* 234, 136–160.

Baba,S., Horie,K., Hokada, T., Owada, M., Adachi, T. and Shiraishi, K. (2015) Multiple Collisions in the East African–Antarctica Orogen: Constraints from Timing of Metamorphism in the Filchnerfjella and Hochlinfjellet Terranes in Central Dronning Maud Land. *The Journal of Geology*, 123, p. 55–78.

Baba,S., Owada, M., and Shiraishi, K. (2008) Contrasting metamorphic P–T path between Schirmacher Hills and Muhlig-Hofmannfjella, central Dronning Maud Land, East Antarctica. pp. 401–417 in Satish-Kumar, M., Motoyoshi, Y., Osanai, Y., Hiroi, Y. & Shiraishi, K. (eds) *Geodynamic Evolution of East Antarctica: A Key to the East–West Gondwana Connection*. Geological Society, London, Special Publications,308.

Bauer W., Thomas R.J., and Jacobs, J. (2003) Proterozoic-Cambrian history of Dronning Maud land in the context of Gondwana assembly. pp247-270 in *Proterozoic East Gondwana: Supercontinent Assembly and Breakup*. Yoshida M., Windley B.F. and Dasgupta S.(eds), Geol. Soc. Lond. Spec. Publ. 206.

Ben Othman, D., Polve, M. and Allegre, C.J. (1984) Nd-Sr isotopic composition of granulites and constraints on the evolution of the lower continental crust. *Natur*e, 307, 510-515.

Bingen, B., Viola, G., Griffin, W.L. Jacobs, J., Engvik, A., Henderson, I.H.C., Boyd, R., Thomas, R.J., Daudi., Skar, O., Key, R.M., Solli, A., Sandstad, J.S., Smethurst, M.and Bjerkgard, T. (2009) Geochronology of the Precambrian crust in the Mozambique belt in NE Mozambique, and implications for Gondwana assembly. *Precambrian Research*, 170, Pages 231-255.

Bingen, B., Viola, G., Griffin, W.L. Jacobs, J., Engvik, A., Henderson, I.H.C., Boyd, R., Thomas, R.J., Daudi., Skar, O., Key, R.M., Solli, A., Sandstad, J.S., Smethurst, M.and Bjerkgard, T. (2009) Gondwana assembly: Geochronology and Hf isotopes constraints from NE Mozambique. http://nora.nerc.ac.uk/id/eprint/5598

Bisnath A., Frimmel H.E., Armstrong R.A. & Board W.S. (2006) Tectonothermal evolution of the Maud Belt: New Shrimp U-Pb zircon data from Gjelsvikfjella, Dronning Maud Land, East Antarctica. *Precambrian Research,* 150, 95-121.

Board W.S. (2001) Tectonothermal evolution of the southern H.U. Sverdrupfjella, western Dronning Maud Land, Antarctica. Ph.D. thesis, University of Cape Town, 205 pp.

Board W.S., Frimmel., H.E., & Armstrong R.A. (2005) Pan-African Tectonism in the western Maud Belt: P-T-t path for High-grade gneisses in the H.U. Sverdrupfjella, East Antarctica. *Journal of Petrology*, 46, 671-699.

Boger S (2011) Antarctica — Before and after Gondwana. *Gondwana Research,* 19, p335–371.

Bumby A., Grantham G.H. and Moabi N. (2019) The structural Evolution of the Straumsnutane and western Sverdrupfjella areas, western Dronning Maud Land, Antarctica – implications for the amalgamation of Gondwana. Abstract International Symposium on Antarctic Earth Science, Incheon, Korea. July 2019.

Byrnes G. (2015) *Tectono-metamorphic history of the reworked, high-grade Maud Belt at central-Eastern H.U. Sverdrupfjella, Antarctica.* unpubl. MSc thesis, University of Cape Town. pp. 126.

Cadoppi, P., Costa, M. and Sacchi, R. (1987) A cross section of the Namama Thrust belt (Mozambique). *Journal of African Earth Sciences*, 6, 493-504.

Collins, A.S. and Pizarevsky S.A. (2005) Amalgamating eastern Gondwana: the evolution of the Circum-Indian Orogens*. Earth-Sci. Rev*., 71 (2005), pp. 229-270

Croaker, M. (1999) *Geological constraints on the evolution of the Urfjell Group, southern Kirwanveggen, western Dronning Maud Land, Antarctica* .Unpubl. M.Sc. thesis, University of Natal.

Daczko N.R., Halpin, J.A., Fitzimmons I.C.W and Whittaker J. (2018) A cryptic Gondwana-forming orogen located in Antarctica. Nature Scientific reports, 8:8371, DOI:10.1038/s41598-018-26530-1

Eglington, B.M. and Harmer, R.E. (1999) GEODATE for Windows version 1: Isotope regression and modelling software. Council for Geoscience Open-file report 1999-0206 O, 24pp.

Elburg,M., Andersen, T., Jacobs,J., Läufer, A. Ruppel, A., Krohne, N., and Damaske D. (2016) One Hundred Fifty Million Years of Intrusive Activity in the Sør Rondane Mountains (East Antarctica): Implications for Gondwana Assembly. *The Journal of Geology*, 124, p. 1–26.

Engvik, A.K. and Elvevold S. (2004) Pan-African extension and near-isothermal exhumation of a granulite facies terrain, Dronning Maud Land, Antarctica. *Geol. Mag*. 141 (6), 2004, pp. 649–660.

Ferrar G.R. (1994) The metamorphic geology of the Armalsryggen, western Dronning Maud Land. Unpubl. MSc Thesis, University of Natal. p135.

Frimmel, H.E. (2004) Formation of a late Mesoproterozoic supercontinent; the South Africa–East Antarctica connection. In: Eriksson, P.G., Altermann, W., Nelson, D.R., Mueller, W.U., Catuneau, O. (Eds.), *The Precambrian Earth; Tempos and Even*ts, vol. 12. Elsevier, Amsterdam, pp. 240–255.

Goldstein SL, O'Nions, R.K., & Hamilton P.J. (1984) A Sm-Nd isotopic study of atmospheric dusts and particulates from major river systems. *Earth and Planetary Science Letters*, 70, p221-236.

Grantham, G.H. (1992) *Geological Evolution of western H.U. Sverdrupfjella, Dronning Maud Land, Antarctica.* Unpublished PhD thesis, University of Natal (Pietermaritzburg). 277pp.

Grantham, G.H., Armstrong. R.A. and Moyes, A.B. (2006). The age, chemistry and structure of mafic dykes at Roerkulten, H.U. Sverdrupfjella, western Dronning Maud Land, Antarctica. pp.213-224 in *Dyke Swarms - Time Markers of Crustal Evolution*. Hanski E., Mertanen S., Ramo T. and Vuollo J. (eds) Proceedings of the Fifth/Fourth International Dyke Conference (IDC5), Rovaniemi, Finland. A.A. Balkema Press.

Grantham, G.H., Groenewald, P.B. and Hunter, D.R. (1988) Geology of the northern H.U. Sverdrupfjella, western Dronning Maud Land and implications for Gondwana reconstructions. *South African Journal Antarctic Research*, 18, 2-10,

Grantham, G.H., Jackson, C., Moyes, A.B., Groenewald, P.B., Harris, P.D., Ferrar, G. & Krynauw, J.R., (1995) The tectonothermal evolution of the Kirwanveggan-H.U. Sverdrupfjella areas, Dronning Maud Land, Antarctica. *Precambrian Re*search, 75, 209-230.

Grantham, G., Kramers, J. and Burger, E.(2019), Ar/Ar data western Dronning Maud Land, Mendeley Data, V2, https://data.mendeley.com/datasets/b84hyp5j93/draft?a=1fc3387e-86fe-4a54-ac73-6660d6f8b1ec

Grantham, G.H., Macey, P.H., Horie,K., Kawakami, T., Ishikawa, I., Satish-Kumar M., Tsuchiya N., Graser P. and Azevedo S. (2013) Comparison of the metamorphic history of the Monapo Complex, northern Mozambique and Balchenfjella and Austhameren areas, Sør Rondane, Antarctica: Implications for the Kuunga Orogeny and the amalgamation of N and S Gondwana *Precambrian Research,* 234 (2013) 85–135.

Grantham, G.H., Macey, P.H., Ingram, B.A., Roberts, M.P., Armstrong, R.A., Hokada, T., Shiraishi, K., Jackson, C., Bisnath, A. and Manhica, V. (2008) Terrane Correlation between Antarctica, Mozambique & Sri Lanka; Comparisons of Geochronology, Lithology, Structure and Metamorphism and possible implications for the geology of southern Africa and Antarctica. *Geodynamic Evolution of East Antarctica: a Key to the East-West Gondwana Connection*. eds M Satish-Kumar, Y Motoyoshi, Y Osanai, Y Hiroi and K Shiraishi, Geol. Soc. of London Spec. Publ., 308, p91-119.

Grantham, G.H., Manhica, A.D.S.T. Armstrong, R.A., Kruger, F.J. and Loubser, M. (2011) New SHRIMP, Rb/Sr and Sm/Nd isotope and whole rock chemical data from central Mozambique and western Dronning Maud Land, Antarctica: Implications for the nature of the eastern margin of the Kalahari Craton and the amalgamation of Gondwana. *Journal of African Earth Sciences*. 59, 74-100.

Grantham, G.H., Moyes, A.B. and Hunter, D.R. (1991) The age, petrogenesis and emplacement of the Dalmatian Granite, H.U. Sverdrupfjella, Dronning Maud Land, Antarctica. *Antarctic. Scie*nce, 3, 197-204.

Groenewald, P.B. and Hunter, D.R. (1991) Granulites of northern H.U. Sverdrupfjella, western Dronning Maud land: metamorphic history from garnet-pyroxene assemblages, coronas and hydration reactions. pps 61-67 in *Geological evolution of Antarctica*. Thomson, M.R.A., Crame, JA. and Thomson, JW. (eds). Int. symp. on Antarctic Earth Sc., Cambridge.

Groenewald, P.B., Grantham, G.H. and Watkeys M. (1991) Geological evidence for a Proterozoic to Mesozoic link between southeastern Africa and Dronning Maud Land, Antarctica. *Journal of the Geological Society,* London, Vol. 148, pp. 1115-1123.

Grosch, E.G., Bisnath, A., Frimmel H.E. and Board W.S. (2007) Geochemistry and tectonic setting of mafic rocks in western Dronning Maud Land, East Antarctica: implications for the geodynamic

evolution of the Proterozoic Maud Belt. *Journal of the Geological Society, Lond*on, Vol. 164, 2007, pp. 465–475.

Grosch, E.G. , Frimmel H.E., Abu-Alam Tamer & Košler J. (2015) Metamorphic and age constraints on crustal reworking in the western H.U. Sverdrupfjella: implications for the evolution of western Dronning Maud Land, Antarctica. *Journal of the Geological Society*, 172, 499-518.

Harmer, R.E., Lee, C.A. and Eglington B.M. (1998) A deep mantle source for carbonatite magmatism: evidence from the nephelinites and carbonatites of the Buhera district, SE Zimbabwe. *Earth and Planetary Science Letters*, 158, 131-142.

Harris P.D. (1999) *The Geological Evolution of Neumayerskarvet in the northern Kirwanveggen, western Dronning Maud Land, Antarctica*. Unpublished PhD Thesis Rand Afrikaans University, 251pp.

Higashino F., Kawakami T., Tsuchiya N., Satish-Kumar M., Ishikawa M., Grantham G.H., Hatori K., Hirata T. (2015) Geochemical behavior of zirconium during upper amphibolite facies metamorphism - a case study from Bratnipene, Sor Rondane Mountains, east Antarctica. *Journal of Mineralogical and Petrological Sciences*, 110, 166-178.

Higashino F., Kawakami T., Satish-Kumar M., Ishikawa M., Maki K., Tsuchiya N., Grantham G.H., Hirata T. (2013) Chlorine-rich fluid or melt activity during granulite facies metamorphism in the Late Proterozoic to Cambrian continental collision zone—An example from the Sør Rondane Mountains, East Antarctica. *Precambrian Research* , 234., 229–246.

Hokada T., Grantham G.H., Arima M., Saito S., Shiraishi K., Armstrong R.A., Eglington B., Misawa K. and Kaiden H. (2019) Stenian A-type granitoids in the Namaqua-Natal Belt, southern Africa, Maud Belt, Antarctica and Nampula Terrane, Mozambique: Rodinia and Gondwana amalgamation implications. Geoscience Frontiers, https://doi.org/10.1016/j.gsf.2019.04.003.

Jackson C. (1999) Characterization of Mesoproterozoic to Paleozoic crustal evolution of western Dronning Maud land. Unpublished report to South African National Antarctic Programme. Study 3. 80.pps

Jacobs J., Elburg M., Laufer A., Kleinhannse I., Henjes-Kunst F., Estrada S., Ruppel A.S., Damaske D., Montero P., Bea F. (2015) Two distinct Late Mesoproterozoic/Early Neoproterozoic basement provinces in central/eastern Dronning Maud Land, East Antarctica: The missing link, 15.21.E *Precambrian Research*, 265, 249–272.

Jacobs, J. Ahrendt, H., Kreutzer, H. and Weber, K. (1995) K-Ar, 40Ar/39Ar and apatite fission-track evidence for Neoproterozoic and Mesozoic basement rejuvenation events in the Heimefrontfjella and Mannefallknausane (East Antarctica). *Precambrian Research*, 75, 251-262.

Jacobs, J. and Thomas R.J. (1994) Oblique collision at about 1.1Ga along the southern margin of the Kaapvaal Craton continent, south east Africa. *Geologische Rundschau*, 83, 322-333.

Jacobs, J. Bauer W. Fanning C.M. (2003a). New age constraints for Grenvillian age metamorphism in western central Dronning Maud land (East Antarctica) and implications for the paleogeography of Kalahari in Rodinia. *Geologische Rundschau*, 92, 301-315.

Jacobs, J. Bauer W. Fanning C.M. (2003c) Late Neoproterozoic/Early Paleozoic events in central Dronning Maud Land and significance for the southern extension of the East African Orogen into East Antarctica. *Precambrian Research* 126, 27-53.

Jacobs, J. Klemd R., Fanning C.M. Bauer W. & Colombo F. (2003b) Extensional collapse of the late Neoproterozoic-early Paleozoic East African-Antarctic Orogen in Central Dronning Maud Land, East Antarctica. pp271-287 in *Proterozoic East Gondwana: Supercontinent Assembly and Breakup*. Yoshida M., Windley B.F. and Dasgupta S. (eds), Geol. Soc. Lond. Spec. Publ. 206.

Jacobs, J. Falter M., Weber K. and Jessberger E.K. (1997) 40Ar/39Ar Evidence for the Structural Evolution of the Heimefront Shear Zone (western Dronning Maud Land) East Antarctica. pp 37-44 In *The*

Antarctic Region: Geological Evolution and processes. Ed C.A. Ricci. Proc. VII Int. Symposium on Antarctic Earth Sciences, Siena, 13-20. Terra Antarctica

Jacobs, J. Fanning C.M., Henjes-Kunst F., Olesch M., and Paech H.J. (1998) Continuation of the Mozambique Belt into East Antarctica: Grenville age metamorphism and Polyphase Pan-African high grade events in Central Dronning Maud Land. *Journal of Geology*, 106, 385-406.

Jacobs, J. Hansen, B.T., Henjes-Kunst, F., Thomas, R.J., Weber, K., Bauer, W., Armstrong, R.A. and Cornell, D.H. (1999) New Age constraints on the Proterozoic/Lower Paleozoic Evolution of Heimefrontfjella, East Antarctica, and its bearing on Rodinia/Gondwana Correlations. Terra Antartica, 6(4), 377-389.

Kamei A., Horie K., Owada M., Yuhara M., Nakano, N., Osanai Y., Adachi T., Hara Y., Terao M., Teuchi S, Shimura T., Tsukada K., Hokada T., Iwata C., Shiraishi K., IshizukaH., Takahashii Y., (2013) Late Proterozoic juvenile arc metatonalite and adakitic intrusions in the SørRondane Mountains, eastern Dronning Maud Land, Antarctica *Precambrian Research* 234, 47– 62.

Kazami S., Tsunogae T., Santosh M., Tsutsumi Y., Takamura Y. (2016) Petrology, geochemistry and zircon U-Pb geochronology of a layered igneous complex from Akarui Point in the Lützow-Holm Complex, East Antarctica: Implications for Antarctica-Sri Lanka correlation. *Journal of Asian Earth Sciences* 130, 206–222.

Kleinschmidt G., Helferich S., Henjes-Kunst F., Jackson C. and Frimmel H.E (2000) The pre-Permo-Carboniferous Rocks and Structures from Southern Kirwanveggen, Dronning Maud Land, Antarctica. *Polarforschung* 66,7 -18.

Krynauw, J.R. and Jackson C. (1996) Geological evolution of western Dronning Maud Land within a Gondwana framework. South African National Antarctic Programme Final Report 1991-1996. Geology Subsection , 1-48.

Li, L. Lin, S., Xing G., Jiang, Y. and He J. (2017) First Direct Evidence of Pan-African Orogeny Associated with Gondwana Assembly in the Cathaysia Block of Southern China. *Nature Scientific* reports, 7, 794. DOI:10.1038/s41598-017-00950-x

Ludwig, K.R. (2001) Isoplot/Ex rev. 2.49: a geochronological tool kit for Microsoft Excel. Berkley Geochronology Center Special Publication No. 1a. 55 pp.

Macey, P.H. Thomas, R.J. Grantham, G.H., Ingram, B.A. Jacobs, J., Armstrong, R.A., Roberts, M.P. Bingen, B. Hollick, L. de Kock,G.S. Viola,G. Bauer, W. Gonzales, E. Bjerkgård, T., Henderson, I.H.C. Sandstad, J.S. Cronwright, M.S. Harley, S., Solli, A. Nordgulen, Ø., Motuza, G. Daudi E. and Manhiça V. (2010) Mesoproterozoic geology of the Nampula Block, northern Mozambique: Tracing fragments of Mesoproterozoic crust in the heart of Gondwana. *Precambrian Research,* 182, 124-148

Marschall H.R., Hawkesworth C.J., and Leat P.T. (2013) Mesoproterozoic subduction under the eastern edge of the Kalahari-Grunehogna Craton preceding Rodinia assembly: The Ritscherflya detrital zircon record, Ahlmannryggen (Dronning Maud Land, Antarctica). *Precambrian Research*, 236, 31-45.

Martin, A.K. and Hartnady, C.J.H. (1986) Plate tectonic development of the southwestern Indian Ocean : a revised reconstruction of East Antarctica and Africa. *Journal Geophysical Research*, 91 (B5) 86, 4767-4787.

Meert J. (2003) A synopsis of events related to the assembly of eastern Gondwana. *Tectonophysics*, 362, 1-40.

Moyes A.B. (1993) The age and origin of the Jutulsessen granitic gneiss, Gjelsvikfjella, Dronning Maud Land. *South African Journal of Antarctic Research*, 23,25-32

Moyes A.B. & Groenewald P.B. (1996) Isotopic constraints on Pan African Metamorphism in Dronning Maud Land, Antarctica. *Chemical Geology*, 129, p247-256

Moyes A.B. and Harris P.D. (1996) Geological evolution of western Dronning Maud Land within a Gondwana framework. South African National Antarctic Programme Final Report 1991-1996. Radiogenic Isotope Geology Project, 1-38.

Moyes A.B., Barton, J.M. and Groenewald, P.B. (1993) Late Proterozoic to early Palaeozoic tectonism in Dronning Maud Land, Antarctica: supercontinental fragmentation and amalgamation. *Journal of the Geological Society of London*, 150, 833-842.

Moyes A.B., Groenewald, P.B. and Brown, R.W. (1993) Isotopic constraints on the age and origin of the Brattskarvet intrusive suite, Dronning Maud Land, Antarctica. *Chemical Geology*, 106, 453-466.

Moyes A.B., Knoper M.W. and Harris P.D. (1997) The age and significance of the Urfjell Group, western Dronning Maud Land. pp 31-36 In *The Antarctic Region: Geological Evolution and processes*. Ed C.A. Ricci. Proc. VII Int. Symposium on Antarctic Earth Sciences, Siena, 13-20. Terra Antarctica

Nakano N., Osanai Y., Kamei A., Satish-Kumar M., Adachi T., Hokada T., Baba S., Toyoshima T (2013) Multiple thermal events recorded in metamorphosed carbonate and associated rocks from the southern Austkampane region in the Sør Rondane Mountains, East Antarctica: A protracted Neoproterozoic history at the Gondwana suture zone. *Precambrian Research*, 234, 161–182.

Ohta Y. G.H. Grantham & P.B. Groenewald (2001) Temakart No. 25, Nature Environment Map H.U. Sverdrupfjella, Dronning Maud Land, East Antarctica, 1:25000, Norwegian Polar Institute, Tromso.

Paulsson, O. and Austrheim H. (2003) A geochronological and geochemical study of rocks from Gjelsvikfjella, Dronning Maud Land, Antarctica—implications for Mesoproterozoic correlations and assembly of Gondwana. *Precambrian Research*, 125, 113-138.

Pauly J., Marschall H.R., Meyer H-P., Chatterjee, N. and Brian Monteleone B. (2016) Prolonged Ediacaran–Cambrian Metamorphic History and Short-lived High-pressure Granulite facies

Metamorphism in the H.U. Sverdrupfjella, Dronning Maud Land (East Antarctica): Evidence for Continental Collision during Gondwana Assembly. *Journal of Petrology*, 57, 185–228.

Ravikant V., Buhn B. and Pimentel M. (2018) Zircon U-Pb age constraints for Tonian-early Cryogenian deposition of metasedimentary rocks from the Schirmacher Oasis, East Antarctica: Implications for correlations across the Mozambique Ocean. *Polar Science, 18, 39-47.*

Renne P. R., Mundil R., Balco G., Min K. and Ludwig K. R. (2010) Joint determination of 40K decay constants and 40Ar*/40K for the Fish Canyon sanidine standard, and improved accuracy for 40Ar/39Ar geochronology. *Geochimicha Cosmochimicha Acta* 74, 5349–5367.

Riedel S., Jacobs J. and Jokat W. (2013) Interpretation of new regional aeromagnetic data over Dronning Maud Land, (East Antarctica). *Tectonophysics*. 585, 161–171.

Riedel S., Jokat, W. and Steinhage D. (2012) Mapping tectonic provinces with airborne gravity and radar data in Dronning Maud Land, East Antarctica. *Geophysical Journal International*, 189, 414–427.

Roberts M.P., Grantham G.H., Cronwright M., Sacchi R., Ingram B.A., Azevedo S., Walliser A. & August R.B. (2005) Preliminary Pressure Temperature Determinations on Granulite-facies Rocks of the Mugeba Klippe, North Central Moçambique GEO2005 p193-194 extended abstracts, Durban, South Africa.

Shiraishi, K., Dunkley D., Hokada T., Fanning, C.M., Kagami, H. and Hamamoto T. (2008) Geochronological constraints of the Late Proterozoic-Cambrian crustal evolution in eastern Dronning Maud Land, East Antarctica: a synthesis of SHRIMP U-Pb age and Nd model age data. *Geodynamic Evolution of East Antarctica : a Key to the East-West Gondwana Connection*. eds M Satish-Kumar, Y Motoyoshi, Y Osanai, Y Hiroi and K Shiraishi, Geol. Soc. of London Spec. Publ., 308, p. 21.67.

Spear F. (1995) *Metamorphic phase equilibria and pressure-temperature-time paths*. Mineralogical Society of America Monograph. 799p.

Stern R.J. (2002) Crustal evolution in the East African Orogen: a neodymium isotopic perspective. *Journal of African Earth Sciences*, 34, 109-117.

Stern R.J. (1994) Arc assembly and continental collision in the Neoproterozoic East African Orogen: Implications for the consolidation of Gondwanaland. *Annual Reviews Earth Science*, 22, 319-351.

Tsukada, K., Yuhara, M., Owada, M., Shimura, T., Kamei, A., Kouchi, Y. and Yamamoto K. (2017) A low-angle brittle shear zone in the western Sør Rondane Mountains, Dronning Maud Land, East Antarctica — Implication for assembly of Gondwanaland. *Journal of Geodynamics*, 111 , 15–30

Tsunogae T., Dunkley D.J., Horie K., Endo T., Miyamoto T., Kato M. (2014) Petrology and SHRIMP zircon geochronology of granulites from Vesleknausen, Lützow-Holm Complex, East Antarctica: Neoarchean magmatism and Neoproterozoic high-grade metamorphism. *Geoscience Frontiers* 5, 167-182.

Veevers J.J. and Saeed A. (2007) Central Antarctic provenance of Permian sandstones in Dronning Maud Land and the Karoo Basin: Integration of U–Pb and TDM ages and host-rock affinity from detrital zircons. *Sedimentary Geology* 202, p. 653–676.

FIGURE CAPTIONS.

Figure 1. Location of the study area in relation to the intersection of the EAO and Kuunga Orogenies in a Gondwana framework. The location of the study area in Antarctica is shown. The Gondwana configuration is modified after Meert (2003) and Daczko et al., (2018).

Figure 2. Map showing the location of $^{40}Ar/^{39}Ar$ samples described in this study from Kirwanveggan and Sverdrupfjella.

Figure 3. Photograph of sandstones and grits with cross bedding from the Urfjell Group at Drapane. The cross bedding is defined by oxide staining from oxidised iron oxides along the foresets .

Figure 4. Thin sections from Sverdrupfjella. Micrographs to show textures of all samples presented in this study. These samples include: (a) sample 008bD, an amphibolite sample from Fuglefjellet; (b) sample 012cG, a gneiss sample from Salknappen; (c) sample 017bD, an amphibolite sample from Vendeholten; (d) sample 032bC an amphibolite sample from Dyna; (e) 036, an amphibolite sample from Brattskarvet; 038bA, (f) a gneiss sample from Gordonnuten.

Figure 5. Thin sections from Kirwanveggan. (a) sample 92/14, a gneiss sample from Neumayerskarvet; (b) sample 92/35, a gneiss sample from Neumayerskarvet; (c) sample 93/41, a gneiss sample from Mjöllföykje; (d) sample 93/61, a gneiss sample from Skappelnabben; (e) 93/77, a gneiss sample from Enden; (f) sample 93/84, a gneiss sample from Hallgrenskarvet and (g) sample 93/89, a gneiss sample from Hallgrenskarvet, (h) UF/2 a quartz arenite from Drapane, Urfjell, Kirwanveggan.

Figure 6. Ar-Ar step heating profiles for hornblende and biotite from Sverdrupfjella.

Figure 7. Ar-Ar step heating profiles for hornblende and biotite from Sverdrupfjella and Kirwanveggan

Figure 8. Ar-Ar step heating profiles for hornblende and biotite from Kirwanveggan

Figure 9. Map showing the distribution of biotite ages from Sverdrupfjella and Kirwanveggan

Figure 10. Map showing the distribution of hornblende ages from Sverdrupfjella and Kirwanveggan.

Figure 11 SHRIMP zircon age data from (A) Urfjell Group (data from Croaker, 1999) (b) Kirwanveggan (c) Sverdrupfjella (d) Gjelsvikfjella (e) Central Dronning Maud Land (f) Sor Rondane. Data sources are shown in Table 6 in Grantham et al., (2019).

Figure 12.(top). Urfjell Nd_i-Sr_i data calculated at 530 Ma compared to data for basement gneisses from Kirwanveggan, Gjelsvikfjella, Sverdrupfjella, CDML and Sor Rondane (data from Croaker 1999; Grantham et al., 2011; Moyes et al., 1993, 1996; Moyes 1993; Paulsen and Austrheim, 2003; Grosch et al., 2007; Table 5, this study) (middle) εNd-εSr calculated at 490 Ma for granites and aplite veins from Sverdrupfjella and Gjelsvikfjella compared to data from the basement gneisses in Sverdrupfjella and Gjelsvikfjella. Data from Grantham et al., (1991), Moyes et al., (2003a,b), Paulsen and Austrheim (2003) and Table 5 this study. (bottom) εNd_t vs Age for granites and aplite veins from Sverdrupfjella and Gjelsvikfjella compared to data from the basement gneisses in Sverdrupfjella and Gjelsvikfjella. The T_{DM} curve is after Goldstein et

al., (1984). T_{DM} model ages are calculated after Ben Othman et. al (1984). The data demonstrate western Sverdrupfjella basement gneisses as a probable source for the ca. 490 Ma old granites but exclude the eastern Sverdrupfjella basement gneisses as a probable source.

Figure 13. Biotite ages from WDML showing location of Urfjell Group at Drapane. Data are from this study as well as from Jacobs et al., (1995), Jacobs et al., (1999) and Kleinschmidt et. al (2000). Note also the interpretation of the broader structure and tectonic units of WDML, Antarctica.

Figure 14. Hornblende ages from WDML. Data are from this study as well as from from Jacobs et al., (1995), Jacobs et al., (1999) and Kleinschmidt et. al (2000). Note also the interpretation of the broader structure and tectonic units of WDML, Antarctica.

Figure 15. Photographs of ~NW-SE oriented field exposures with annotated interpretations from Salknappen (top) and Skarsnuten (bottom) showing top-to-the-S-SE senses of shear involving both compressional and extensional senses of displacement along ca. 490 Ma old Dalmatian Granite veins (in red). In the Skarsnuten section, top-to-the-NW vergant D1-D2 isoclinals folds defined by anatectic granitic sheets are seen (in pale blue).

Figure 16. (a) Large scale interpretation of the regional structure of western and central Dronning Maud Land overlain on aeromagnetic data modified after Riedel et al., (2013). (b) Large scale interpretation of the regional structure of western and central Dronning Maud Land

overlain on inferred crustal thicknesses from aerogravity data modified after Riedel et al., (2012). The contours are from Riedel et al., (2012) and reflect thickness of crust estimates. The "teeth" on the thrust fault represent dip direction and dip beneath the hanging wall of the nappe complex overlying eastern Sverdrupfjella.

Figure 17. A simplified geological map of reconstructed Gondwana showing the various tectonic unit equivalents between southern Africa and Dronning Maud land Antarctic. The dashed line reflects the cross section line for the interpretive cross section shown in Figure 18.

Figure 18. Interpretive cross section from N. Mozambique to southern WDML, modified after Grantham et al., (2008). The map in Figure 17 reflects current positions of geological units and inferred structures.

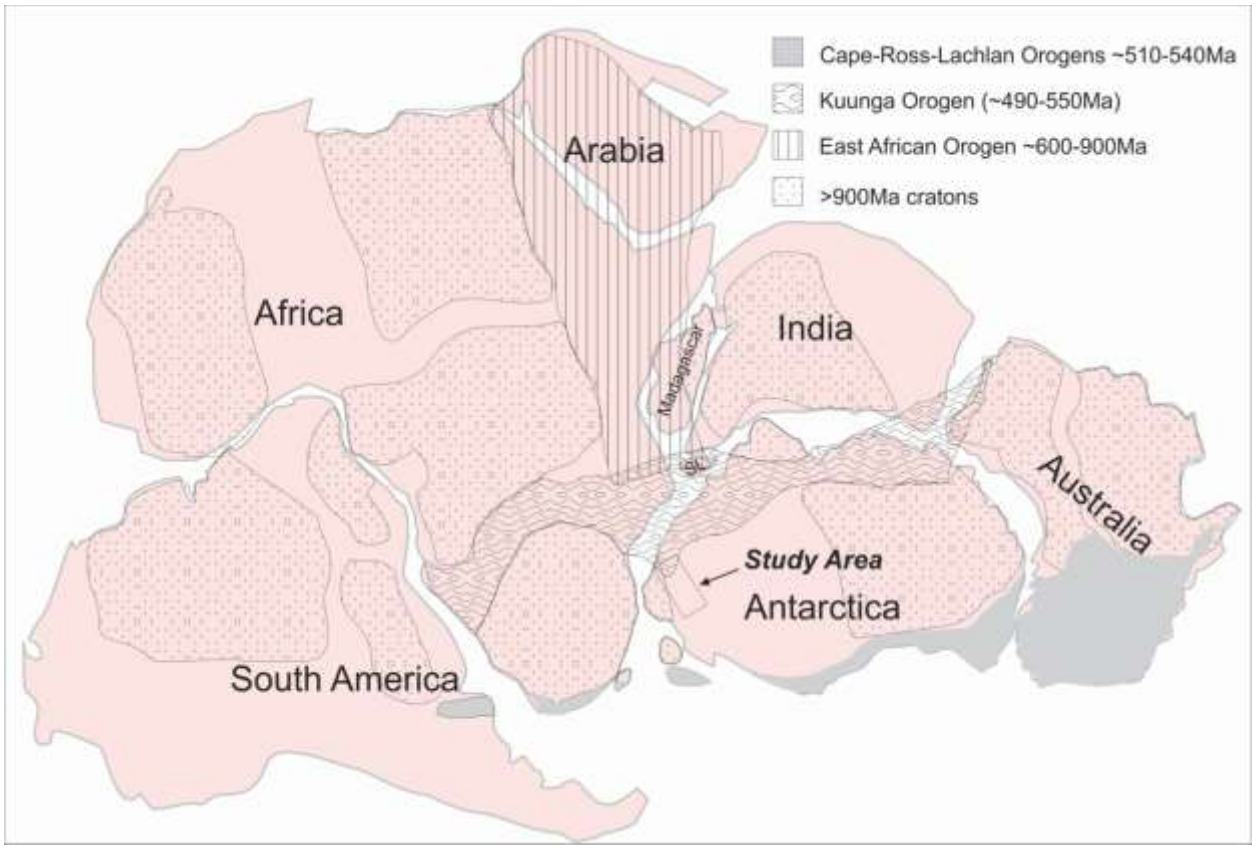
Cape-Ross-Lachlan Orogens ~510-540Ma
Kuunga Orogen (~490-550Ma)
East African Orogen ~600-900Ma
>900Ma cratons
Arabia
Africa
India
Madagascar
Australia
Study Area
Antarctica
South America
Fig 1.

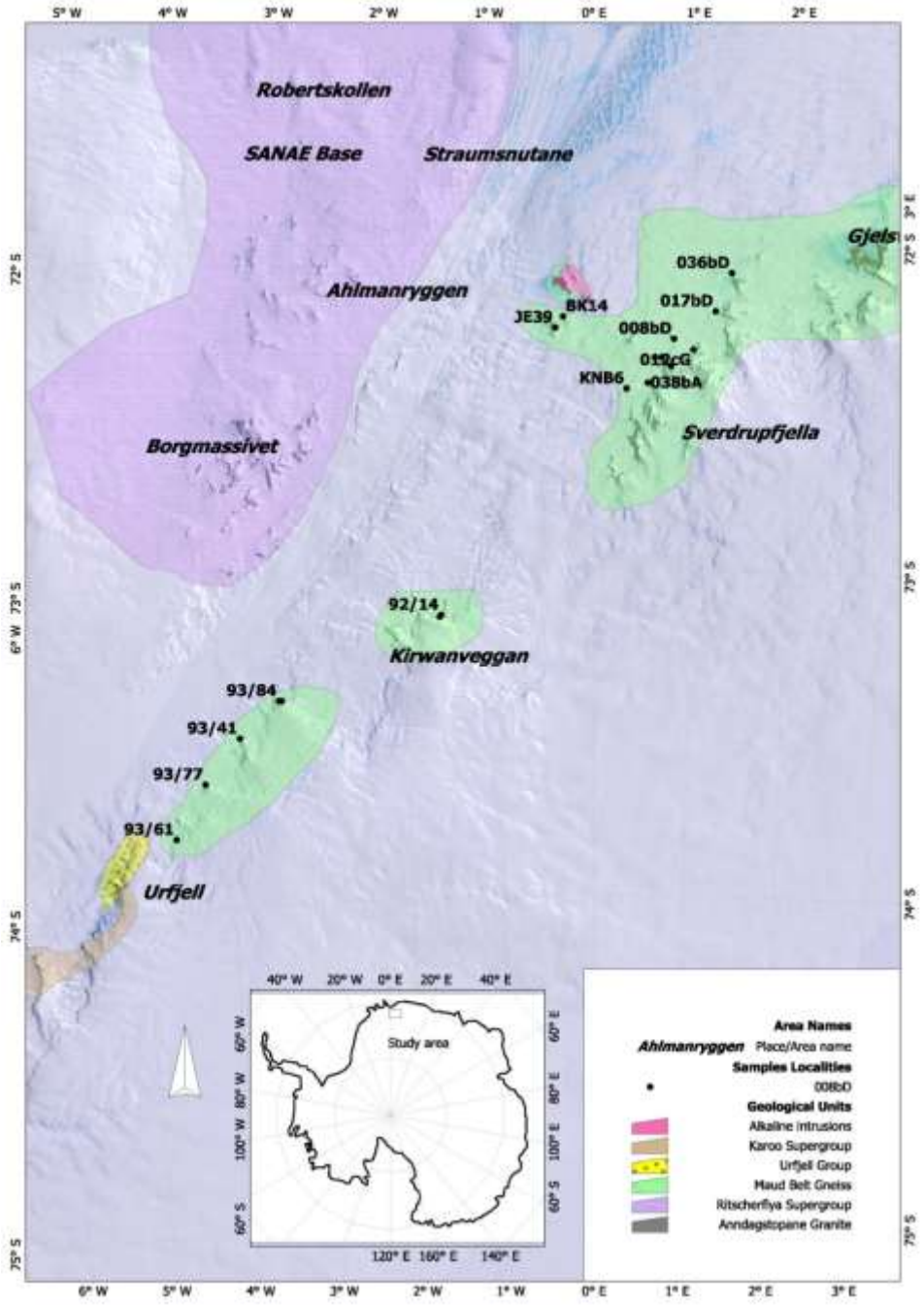
Robertskollen
SANAE Base
Straumsnutane
Gjelsvikfjella
Ahlmannryggen
036bD
017bD
BK14
JE39
008bD
KNB6
038bA
Sverdrupfjella
Borgmassivet
92/14
Kirwanveggan
93/84
93/41
93/77
93/61
Urfjell
Study area
Area Names
Ahlmannryggen Place/Area name
Samples Localities
008bD
Geological Units
Alkaline intrusions
Karoo Supergroup
Urfjell Group
Maud Belt Gneiss
Ritscherflya Supergroup
Anndalsstopane Granite

Fig.2

Fig 3.

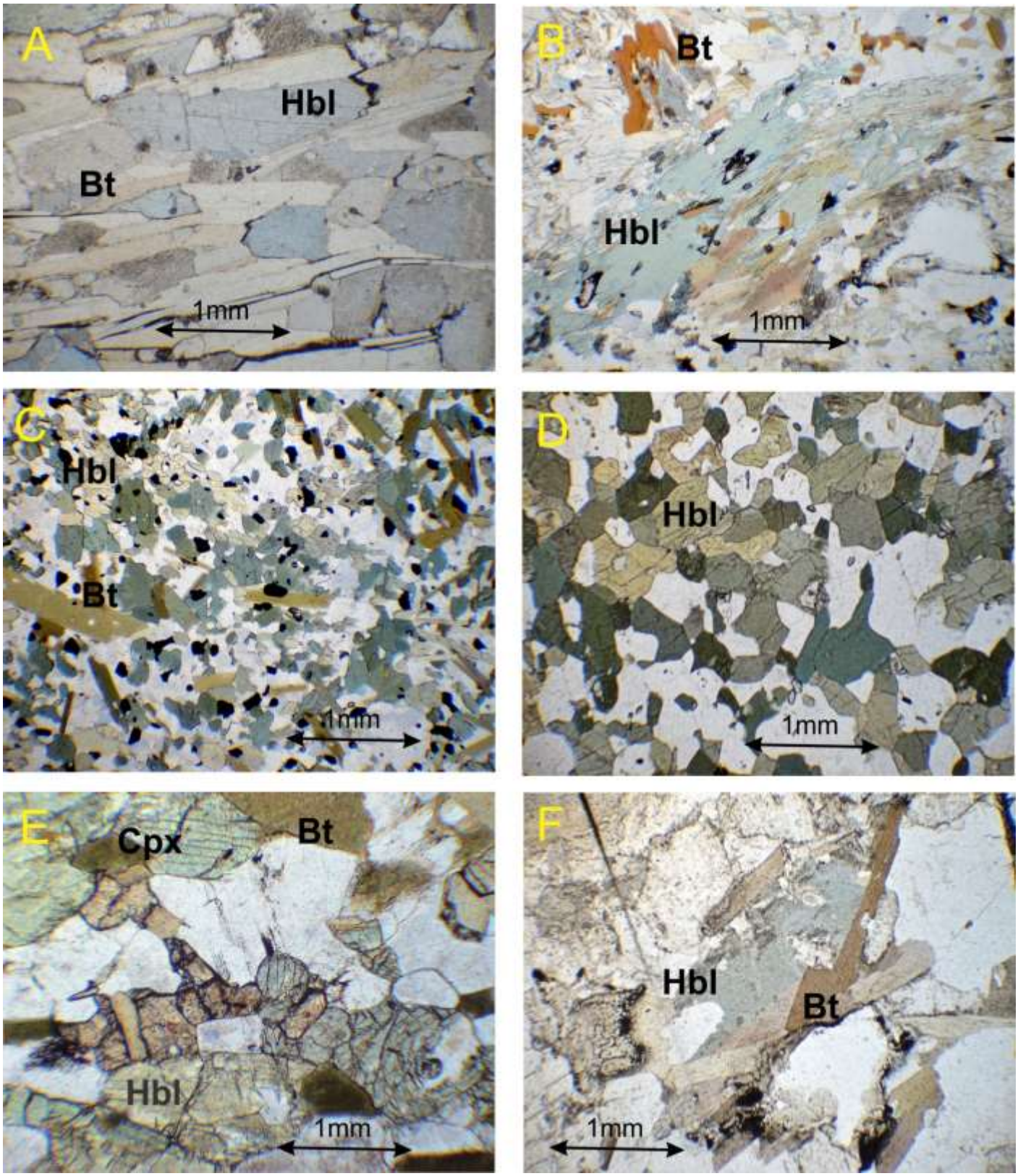
A
Hbl
Bt
1mm
B
Bt
Hbl
1mm
C
Hbl
Bt
1mm
D
Hbl
1mm
E
Cpx
Bt
Hbl
1mm
F
Hbl
Bt
1mm
Fig 4.

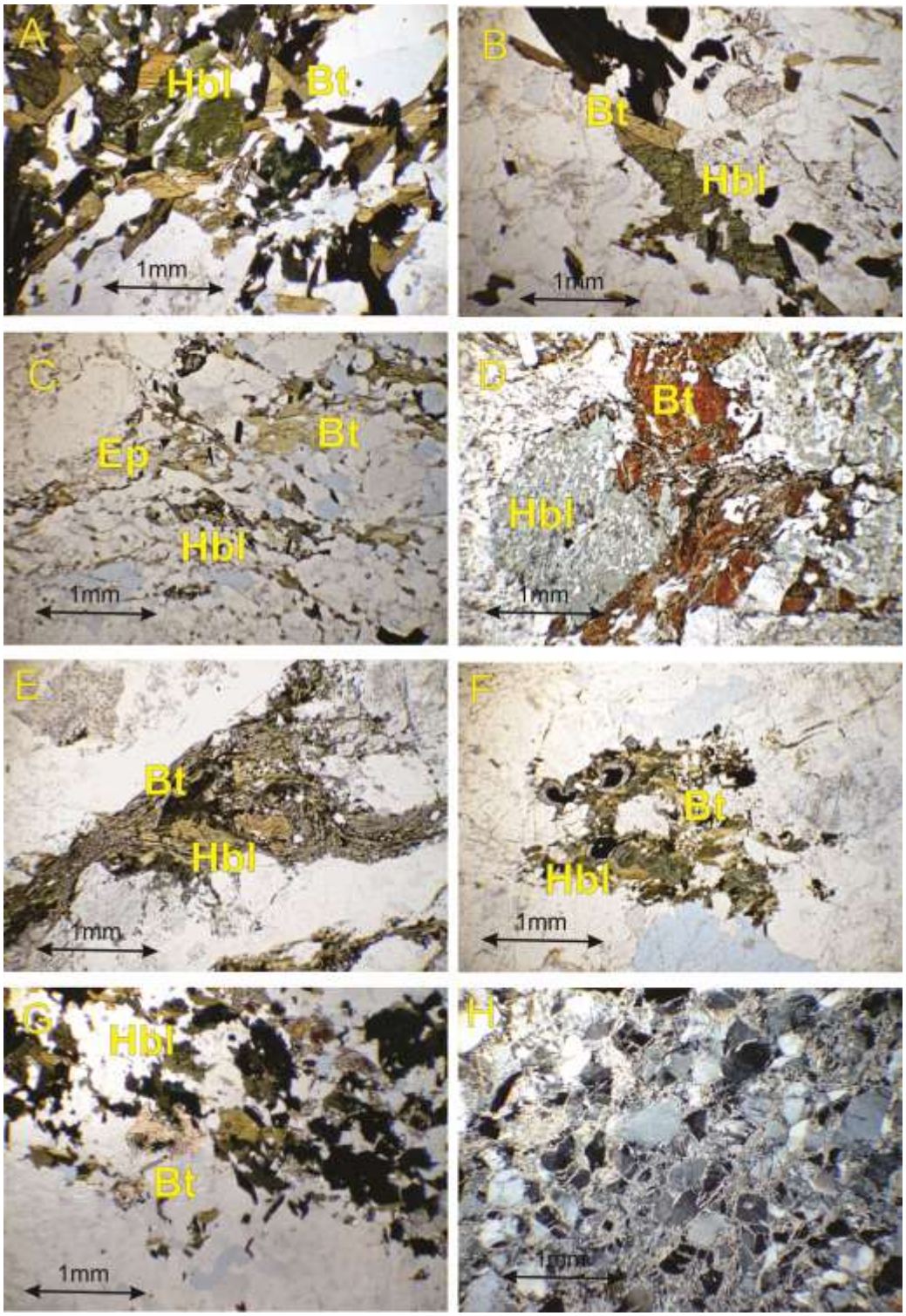
A
Hbl
Bt
1mm
B
Bt
Hbl
1mm
C
Ep
Bt
Hbl
1mm
D
Bt
Hbl
1mm
E
Bt
Hbl
1mm
F
Bt
Hbl
1mm
G
Hbl
Bt
1mm
H
1mm

Fig 5

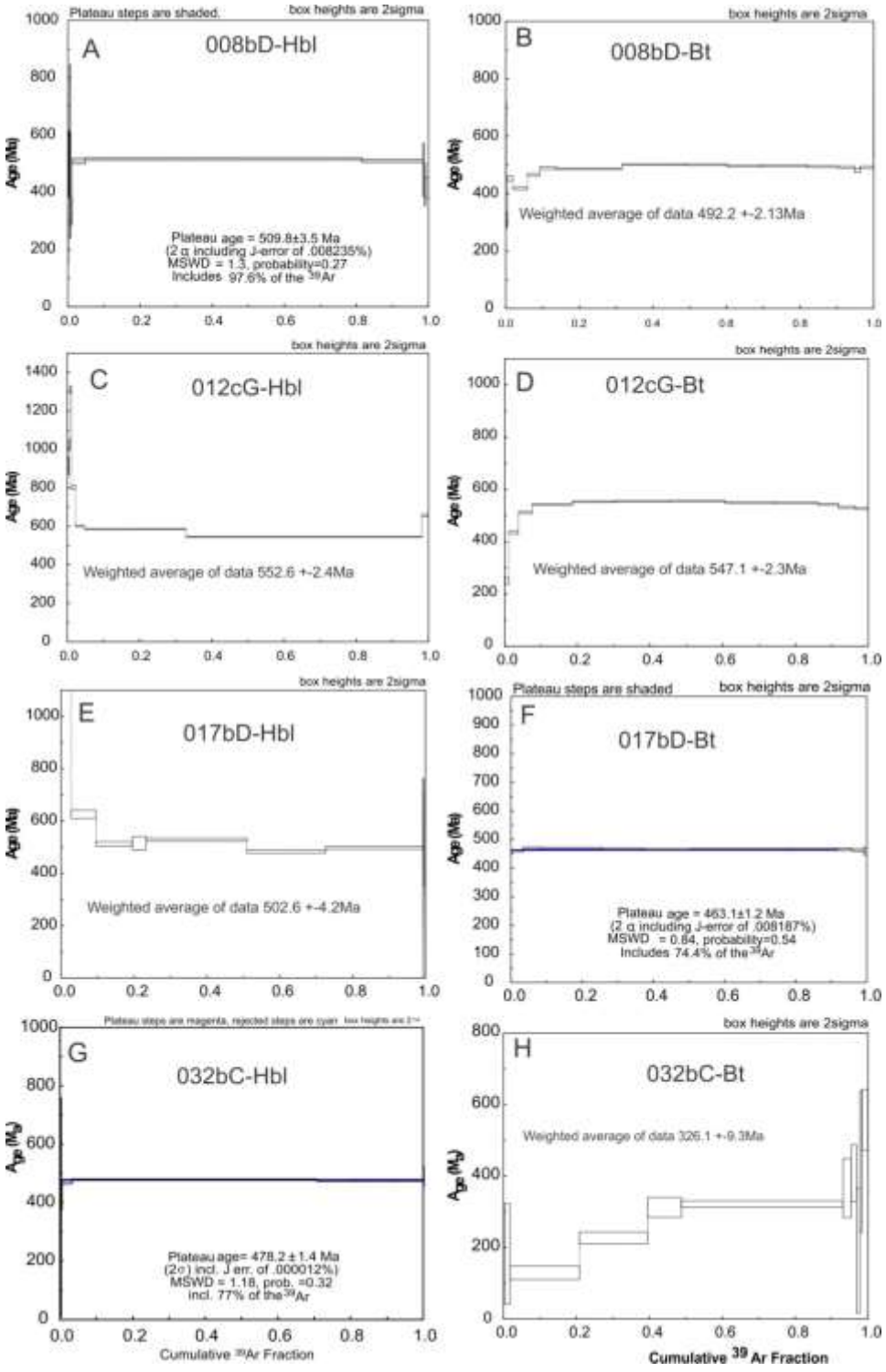
Plateau steps are shaded.
box heights are 2sigma
A
008bD-Hbl
Plateau age = 509.8±3.5 Ma
(2 σ including J-error of .008235%)
MSWD = 1.3, probability=0.27
Includes 97.6% of the 39Ar
B
008bD-Bt
Weighted average of data 492.2 +-2.13Ma
C
012cG-Hbl
Weighted average of data 552.6 +-2.4Ma
D
012cG-Bt
Weighted average of data 547.1 +-2.3Ma
E
017bD-Hbl
Weighted average of data 502.6 +-4.2Ma
Plateau steps are shaded
F
017bD-Bt
Plateau age = 463.1±1.2 Ma
(2 σ including J-error of .008187%)
MSWD = 0.84, probability=0.54
Includes 74.4% of the 39Ar
G
032bC-Hbl
Plateau age= 478.2 ± 1.4 Ma
(2σ) incl. J err. of .000012%)
MSWD = 1.18, prob. =0.32
incl. 77% of the 39Ar
H
032bC-Bt
Weighted average of data 326.1 +-9.3Ma
Age (Ma)
Cumulative 39Ar Fraction

Fig. 6

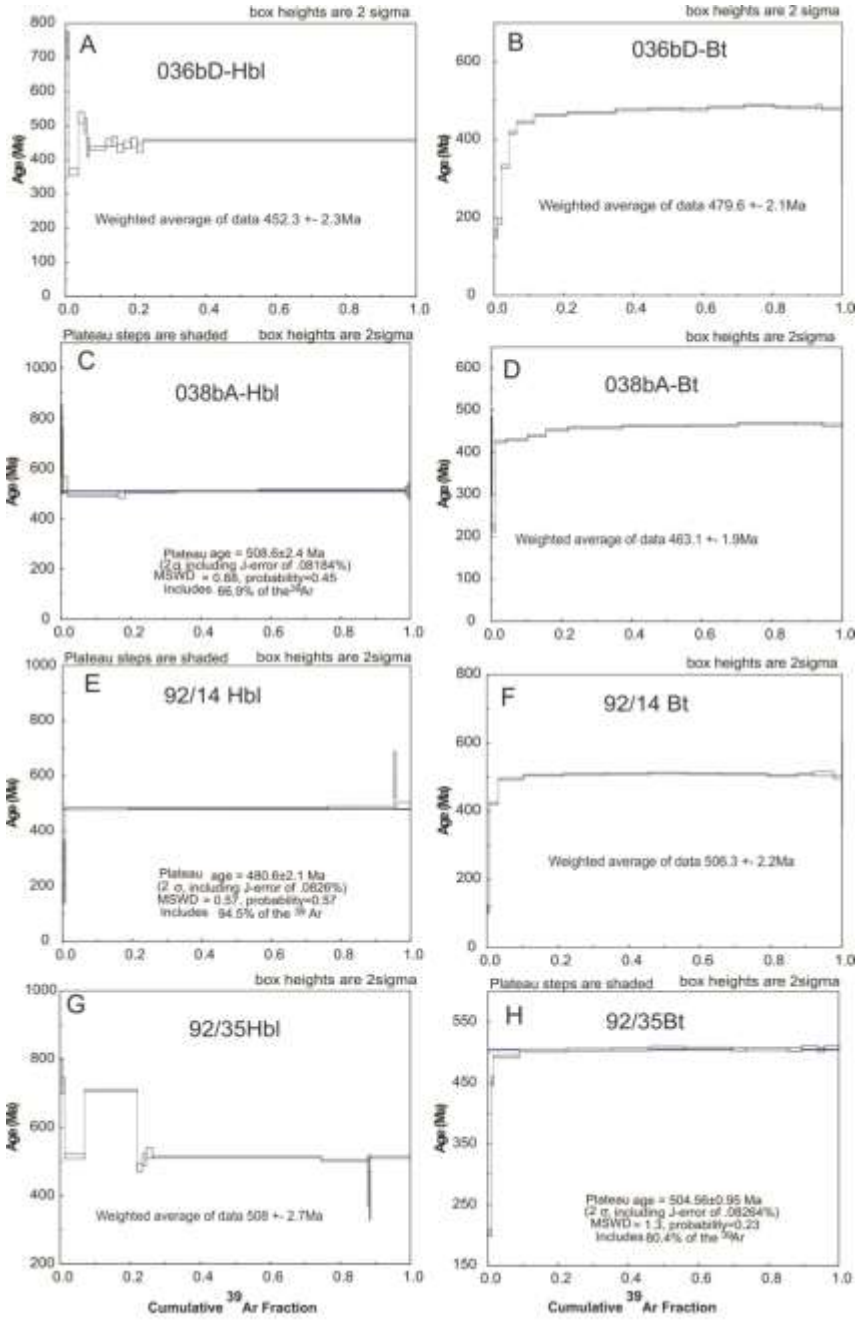
box heights are 2 sigma
A
036bD-Hbl
Weighted average of data 452.3 +- 2.3Ma
B
036bD-Bt
Weighted average of data 479.6 +- 2.1Ma
Plateau steps are shaded
box heights are 2sigma
C
038bA-Hbl
Plateau age = 508.6±2.4 Ma
(2 σ, including J-error of .08184%)
MSWD = 0.88, probability=0.45
Includes 66.9% of the 39Ar
D
038bA-Bt
Weighted average of data 463.1 +- 1.9Ma
E
92/14 Hbl
Plateau age = 480.6±2.1 Ma
(2 σ, including J-error of .0826%)
MSWD = 0.57, probability=0.57
Includes 94.5% of the 39 Ar
F
92/14 Bt
Weighted average of data 506.3 +- 2.2Ma
G
92/35Hbl
Weighted average of data 508 +- 2.7Ma
H
92/35Bt
Plateau age = 504.56±0.95 Ma
(2 σ, including J-error of .08264%)
MSWD = 1.3, probability=0.23
Includes 80.4% of the 39Ar
Age (Ma)
Cumulative 39 Ar Fraction

Fig. 7

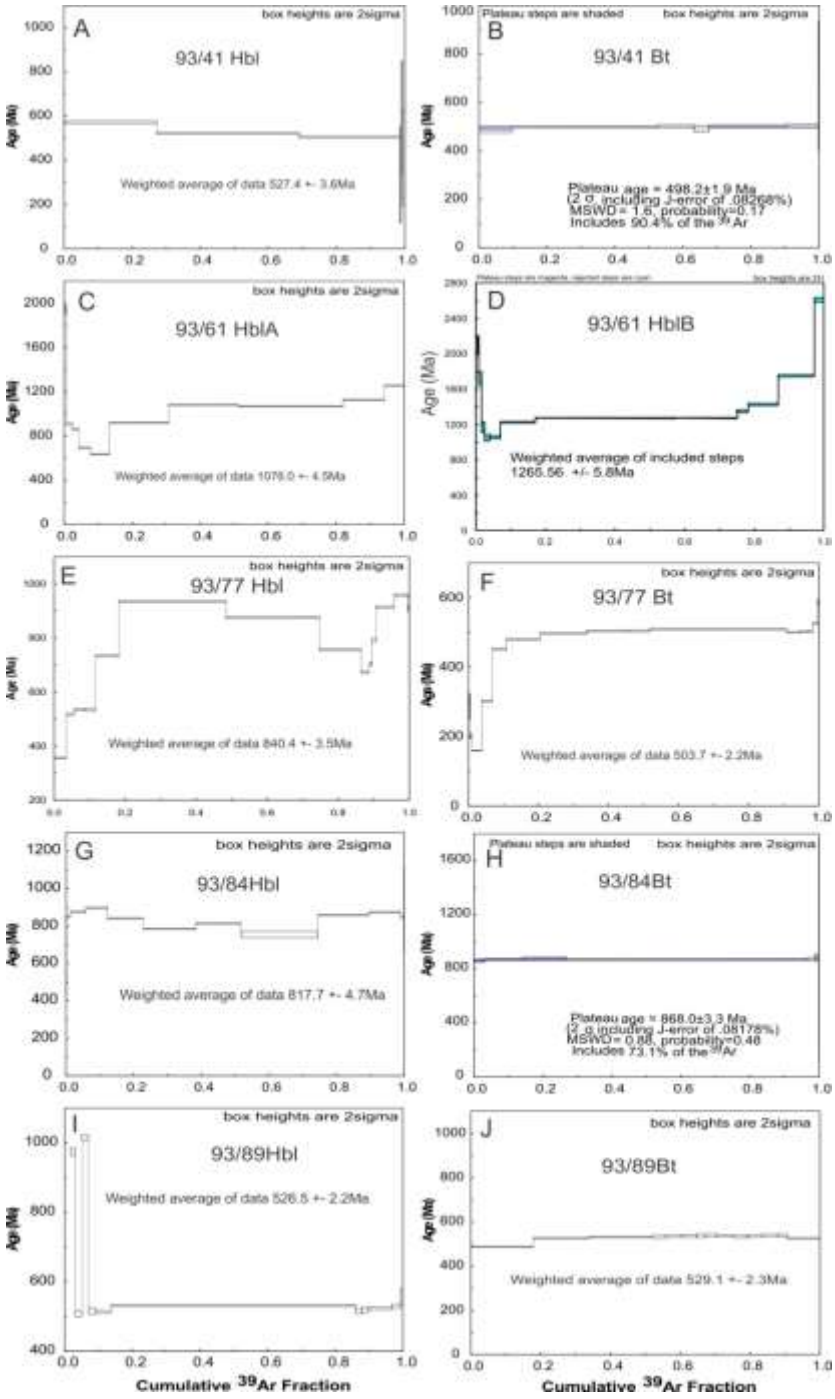
A
93/41 Hbl
box heights are 2sigma
Weighted average of data 527.4 +- 3.6Ma
B
93/41 Bt
Plateau steps are shaded
box heights are 2sigma
Plateau age = 498.2±1.9 Ma
(2 σ, including J-error of .08268%)
MSWD = 1.6, probability=0.17
Includes 90.4% of the 39Ar
C
93/61 HblA
box heights are 2sigma
Weighted average of data 1078.0 +- 4.5Ma
D
93/61 HblB
Age (Ma)
Weighted average of included steps
1265.56 +/- 5.8Ma
E
93/77 Hbl
box heights are 2sigma
Weighted average of data 840.4 +- 3.5Ma
F
93/77 Bt
box heights are 2sigma
Weighted average of data 503.7 +- 2.2Ma
G
93/84Hbl
box heights are 2sigma
Weighted average of data 817.7 +- 4.7Ma
H
93/84Bt
Plateau steps are shaded
box heights are 2sigma
Plateau age = 868.0±3.3 Ma
(2 σ, including J-error of .08178%)
MSWD = 0.88, probability=0.46
Includes 73.1% of the 39Ar
I
93/89Hbl
box heights are 2sigma
Weighted average of data 526.5 +- 2.2Ma
J
93/89Bt
box heights are 2sigma
Weighted average of data 529.1 +- 2.3Ma
Age (Ma)
Cumulative 39Ar Fraction
Cumulative 39Ar Fraction

Fig. 8

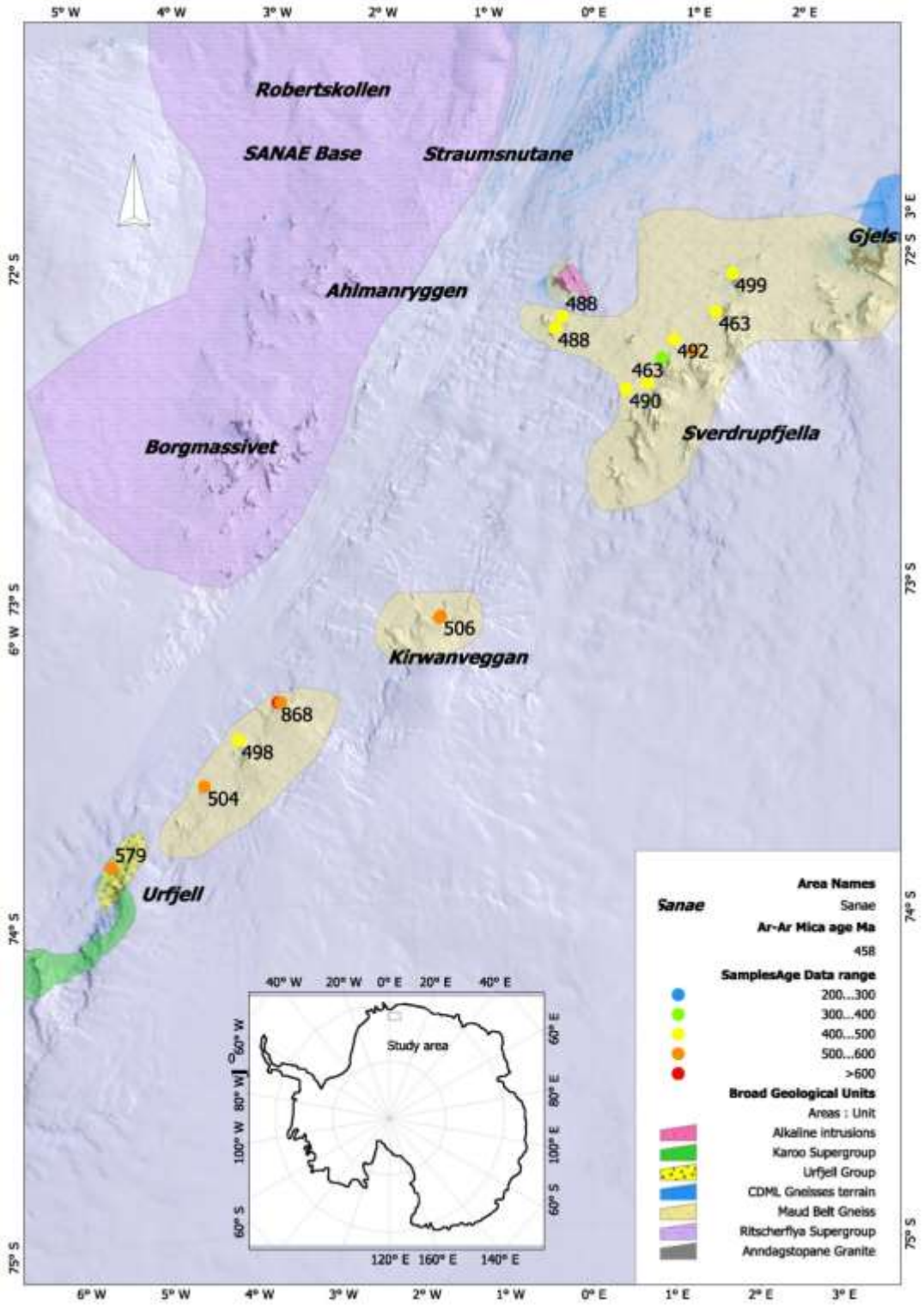
Robertskollen
SANAE Base
Straumsnutane
Ahlmanryggen
Borgmassivet
Gjelsvikfjella
Sverdrupfjella
Kirwanveggan
Urfjell
488
488
499
463
492
463
490
506
868
498
504
579
Area Names
Sanae
Sanae
Ar-Ar Mica age Ma
458
SamplesAge Data range
200...300
300...400
400...500
500...600
>600
Broad Geological Units
Areas : Unit
Alkaline intrusions
Karoo Supergroup
Urfjell Group
CDML Gneisses terrain
Maud Belt Gneiss
Ritscherflya Supergroup
Anndagstopane Granite
Study area
5° W
4° W
3° W
2° W
1° W
0° E
1° E
2° E
3° E
72° S
73° S
74° S
75° S
6° W
40° W
20° W
0° E
20° E
40° E
60° W
80° W
100° W
120° W
60° E
80° E
100° E
120° E
140° E
160° E
60° S

Fig 9

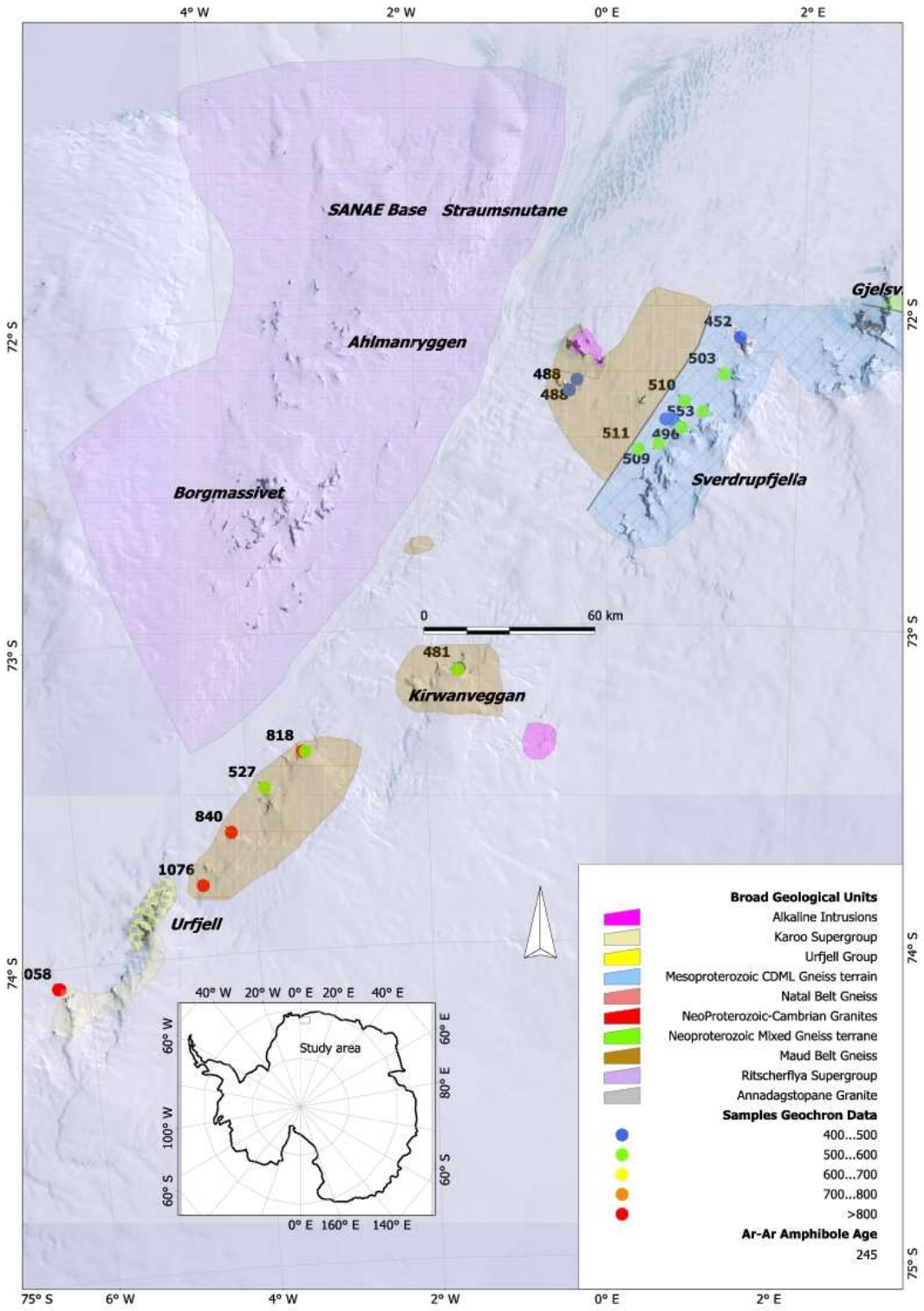
4° W
2° W
0° E
2° E
72° S
73° S
74° S
75° S
6° W
SANAE Base
Straumsnutane
Ahlmanryggen
Borgmassivet
Gjelsv
Sverdrupfjella
Kirwanveggan
Urfjell
452
503
488
488
510
553
511
496
509
481
818
527
840
1076
058
0
60 km
Broad Geological Units
Alkaline Intrusions
Karoo Supergroup
Urfjell Group
Mesoproterozoic CDML Gneiss terrain
Natal Belt Gneiss
NeoProterozoic-Cambrian Granites
Neoproterozoic Mixed Gneiss terrane
Maud Belt Gneiss
Ritscherflya Supergroup
Annadagstopane Granite
Samples Geochron Data
400...500
500...600
600...700
700...800
>800
Ar-Ar Amphibole Age
245
40° W
20° W
0° E
20° E
40° E
60° W
100° W
60° S
80° E
60° E
0° E
160° E
140° E
Study area

Fig 10.

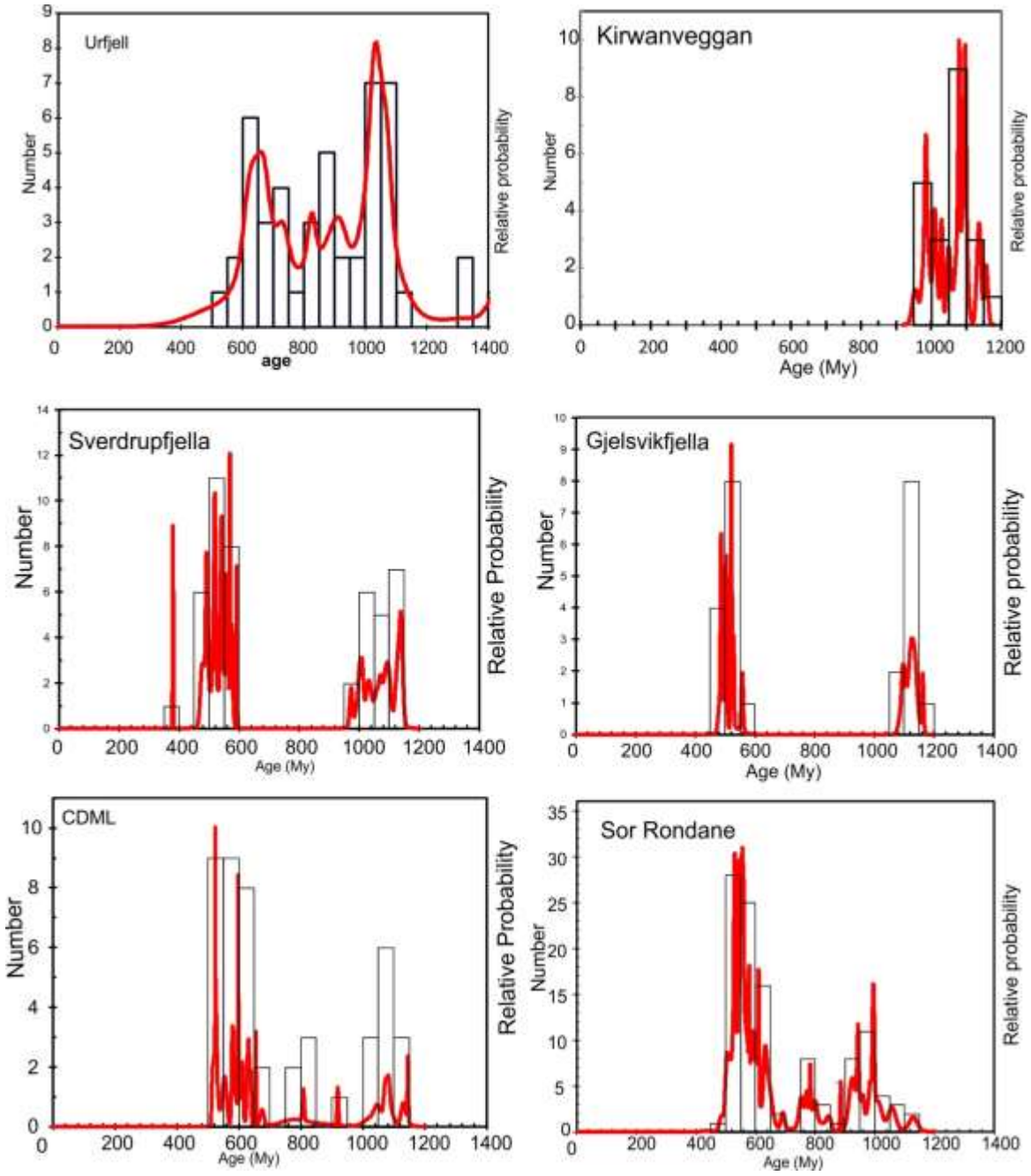
Urfjell
Number
Relative probability
age
Kirwanveggan
Number
Relative probability
Age (My)
Sverdrupfjella
Number
Relative Probability
Age (My)
Gjelsvikfjella
Number
Relative probability
Age (My)
CDML
Number
Relative Probability
Age (My)
Sor Rondane
Number
Relative probability
Age (My)

Fig. 11

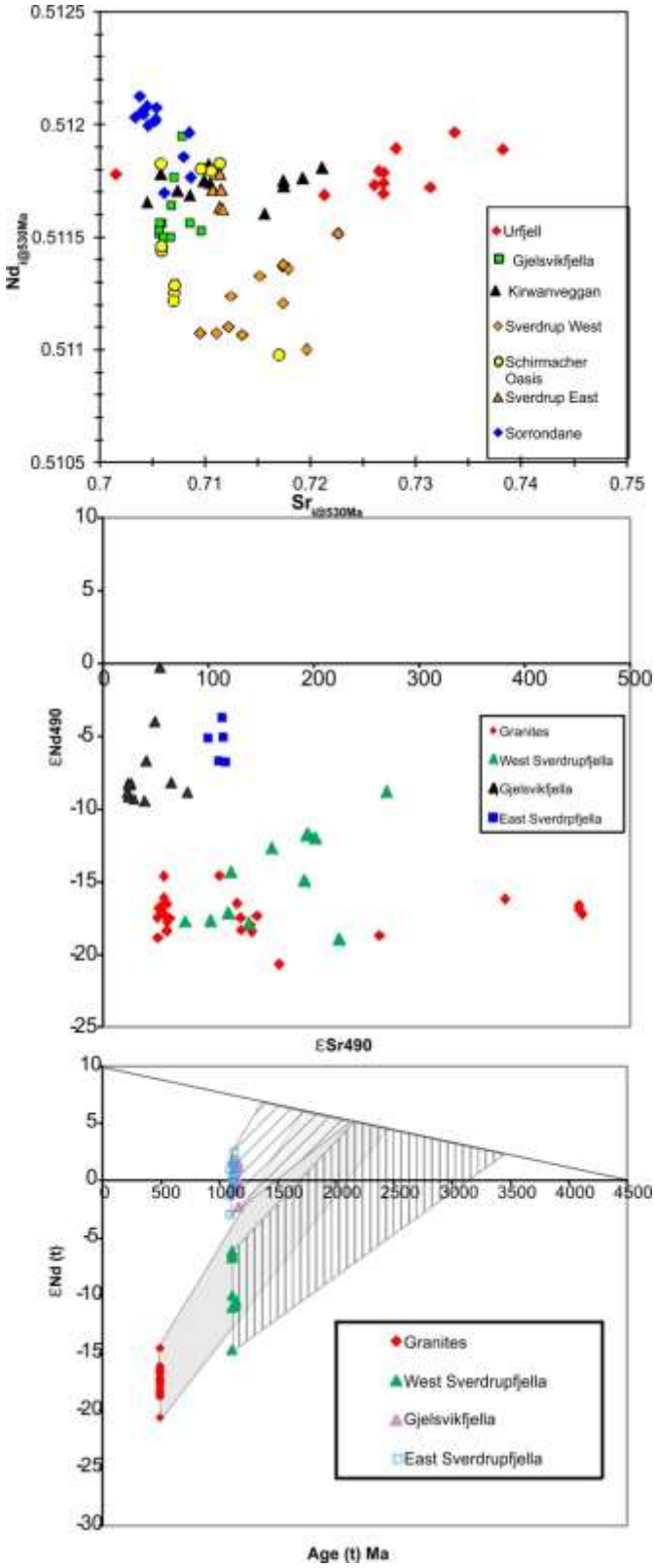
0.5125
0.512
0.5115
0.511
0.5105
0.7
0.71
0.72
0.73
0.74
0.75
Urfjell
Gjelsvikfjella
Kirwanveggan
Sverdrup West
Schirmacher Oasis
Sverdrup East
Sorrondane
10
5
0
-5
-10
-15
-20
-25
0
100
200
300
400
500
εNd490
εSr490
Granites
West Sverdrupfjella
Gjelsvikfjella
East Sverdrpfjella
10
5
0
-5
-10
-15
-20
-25
-30
0
500
1000
1500
2000
2500
3000
3500
4000
4500
εNd (t)
Granites
West Sverdrupfjella
Gjelsvikfjella
East Sverdrupfjella
Age (t) Ma

Fig. 12

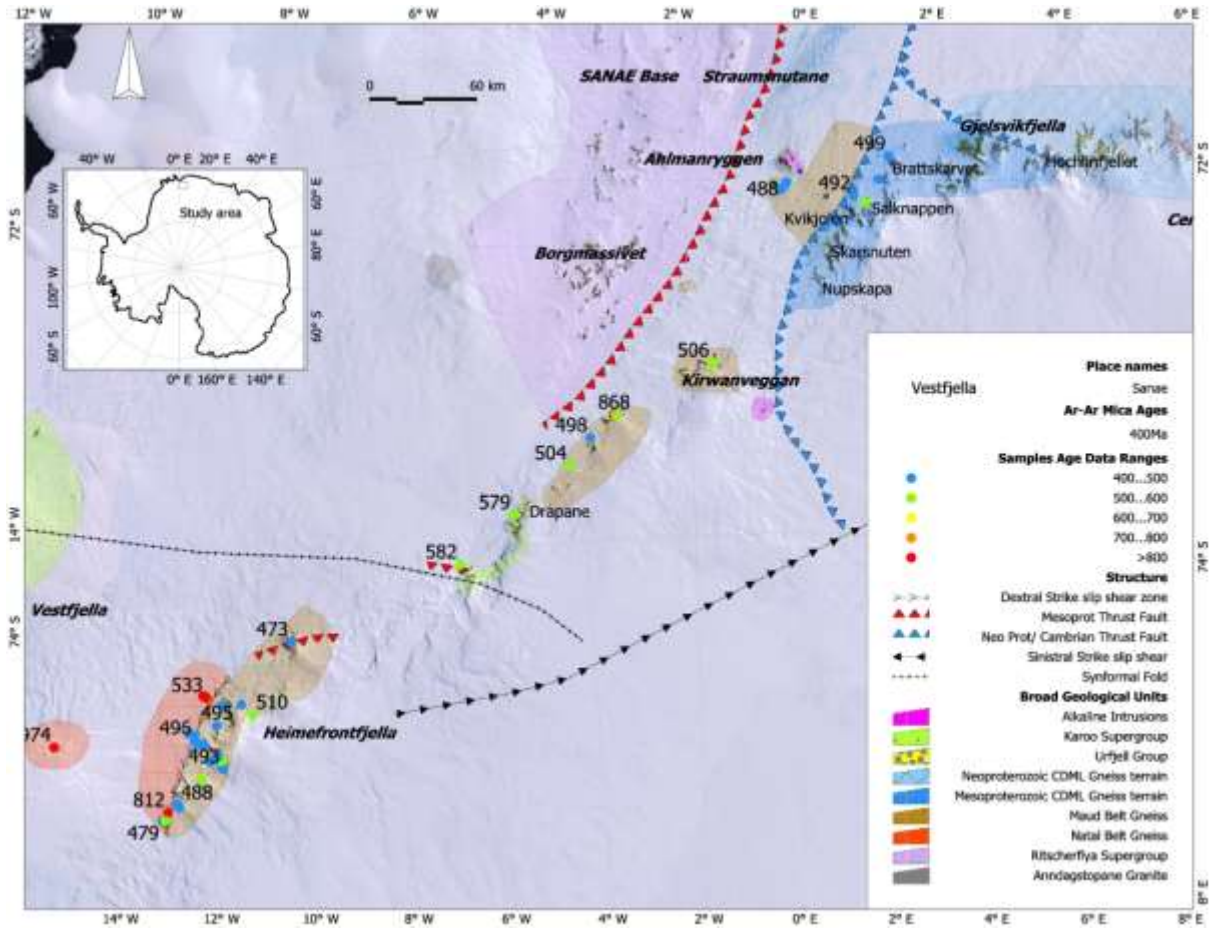
SANAE Base
Straumsnutane
Ahlmannryggen
Gjelsvikfjella
Borgmassivet
Kirwanveggan
Vestfjella
Heimefrontfjella
Drapane
Brattskarvet
Hochlinfjellet
Kvikjokken
Falknappen
Skarsnuten
Nupskapa
Study area
0 60 km
Vestfjella
Place names
Sanae
Ar-Ar Mica Ages
400Ma
Samples Age Data Ranges
400...500
500...600
600...700
700...800
>800
Structure
Dextral Strike slip shear zone
Mesoprot Thrust Fault
Neo Prot/ Cambrian Thrust Fault
Sinistral Strike slip shear
Synformal Fold
Broad Geological Units
Alkaline Intrusions
Karoo Supergroup
Urfjell Group
Neoproterozoic CDML Gneiss terrain
Mesoproterozoic CDML Gneiss terrain
Maud Belt Gneiss
Natal Belt Gneiss
Ritscherflya Supergroup
Anndagstopane Granite
Fig. 13

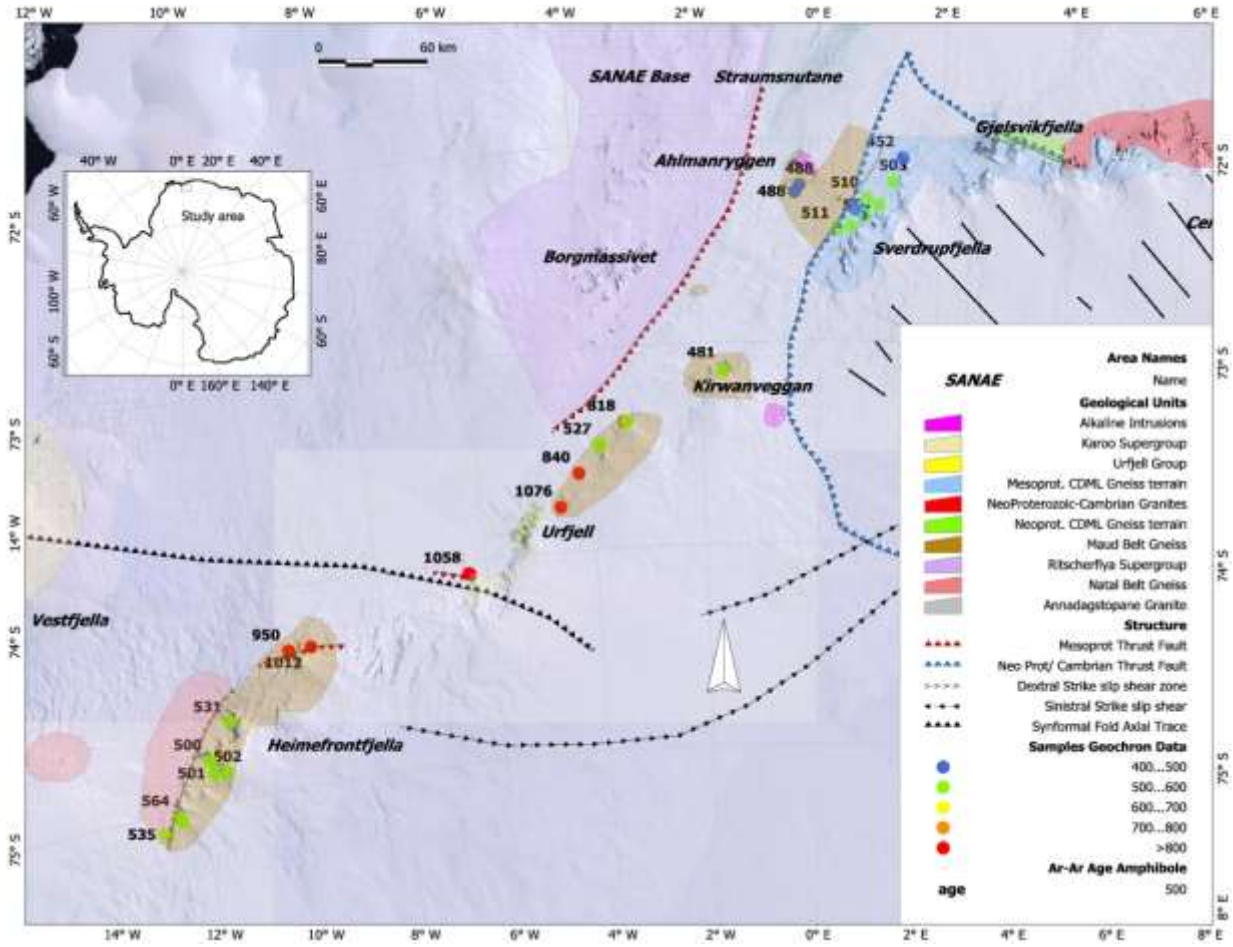
SANAE Base
Straumsnutane
Gjelsvikfjella
Ahlmannryggen
Borgmassivet
Sverdrupfjella
Kirwanveggan
Urfjell
Vestfjella
Heimefrontfjella
Study area
0 60 km
452
503
488
488
510
511
481
818
527
840
1076
1058
950
1012
531
500
502
501
564
535
Area Names
SANAE
Name
Geological Units
Alkaline Intrusions
Karoo Supergroup
Urfjell Group
Mesoprot. CDML Gneiss terrain
NeoProterozoic-Cambrian Granites
Neoprot. CDML Gneiss terrain
Maud Belt Gneiss
Ritscherflya Supergroup
Natal Belt Gneiss
Annadagstopane Granite
Structure
Mesoprot Thrust Fault
Neo Prot/ Cambrian Thrust Fault
Dextral Strike slip shear zone
Sinistral Strike slip shear
Synformal Fold Axial Trace
Samples Geochron Data
400...500
500...600
600...700
700...800
>800
Ar-Ar Age Amphibole
age
500

Fig. 14

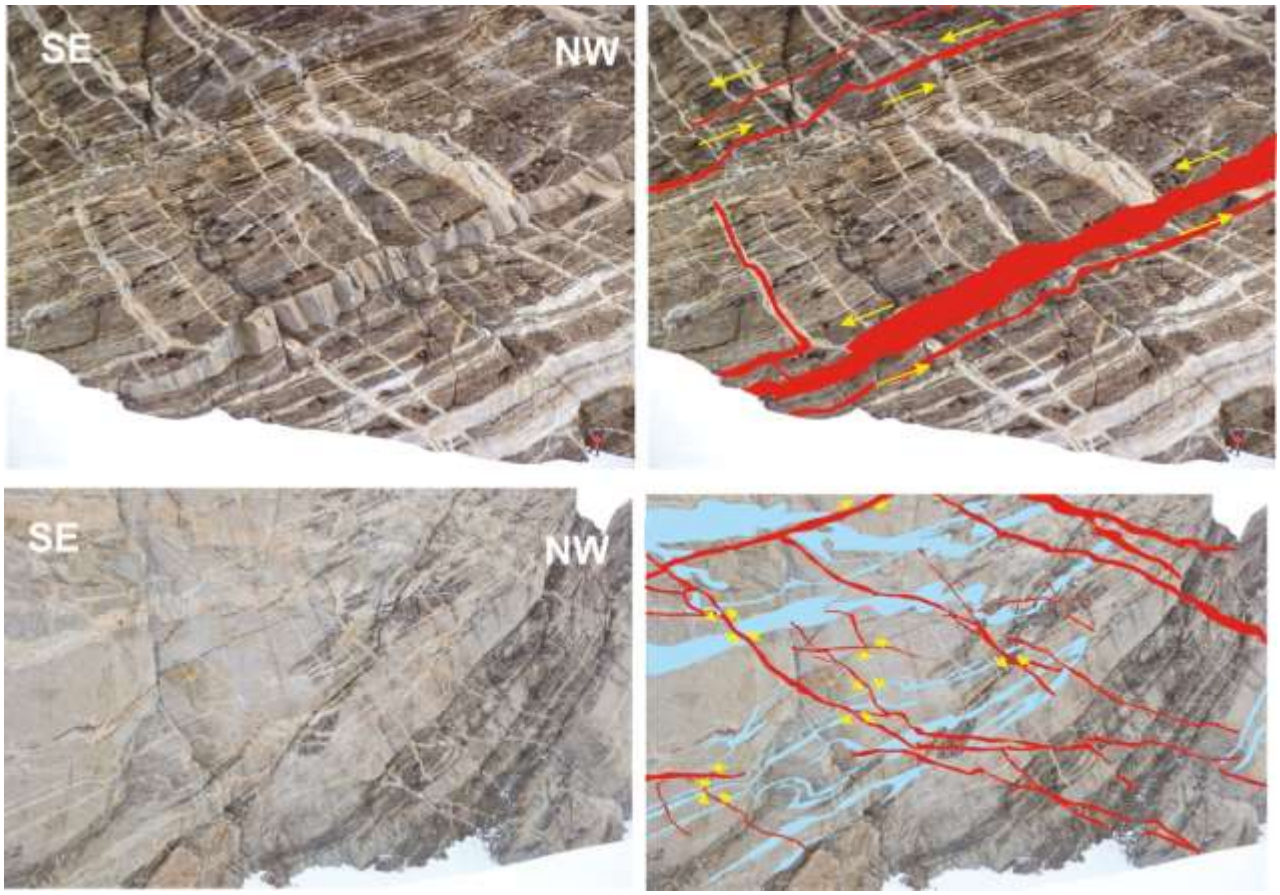

Fig 15.

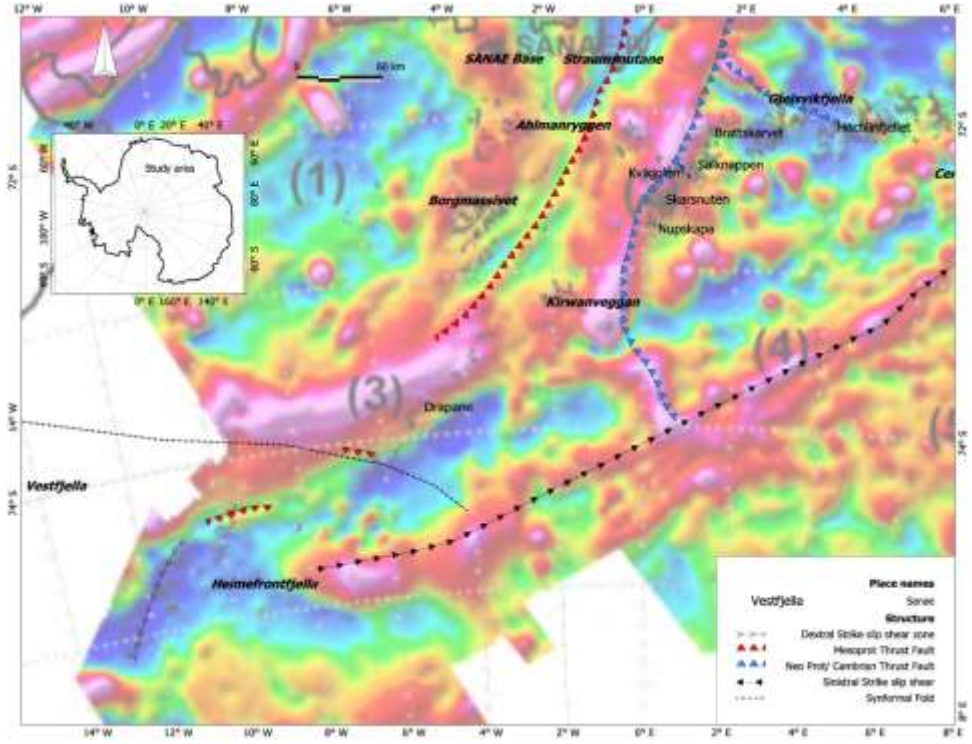

Fig 16a

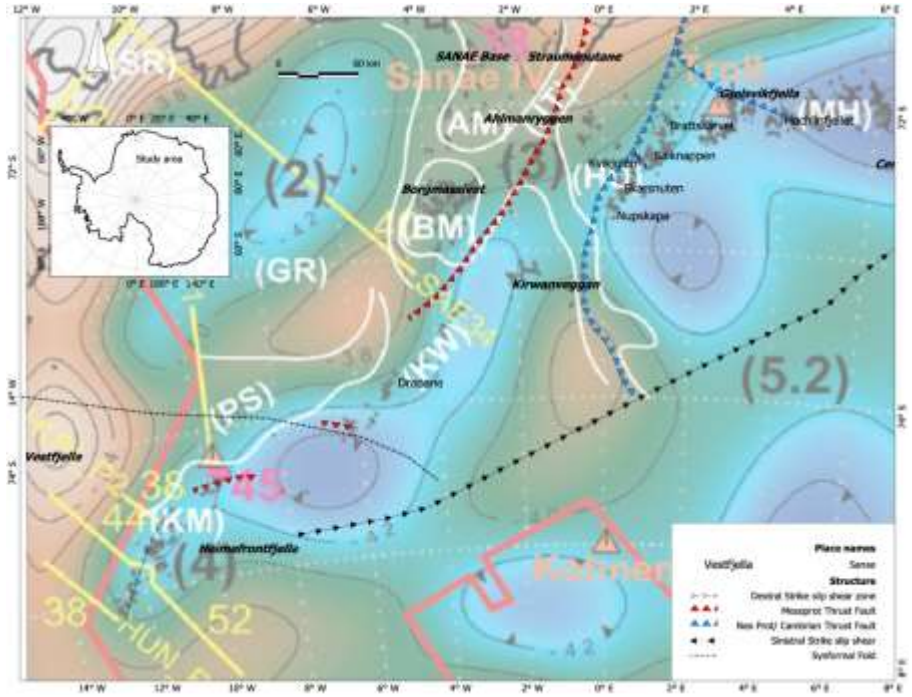

Fig 16 b

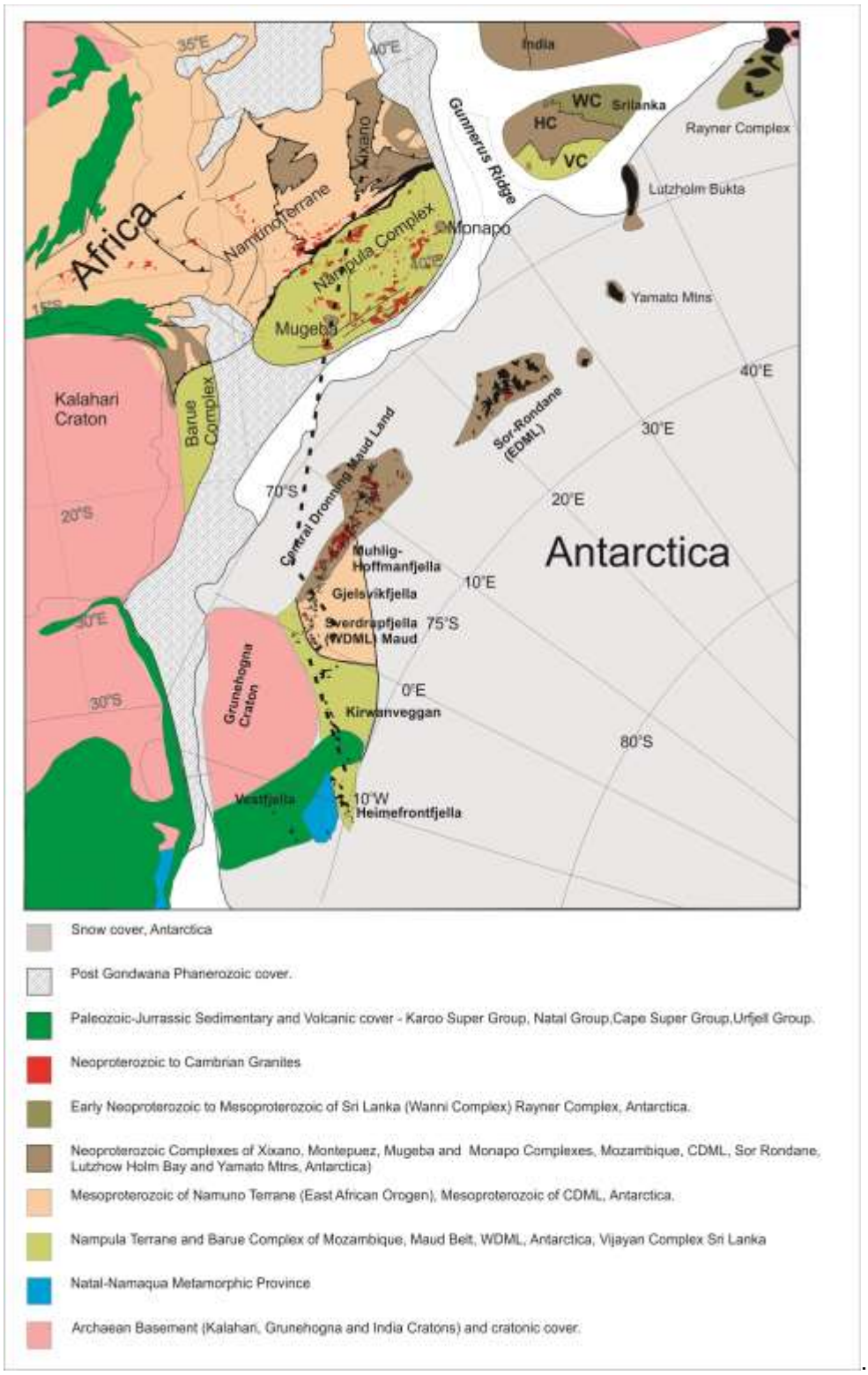
India
WC
Srilanka
HC
VC
Rayner Complex
Gunnerus Ridge
Lutzholm Bukta
Africa
Namuno Terrane
Xixano
Nampula Complex
Monapo
Mugeba
Yamato Mtns
Kalahari Craton
Barue Complex
Sor-Rondane (EDML)
Central Dronning Maud Land
Muhlig-Hoffmanfjella
Gjelsvikfjella
Sverdrupfjella (WDML) Maud
Grunehogna Craton
Kirwanveggan
Vestfjella
Heimefrontfjella
Antarctica
35°E
40°E
30°E
20°E
10°E
0°E
10°W
20°S
30°S
70°S
75°S
80°S
Snow cover, Antarctica
Post Gondwana Phanerozoic cover.
Paleozoic-Jurrassic Sedimentary and Volcanic cover - Karoo Super Group, Natal Group,Cape Super Group,Urfjell Group.
Neoproterozoic to Cambrian Granites
Early Neoproterozoic to Mesoproterozoic of Sri Lanka (Wanni Complex) Rayner Complex, Antarctica.
Neoproterozoic Complexes of Xixano, Montepuez, Mugeba and Monapo Complexes, Mozambique, CDML, Sor Rondane, Lutzhow Holm Bay and Yamato Mtns, Antarctica)
Mesoproterozoic of Namuno Terrane (East African Orogen), Mesoproterozoic of CDML, Antarctica.
Nampula Terrane and Barue Complex of Mozambique, Maud Belt, WDML, Antarctica, Vijayan Complex Sri Lanka
Natal-Namaqua Metamorphic Province
Archaean Basement (Kalahari, Grunehogna and India Cratons) and cratonic cover.

Fig. 17

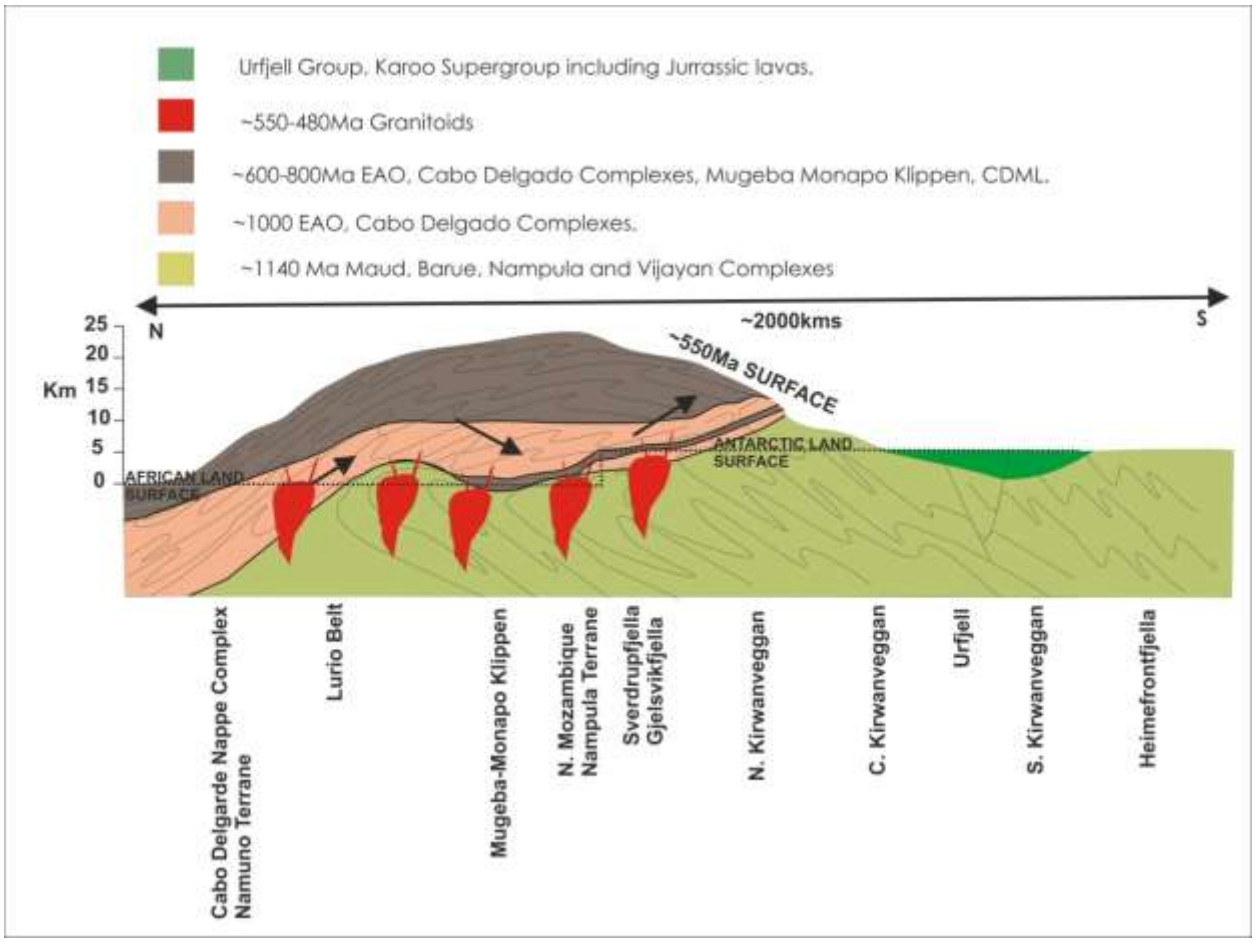
Urfjell Group, Karoo Supergroup including Jurrassic lavas.
~550-480Ma Granitoids
~600-800Ma EAO, Cabo Delgado Complexes, Mugeba Monapo Klippen, CDML.
~1000 EAO, Cabo Delgado Complexes.
~1140 Ma Maud, Barue, Nampula and Vijayan Complexes
N
~2000kms
S
Km
25
20
15
10
5
0
~550Ma SURFACE
AFRICAN LAND SURFACE
ANTARCTIC LAND SURFACE
Cabo Delgarde Nappe Complex
Namuno Terrane
Lurio Belt
Mugeba-Monapo Klippen
N. Mozambique
Nampula Terrane
Sverdrupfjella
Gjelsvikfjella
N. Kirwanveggan
C. Kirwanveggan
Urfjell
S. Kirwanveggan
Heimefrontfjella

Fig 18.

Sample No.	Area	Bt	Hbl	Cpx	Fsp	Qtz	Opaques	Garnet	Epidote	TTn	Chl
036bD	Svdf	20	25	15	30	5	5				
017bD	Svdf	15	30		40	10	5				
008bD	Svdf	40	45		8	2	5				
012cG	Svdf	35	25		30	10	5		tr		
032bC	Svdf		45		40	10	tr		tr		
038bA	Svdf	15	30		45	10					
92/14	Kwgn	25	25		20	25	5				
92/35	Kwgn	15	10		45	25	2	3			
93/84	Kwgn	10	20		40	25	3			2	
93/89	Kwgn	15	20		35	20	5	3		2	
93/41	Kwgn	10	5		45	30	5				
93/77	Kwgn	10	5		40	35	2		3		5
93/61	Kwgn	10	20	5	35	25	2		1		

Table 1. Table summarising the mineralogy of the samples with biotite- hornblende pairs. Samples are arranged from north (top) to south (bottom). Svdf=Sverdrupfjella. Kwgn=Kirwanveggan.

Sample	Amphibole Age	Biotite Age	Rock Type	Location
008bD	509.8 ±-4.3	492.2 ±2.1	Amphibolite	Fuglefjellet, Sverdrupfjella
012cG	552.6 ±2.4	547.1 ±2.3	Garnet gneiss	Salknappen, Sverdrupfjella
017bD	502.6 ±4.2	463.1 ±2.6	Amphibolite	Vendeholten, Sverdrupfjella
032bC	468.3 ±1.5	326.1 ±9.3	Amphibolite	Dyna, Sverdrupfjella
036bD	452.7 ± 2.3	499.4 ±2.73 479.6 ± 1.9	Amphibolite	Brattskarvet, Sverdrupfjella
038bA	508.6 ±2.4	463.1 ±1.2	Gneiss	Gordonnuten, Sverdrupfjella
92/14	480.6 ±2.1	506.3 ± 2.2	Gneiss	Neumayerskarvet, Kirwanveggan
92/35	508.0 ±2.7	504.6 ± 1.00	Gneiss	Neumayerskarvet, Kirwanveggan
93/41	527.4 ±3.6	498.2 ±1.9	Gneiss	Mjöllföykje, Kirwanveggan
93/61	1265.6 ± 5.8 1076.5 ± 4.5	No data	Gneiss	Skappelnabben, Kirwanveggan
93/77	840.4 ±3.5	503.7 ±2.2	Gneiss	Enden, Kirwanveggan
93/84	817.7 ± 4.7	868 ± 3.3	Gneiss	Hallgrenskarvet, Kirwanveggan
93/89	526.5 ±2.2	529.1 ±2.4	Gneiss	Hallgrenskarvet, Kirwanveggan

Table 2. Summary of ages from the various samples from Sverdrupfjella and Kirwanveggan.

Area	Sample no.	Hbl age	Bt age	difference	Cooling rate °C per My	Erosion rate equivalent @ 25°C/km in mm/yr
Sverdrupfjella	008bD	509.8	492.2	17.6	11.4	0.45
Sverdrupfjella	012cG	552.6	547.1	5.5	36.4	1.45
Sverdrupfjella	017bd	502.6	463.1	39.5	5.1	0.20
Sverdrupfjella	032bC	468.3	326.1	142.2	1.4	0.06
Sverdrupfjella	036bD	452.7	479.6	-36.3	-5.5	-0.22
Sverdrupfjella	038bA	508.6	463.1	45.5	4.4	0.18
Kirwanveggan	92/14	480.6	506.3	-25.7	-7.8	-0.31
Kirwanveggan	92/35	508	504.6	3.4	58.1	2.33
Kirwanveggan	93/41	527	498.2	28.8	6.9	0.28
Kirwanveggan	93/61	1076.5	no sample			
Kirwanveggan	93/77	840.4	503.7	336.7	0.6	0.02
Kirwanveggan	93/84	817.7	868	-50	-4	0.03
Kirwanveggan	93/89	526.5	529.1	-2.6	-76.9	-3.08

Table 3. Summarised differences in age differences between hornblende and biotite and calculated cooling rate assuming a 200°C difference in closure temperature between hornblende and biotite. Erosion rate equivalent is calculated assuming a geothermal gradient of 25°C/km.

Sample	Ar/Ar age Mica	Ar/Ar Error Mica	Ar/Ar age Amph	Ar/Ar error Amph	Reference
D3			478.0	7	Board, 2001
DY11			496.0	4	Board, 2001
KK12			520.0	12	Board, 2001
JE39	488.0	3	488.0	4	Board, 2001
BK14	488.0	3	488.0	4	Board, 2001
KNB26	490.0	5	511.0	4	Board, 2001
10Kn94	579.0	4			Croaker 1999
Bvs	533	12			Jacobs et al., 1995
GZ27	476	10			Jacobs et al., 1995
J 1028	476	10			Jacobs et al., 1995
J 14.2/5 bt	494	10			Jacobs et al., 1995
J 14.2/5MS	498	10			Jacobs et al., 1995
J1.2/9BT	475	10			Jacobs et al., 1995
J1.2/9MS	489	10			Jacobs et al., 1995
J10.2./9bt	469	10			Jacobs et al., 1995
J10.2./9MS	484	10			Jacobs et al., 1995
J1013	508	11			Jacobs et al., 1995
J1057	510	11			Jacobs et al., 1995
J11 2/21BT	495	10			Jacobs et al., 1995
J11 2/24 PSEUDOTACH	395	9			Jacobs et al., 1995
J1102	497	11			Jacobs et al., 1995
J1160	477	10			Jacobs et al., 1995
J1553	530	13			Jacobs et al., 1995
J7.2/7bt	499	10			Jacobs et al., 1995
J7.2/7MS	508	11			Jacobs et al., 1995
J9.2/3	496	10			Jacobs et al., 1995
J950MS	510	11			Jacobs et al., 1995
J965	499	11			Jacobs et al., 1995
J5.2/3	478	10			Jacobs et al., 1995
Pvu1-2	962	20			Jacobs et al., 1995
PVu2.3	966	20			Jacobs et al., 1995
PVU3-4	987	20			Jacobs et al., 1995
W14.2/3	974	20			Jacobs et al., 1995
W2.2./1	473	11			Jacobs et al., 1995
W23.1./7	960	20			Jacobs et al., 1995
W30.1./3	493	10			Jacobs et al., 1995
W6.2/4	812	17			Jacobs et al., 1995
W7.2./6	470	10			Jacobs et al., 1995
W8.2./3	488	10			Jacobs et al., 1995
W8.2/3M	486	10			Jacobs et al., 1995
J1145.5			501.0	2.1	Jacobs et al., 1999
W3.2.88 /20			500.0	3.7	Jacobs et al., 1999
J1176	468.0	5.0	502.0	2.3	Jacobs et al., 1999

J1.2.94/1	469.0	5.0			Jacobs et al., 1999
J23.1.94/13	479.0	5.0	535.0	13	Jacobs et al., 1999
GZ 44	494.0	3.0			Jacobs et al., 1999
J23.1.94/1	498.0	5.0	565.0	21.0	Jacobs et al., 1999
W23.1.94/3	509.0	5.0	506.0	8.0	Jacobs et al., 1999
J25.1.94/3			495.0	5.0	Jacobs et al., 1999
W12.1.86/1			1012.0	14.0	Jacobs et al., 1999

References.

Board W.S. (2001) *Tectonothermal evolution of the southern H.U. Sverdrupfjella, western Dronning Maud Land, Antarctica.* Ph.D. thesis, University of Cape Town, 205 pp.

Croaker, M. (1999) *Geological constraints on the evolution of the Urfjell Group, southern Kirwanveggen, western Dronning Maud Land, Antarctica* .Unpubl. M.Sc. thesis, University of Natal.

Jacobs, J. Ahrendt, H., Kreutzer, H. and Weber, K. (1995) K-Ar, 40Ar/39Ar and apatite fission-track evidence for Neoproterozoic and Mesozoic basement rejuvenation events in the Heimefrontfjella and Mannefallknausane (East Antarctica). *Precambrian Research*, 75, 251-262.

Jacobs, J. Hansen, B.T., Henjes-Kunst, F., Thomas, R.J., Weber, K., Bauer, W., Armstrong, R.A. and Cornell, D.H. (1999) New Age constraints on the Proterozoic/Lower Paleozoic Evolution of Heimefrontfjella, East Antarctica, and its bearing on Rodinia/Gondwana Correlations. Terra Antartica, 6(4), 377-389.

Sverdrupfjella	Sample	Rb	Sr	$^{87}Rb/^{86}Sr$	$^{87}Sr/^{86}Sr$	Precision	Sm	Nd	$^{147}Sm/^{144}Nd$	$^{143}Nd/^{144}Nd$	Precision
Dalmatian Granite	dvg2	182.3	273.4	1.94	0.72942	0.00001	2.405	14.205	0.1023	0.51128	0.00003
Dalmatian Granite	dvg-dal	231.4	271.4	2.48	0.73173	0.00001	2.368	15.27	0.0937	0.51142	0.00003
Dalmatian Granite	kk7	202.8	389.4	1.51	0.72386	0.00001	3.406	23.352	0.0882	0.51140	0.00003
Dalmatian Granite	kk6	185.1	244.5	2.19	0.72718	0.00015	3.671	27.022	0.0821	0.51153	0.00002
Dalmatian Granite	kk5	208.9	249	2.44	0.7301	0.00001	4.58	24.481	0.1131	0.51153	0.00004
Dalmatian Granite	bk62	199.2	235.4	2.46	0.75331	0.00001	3.265	16.695	0.1182	0.51151	0.00003
Dalmatian Granite	bk59	214.1	196.4	3.17	0.7531	0.00001	1.874	9.464	0.1197	0.51153	0.00003
Dalmatian Granite	bk58	219.5	192.2	3.32	0.75908	0.00003	2.135	10.654	0.1211	0.51157	0.00002
Dalmatian Granite	bk4	198.4	233.2	2.47	0.75315	0.00001	1.375	6.768	0.1228	0.51155	0.00003
Salknappen Granite Gneiss	SA 10	107	293	1.0578	0.71969	0.00001	9.252	37.962	0.1473	0.51214	0.00002
Salknappen Granite Gneiss	SA 09	111	300	1.0718	0.71960	0.00003	6.243	25.523	0.1479	0.51222	0.00002
Salknappen Granite Gneiss	SA 08	108	274	1.1418	0.72003	0.00001	5.293	23.575	0.1357	0.51225	0.00002
Kirwanveggan											
Kvervelnatten Orthogneiss	93/29	50.01	895.8	0.1615	0.70573	0.00015	5.966	37.29	0.096708	0.51199	0.00003
Kvervelnatten Orthogneiss	93/36	59.41	748.7	0.2296	0.70753	0.00013	9.718	44.4	0.13231	0.51224	0.00001
Issfosnippa Granite Gneiss	92/81	111.2	491.8	0.6546	0.71349	0.0002	8.039	51.34	0.09465	0.51201	0.00002
Issfosnippa Granite Gneiss	92/86	144.7	238.4	1.7601	0.73076	0.0019	2.651	15.67	0.102264	0.51208	0.00001
Kirwanveggan Megacrystic Orthogneiss	92/14	76.08	363.2	0.6065	0.71448	0.00016	10.79	51.56	0.126503	0.51219	0.00006
Kirwanveggan Megacrystic Orthogneiss	92/17	84.56	395.3	0.6192	0.71206	0.00017	11.94	56.45	0.127858	0.51215	0.00002

Kirwanveggan Megacrystic Orthogneiss	92/18	95.19	307	0.8979	0.71712	0.00015	14.74	70.21	0.126911	0.51226	0.00001
Kirwanveggan Megacrystic Orthogneiss	92/19	101.6	310	0.9492	0.71765	0.00014	14.11	64.25	0.132754	0.51220	0.00004
Garnet Kyanite granite Neuemeyerskarvet	92/26	130.7	221.3	1.7132	0.73403	0.00017	6.356	24.71	0.155496	0.51235	0.00004
Garnet Kyanite granite Neuemeyerskarvet	92/33	129.7	270.3	1.3908	0.72615	0.00013	2.934	21.5	0.082487	0.51189	0.00002
Garnet Kyanite granite Neuemeyerskarvet	92/51	65.67	198.3	0.9597	0.72468	0.00035	4.582	21.48	0.128948	0.51220	0.00003
Garnet Kyanite granite Neuemeyerskarvet	92/53	137.1	238.3	1.6685	0.73186	0.0002	6.599	27.34	0.145911	0.51233	0.00003
Garnet Kyanite granite Neuemeyerskarvet	92/65	20.12	218.6	0.2665	0.71624	0.00015	0.9537	10.87	0.053033	0.51195	0.00004

Table 5.

Unit	Method	Age	Error	Crystalisation or metamorphic	Source reference	Area
grey gneiss 1701/2	SHRIMP	1061	56	met	Jacobs et al., (2003a)	CDML
grey gneiss 1701/2	SHRIMP	528	10	met	Jacobs et al., (2003a)	CDML
augen gneiss 1512/1	SHRIMP	1049	19	met	Jacobs et al., (2003a)	CDML
augen gneiss 2412/4	SHRIMP	1096	8	cryst	Jacobs et al., (2003a)	Gjelsvikfjella
grey migm gneiss 2712/4	SHRIMP	1115	12	cryst	Jacobs et al., (2003a)	Gjelsvikfjella
augen gneiss 1512/1	SHRIMP	1123	21	cryst	Jacobs et al., (2003a)	Gjelsvikfjella
grey gneiss 1701/2	SHRIMP	1142	21	cryst	Jacobs et al., (2003a)	Gjelsvikfjella
MIGM AUGEN GNEISS	SHRIMP	1137	14	cryst	Jacobs et al., (2003a)	Gjelsvikfjella
leucosome	SHRIMP	516	5	met	Jacobs et al., (1998)	CDML
rimj1704	SHRIMP	522	10	met	Jacobs et al., (1998)	CDML
rimj1795	SHRIMP	557	11	met	Jacobs et al., (1998)	CDML
j1886 charnockite	SHRIMP	544	15	met	Jacobs et al., (1998)	CDML
anorthositerimj1955	SHRIMP	555	11	met	Jacobs et al., (1998)	CDML
metrimj1704	SHRIMP	1084	8	met	Jacobs et al., (1998)	CDML
FELSIC GNEISSj1671	SHRIMP	1073	9	cryst	Jacobs et al., (1998)	CDML
felsicgneissj1704	SHRIMP	1137	21	cryst	Jacobs et al., (1998)	CDML
felsic gneissj1795	SHRIMP	1076	14	cryst	Jacobs et al., (1998)	CDML
orthogneissj1736	SHRIMP	1086	20	cryst	Jacobs et al., (1998)	CDML
orthogneissj1797	SHRIMP	1087	28	cryst	Jacobs et al., (1998)	CDML
metagranodioritej1698	SHRIMP	530	8	cryst	Jacobs et al., (1998)	CDML
metaleucogranite j1695	SHRIMP	527	6	cryst	Jacobs et al., (1998)	CDML
felsicgneissj1838	SHRIMP	1130	12	cryst	Jacobs et al., (1998)	CDML
charnockitej1886	SHRIMP	608	9	cryst	Jacobs et al., (1998)	CDML
anorthositej1955	SHRIMP	600	12	cryst	Jacobs et al., (1998)	CDML
anorthositerj1958	SHRIMP	583	7	cryst	Jacobs et al., (1998)	CDML
zwiesel gabbro	SHRIMP	527	5	cryst	Jacobs et al., (2003b)	CDML
zwiesel gabbro	SHRIMP	521	6	cryst	Jacobs et al., (2003b)	CDML
MS-01 metapelite	LA-ICPMS	763	69	met	Ravikant et al., (2018)	CDML

MS-05 calc silicate	LA-ICPMS	843	87	met	Ravikant et al., (2018)	CDML
Sr04 granite	LA-ICPMS	830	240	cryst	Ravikant et al., (2018)	CDML
MS-02 quartzite	LA-ICPMS	1018	33	detrital	Ravikant et al., (2018)	CDML
MS 4granite	LA-ICPMS	783	68	cryst	Ravikant et al., (2018)	CDML
B01122102B	SHRIMP	633	4	met	Baba et al., (2015)	CDML
B01122102B	SHRIMP	598	1	met	Baba et al., (2015)	CDML
B01122103	SHRIMP	599	1	met	Baba et al., (2015)	CDML
B02010301K3	SHRIMP	525	1	met	Baba et al., (2015)	CDML
stabben gabbro	SHRIMP	487	4	cryst	Bisnath et al., (2006)	Gjelsvikfjella
granite APLITE dykes	SHRIMP	497	5	cryst	Bisnath et al., (2006)	Gjelsvikfjella
augen gneiss	SHRIMP	1104	8	cryst	Bisnath et al., (2006)	Gjelsvikfjella
grey migm augen gneiss	SHRIMP	1124	11	cryst	Bisnath et al., (2006)	Gjelsvikfjella
granite gneiss	SHRIMP	1133	16	cryst	Bisnath et al., (2006)	Gjelsvikfjella
BANDED GNEISS	SHRIMP	1091	16	cryst	Bisnath et al., (2006)	Gjelsvikfjella
granite gneiss	SHRIMP	1130	19	cryst	Bisnath et al., (2006)	Gjelsvikfjella
MIGMATITE GNEISS	SHRIMP	529	4	met	Bisnath et al., (2006)	Gjelsvikfjella
L INTERCEPT ABA/32	SHRIMP	527	50	met	Bisnath et al., (2006)	Gjelsvikfjella
HOMOGENEOUS MIGMATITE	SIMS	1163	6	cryst	Paulsson and Austrheim (2003)	Gjelsvikfjella
STABBEN SYENITE	SIMS	500	8	cryst	Paulsson and Austrheim (2003)	Gjelsvikfjella
ZIRCON OVERGROWTHS	SIMS	504	6	met	Paulsson and Austrheim (2003)	Gjelsvikfjella
AGE OF MIGMATISATION	tims	504	4	met	Paulsson and Austrheim (2003)	Gjelsvikfjella
lamprophyre dyke /2312/2	SHRIMP	523	5	cryst	Jacobs et al., (2003c)	Gjelsvikfjella
charnockite 1301/2	SHRIMP	521	3	cryst	Jacobs et al., (2003c)	Gjelsvikfjella
STABBEN GABBRO	SHRIMP	483	11	cryst	Jacobs et al., (2003c)	Gjelsvikfjella
granite dyke gygra	SHRIMP	487	4	cryst	Jacobs et al., (2003c)	Gjelsvikfjella
leucosome-1301/2	SHRIMP	521	3	met	Jacobs et al., (2003c)	Gjelsvikfjella
leucosome-0801/3	SHRIMP	558	6	met	Jacobs et al., (2003c)	Gjelsvikfjella
KYANITE LEUCOGNEISS	SHRIMP	1096	10	cryst	Harris P.D. (1999)	Kirwanveggan
BT GRT MIGMATITE	SHRIMP	1157	10	cryst	Harris P.D. (1999)	Kirwanveggan
INTRUSIVE LEUCOGNEISS	SHRIMP	1101	13	cryst	Harris P.D. (1999)	Kirwanveggan

MEGACRYSTIC ORTHOGNEISS	SHRIMP	1088	10	cryst	Harris P.D. (1999)	Kirwanveggan
PEGMATITE VEIN	SHRIMP	1079	6	cryst	Harris P.D. (1999)	Kirwanveggan
LEUCOSOME MIGM GNEISS	SHRIMP	1098	5	met	Harris P.D. (1999)	Kirwanveggan
KYANITE LEUCOGNEISS	SHRIMP	1096	10	met	Harris P.D. (1999)	Kirwanveggan
KVERVELKATTEN	SHRIMP	1134	11	cryst	Jackson (1999)	Kirwanveggan
KVERVELKATTEN AMPH POD	SHRIMP	1139	10	cryst	Jackson (1999)	Kirwanveggan
MEGACRYSTIC AUGEN GNEISS	SHRIMP	1074	11	cryst	Jackson (1999)	Kirwanveggan
LEUCOPEGMATITE CJK155	SHRIMP	1050	10	cryst	Jackson (1999)	Kirwanveggan
PORPHYRITIC GRANITE DYKE	SHRIMP	1011	8	cryst	Jackson (1999)	Kirwanveggan
LEUCOGRANITE	SHRIMP	990	12	cryst	Jackson (1999)	Kirwanveggan
GRANITE DYKE	SHRIMP	980	13	cryst	Jackson (1999)	Kirwanveggan
AMPH DYKE	SHRIMP	986	6	cryst	Jackson (1999)	Kirwanveggan
BANDED BT GNEISS	SHRIMP	1081	4	cryst	Jackson (1999)	Kirwanveggan
BANDED BT GNEISS	SHRIMP	994	22	cryst	Jackson (1999)	Kirwanveggan
LEUCOSOME	SHRIMP	1031	6	met	Jackson (1999)	Kirwanveggan
MONAZITE	SHRIMP	956	17	met	Jackson (1999)	Kirwanveggan
TITANITE	SHRIMP	1015	16	met	Jackson (1999)	Kirwanveggan
TITANITE	SHRIMP	1003	9	cryst	Jackson (1999)	Kirwanveggan
Grey gneiss	SHRIMP	1143	11	cryst	Jackson (1999)	Kirwanveggan
RIM KVERVELKNATTEN	SHRIMP	1060	22	met	Krynauw and Jackson (1996)	Kirwanveggan
DALMATIAN	SHRIMP	489	10	cryst	Krynauw and Jackson (1996)	Sverdrupfjella
Brattskarvet	SHRIMP	474	10	cryst	Krynauw and Jackson (1996)	Sverdrupfjella
LATE FELSIC DYKE	SHRIMP	1011	8	cryst	Moyes and Harris (1996)	Sverdrupfjella
SVEABREEN GRANITE	SHRIMP	1127	12	cryst	Moyes and Harris (1996)	Sverdrupfjella
FUGITIVE GRANITE	SHRIMP	1131	25	cryst	Moyes and Harris (1996)	Sverdrupfjella
FUGITIVE GRANITE	SHRIMP	1061	14	cryst	Moyes and Harris (1996)	Sverdrupfjella
ROERKULTEN GRANITE	SHRIMP	1103	13	cryst	Moyes and Harris (1996)	Sverdrupfjella
ROOTSHORGA PARA	SHRIMP	1092	13	cryst	Moyes and Harris (1996)	Sverdrupfjella
GRANITE GNEISS	SHRIMP	1132	16	cryst	Board et al., (2005)	Sverdrupfjella
TABULAR GRANITE	SHRIMP	1072	10	cryst	Board et al., (2005)	Sverdrupfjella

granite dykes	SHRIMP	480	10	cryst	Board et al., (2005)	Sverdrupfjella
GRANITE GTNEISS RIM	SHRIMP	1031	47	met	Board et al., (2005)	Sverdrupfjella
METAPELITEwbsv025	SHRIMP	1044	47	met	Board et al., (2005)	Sverdrupfjella
METAPELITEwbsv025	SHRIMP	540	6	met	Board et al., (2005)	Sverdrupfjella
TABULAR GRANITE	SHRIMP	565	11	met	Board et al., (2005)	Sverdrupfjella
TABULAR GRANITE	SHRIMP	996	17	met	Board et al., (2005)	Sverdrupfjella
LEUCOSOME wbsv071	SHRIMP	1035	31	met	Board et al., (2005)	Sverdrupfjella
LEUCOSOME lower intercept	SHRIMP	499	17	met	Board et al., (2005)	Sverdrupfjella
LEUCOSOME wbsv074	SHRIMP	515	7	met	Board et al., (2005)	Sverdrupfjella
LEUCOSOME wbsv113	SHRIMP	1032	15	met	Board et al., (2005)	Sverdrupfjella
LEUCOSOME wbsv113	SHRIMP	503	35	met	Board et al., (2005)	Sverdrupfjella
LEUCOSOME wbsv114	SHRIMP	525	35	met	Board et al., (2005)	Sverdrupfjella
LEUCOSOME wbsv116	SHRIMP	519	4	met	Board et al., (2005)	Sverdrupfjella
Midbressrabben Diorite	SHRIMP	1140	10	cryst	Grantham et al., (2011)	Sverdrupfjella
Grey gneiss Jutulrora JW4	SHRIMP	1139	12	cryst	Grantham et al., (2011)	Sverdrupfjella
Augen gneiss SA 10	SHRIMP	1096	14	cryst	Hokada et al., (2019)	Sverdrupfjella
Rim sa10	SHRIMP	538	25	met	Hokada et al., (2019)	Sverdrupfjella
Mafic dyke	SHRIMP	523	21	met	Grantham et al., (2006)	Sverdrupfjella
Z-7-14-15	SIMS	493.7	7.4	met	Pauly et al., (2016)	Sverdrupfjella
Z-7-14-15	SIMS	542.3	3.8	met	Pauly et al., (2016)	Sverdrupfjella
Z-7-14-15	SIMS	555.8	2.8	met	Pauly et al., (2016)	Sverdrupfjella
Z-7-14-15	SIMS	569.7	1.4	met	Pauly et al., (2016)	Sverdrupfjella
Z-7-14-15	SIMS	592.6	2.1	met	Pauly et al., (2016)	Sverdrupfjella
Sample Z7-15-2	SIMS	550	8.5	met	Pauly et al., (2016)	Sverdrupfjella
Sample Z7-15-2	SIMS	575.8	9.4	met	Pauly et al., (2016)	Sverdrupfjella
Sample Z7-15-2	SIMS	973.6	8.8	xenocryst	Pauly et al., (2016)	Sverdrupfjella
Z-7-16-4	SIMS	379.7	1.7	met	Pauly et al., (2016)	Sverdrupfjella
Z-7-16-4	SIMS	491.4	4.3	met	Pauly et al., (2016)	Sverdrupfjella
Z-7-16-4	SIMS	517.5	8.6	met	Pauly et al., (2016)	Sverdrupfjella
Z-7-16-4	SIMS	562	3.4	met	Pauly et al., (2016)	Sverdrupfjella

Sample Z7-15-5	SIMS	521.2	4.6	met	Pauly et al., (2016)	Sverdrupfjella
Sample Z7-15-5	SIMS	541.9	7.5	met	Pauly et al., (2016)	Sverdrupfjella
Sample Z7-15-5	SIMS	575.3	5.6	met	Pauly et al., (2016)	Sverdrupfjella
Sample Z7-15-5	SIMS	1083	12	xenocryst	Pauly et al., (2016)	Sverdrupfjella
K08122101a meta tonalite	SHRIMP	995	3	cryst	Kamei et al., (2013)	Sor Rondane
K08122301d meta tonalite	SHRIMP	772	4	cryst	Kamei et al., (2013)	Sor Rondane
k09012401a metatonalite	SHRIMP	998	3	cryst	Kamei et al., (2013)	Sor Rondane
S08121201b metatonalite	SHRIMP	945	2	cryst	Kamei et al., (2013)	Sor Rondane
K09012201e metatonalite	SHRIMP	996	3	cryst	Kamei et al., (2013)	Sor Rondane
K09011101a metatonalite	SHRIMP	943	3	cryst	Kamei et al., (2013)	Sor Rondane
K09010703a metatonalite	SHRIMP	996	3	cryst	Kamei et al., (2013)	Sor Rondane
K09010801e metagabbro	SHRIMP	930	10	cryst	Kamei et al., (2013)	Sor Rondane
2703N calc silicate	LAICPMS	548	4	cryst	Nakano et al. (2013)	Sor Rondane
2902E calc silicate	LAICPMS	552	4	cryst	Nakano et al. (2013)	Sor Rondane
27030 amphibolite	LAICPMS	756	6	cryst	Nakano et al. (2013)	Sor Rondane
2703p amphibolite	LAICPMS	769	11	cryst	Nakano et al. (2013)	Sor Rondane
2703q hornblendite	LAICPMS	544	10	cryst	Nakano et al. (2013)	Sor Rondane
2901a Grt qf geniss	LAICPMS	1063	14	cryst	Nakano et al. (2013)	Sor Rondane
2901b-2 Grt qf gneiss	LAICPMS	1057	12	cryst	Nakano et al. (2013)	Sor Rondane
2702 a Grt Bt felsic gneiss	LAICPMS	750	7	cryst	Nakano et al. (2013)	Sor Rondane
2702 a Grt Bt felsic gneiss	LAICPMS	648	11	met	Nakano et al. (2013)	Sor Rondane
2902J metagranite	LAICPMS	557	4	cryst	Nakano et al. (2013)	Sor Rondane
2901d amphibolite	LAICPMS	755	38	cryst	Nakano et al. (2013)	Sor Rondane
2702b amphibolite	LAICPMS	648	7	cryst	Nakano et al. (2013)	Sor Rondane
27t02d grt sill gneiss	LAICPMS	639	11	met	Nakano et al. (2013)	Sor Rondane
85011503D enderbite	SHRIMP	951	17	cryst	Shiraishi et al. (2008)	Sor Rondane
85011503D enderbite	SHRIMP	602	15	met	Shiraishi et al. (2008)	Sor Rondane
84022004 grt bt gneiss	SHRIMP	1014	15	inherit	Shiraishi et al. (2008)	Sor Rondane
84022004 grt bt gneiss	SHRIMP	791	10	met	Shiraishi et al. (2008)	Sor Rondane
85020401C grt sill gneiss	SHRIMP	1009	13	inherit	Shiraishi et al. (2008)	Sor Rondane

9032401 grt sill gneiss	SHRIMP	1125	15	met	Shiraishi et al. (2008)	Sor Rondane
9032401 grt sill gneiss	SHRIMP	637	67	met	Shiraishi et al. (2008)	Sor Rondane
90102801A hbl bt gneiss	SHRIMP	1133	12	cryst	Shiraishi et al. (2008)	Sor Rondane
90102801A hbl bt gneiss	SHRIMP	516	8	met	Shiraishi et al. (2008)	Sor Rondane
90112102A grt bt gneiss	SHRIMP	601	6	met	Shiraishi et al. (2008)	Sor Rondane
90112302b hbl bt gneiss	SHRIMP	795	17	cryst	Shiraishi et al. (2008)	Sor Rondane
90112302b hbl bt gneiss	SHRIMP	605	70	met	Shiraishi et al. (2008)	Sor Rondane
90112302b hbl bt gneiss	SHRIMP	983	17	cryst	Shiraishi et al. (2008)	Sor Rondane
90112302a btgranite	SHRIMP	549	13	cryst	Shiraishi et al. (2008)	Sor Rondane
9031507 metatonalite	SHRIMP	920	8	cryst	Shiraishi et al. (2008)	Sor Rondane
9031507 metatonalite	SHRIMP	517	5	met	Shiraishi et al. (2008)	Sor Rondane
85012817 bt gneiss	SHRIMP	653	11	cryst	Shiraishi et al. (2008)	Sor Rondane
85012817 bt gneiss	SHRIMP	571	5	met	Shiraishi et al. (2008)	Sor Rondane
Mylonitised granite	SHRIMP	572	8	met	Shiraishi et al. (2008)	Sor Rondane
Ts11021401b1	LAICPMS	847	8	met	Kazami et al., (2016)	Lutzoholm Bukta
TS11012406B	LAICPMS	591	3	met	Tsunogae et al., (2014)	Lutzoholm Bukta
TS11012406B	LAICPMS	548	7	met	Tsunogae et al., (2014)	Lutzoholm Bukta
TK2010011501A.	LAICPMS	603	14	met	Higashino et al., (2013)	Sor Rondane
TK2010011501A.	LAICPMS	590	11	met	Higashino et al., (2013)	Sor Rondane
7121003a opx felsic gneiss	SHRIMP	990	55	cryst	Adachi et al., (2013)	Sor Rondane
7121003a opx felsic gneiss	SHRIMP	827	15	met	Adachi et al., (2013)	Sor Rondane
bc0801302c grt bt sill gneiss	SHRIMP	1057	12	met	Adachi et al., (2013)	Sor Rondane
bc0801502b grt bt gneiss	SHRIMP	784	2	cryst	Adachi et al., (2013)	Sor Rondane
bc0801502b grt bt gneiss	SHRIMP	692	6	met	Adachi et al., (2013)	Sor Rondane
7121003d pegmatite	SHRIMP	546	4	cryst	Adachi et al., (2013)	Sor Rondane
bc07121703a pegmatite	SHRIMP	546	5	cryst	Adachi et al., (2013)	Sor Rondane
ac07121901a hbl bt gneiss	SHRIMP	887	2	cryst	Adachi et al., (2013)	Sor Rondane
bc07122805c hbl bt gneiss	SHRIMP	637	5	cryst	Adachi et al., (2013)	Sor Rondane
ac07121501u granite	SHRIMP	502	4	cryst	Adachi et al., (2013)	Sor Rondane
ac07121601a granite	SHRIMP	513	4	cryst	Adachi et al., (2013)	Sor Rondane

ac08012001a hbl bt gneiss	SHRIMP	564	3	met	Adachi et al., (2013)	Sor Rondane
b08012201i grt hbl bt gneiss	SHRIMP	986	4	cryst	Adachi et al., (2013)	Sor Rondane
b08012304e grt hbl bt gneiss	SHRIMP	1000	15	cryst	Adachi et al., (2013)	Sor Rondane
b08012304e grt hbl bt gneiss	SHRIMP	546	6	met	Adachi et al., (2013)	Sor Rondane
bc08010604a grt bt geniss	SHRIMP	1015	11	cryst	Adachi et al., (2013)	Sor Rondane
bc08010604a grt bt geniss	SHRIMP	605	4	met	Adachi et al., (2013)	Sor Rondane
tc43	LAICPMS	637	6	cryst	Elburg et al., (2016)	Sor Rondane
mesr12	LAICPMS	577	6	cryst	Elburg et al., (2016)	Sor Rondane
mesr82	LAICPMS	572	4	cryst	Elburg et al., (2016)	Sor Rondane
mesr89	LAICPMS	560	9	cryst	Elburg et al., (2016)	Sor Rondane
mesr75	LAICPMS	566	4	cryst	Elburg et al., (2016)	Sor Rondane
mesr30	LAICPMS	551	8	cryst	Elburg et al., (2016)	Sor Rondane
mesr121	LAICPMS	532	3	cryst	Elburg et al., (2016)	Sor Rondane
mesr80	LAICPMS	529	5	cryst	Elburg et al., (2016)	Sor Rondane
mesr123	LAICPMS	528	4	cryst	Elburg et al., (2016)	Sor Rondane
mesr118	LAICPMS	527	5	cryst	Elburg et al., (2016)	Sor Rondane
mesr113	LAICPMS	509	12	cryst	Elburg et al., (2016)	Sor Rondane
mesr22	LAICPMS	506	4	cryst	Elburg et al., (2016)	Sor Rondane
j214a_1 fg granitoid gneiss	SHRIMP	961	4	cryst	Jacobs et al., (2015)	Eastern DML
j12121e amphibole gneiss	SHRIMP	925	11	cryst	Jacobs et al., (2015)	Eastern DML
j1214a_2 granitoid gneiss	SHRIMP	980	8	cryst	Jacobs et al., (2015)	Eastern DML
j1211a_1 granite gneiss	SHRIMP	930	12	cryst	Jacobs et al., (2015)	Eastern DML
j1211a_1 granite gneiss	SHRIMP	551	14	met	Jacobs et al., (2015)	Eastern DML
j1211a_1 granite gneiss	SHRIMP	486	7	met	Jacobs et al., (2015)	Eastern DML
j1213b enderbite gneiss	SHRIMP	930	9	cryst	Jacobs et al., (2015)	Eastern DML
j1213b enderbite gneiss	SHRIMP	950	5	cryst	Jacobs et al., (2015)	Eastern DML
j1211b_1 grt migmatite	SHRIMP	546	3	met	Jacobs et al., (2015)	Eastern DML
j1211b_2 metagabbro	SHRIMP	916	13	cryst	Jacobs et al., (2015)	Eastern DML
j1213c pegmatite gneiss	SHRIMP	597	7	cryst	Jacobs et al., (2015)	Eastern DML
j1212a granite gneiss	SHRIMP	524	7	cryst	Jacobs et al., (2015)	Eastern DML

j1213d pegmatite gneiss	SHRIMP	582	5	cryst	Jacobs et al., (2015)	Eastern DML
j1212c granite sheet	SHRIMP	528	6	cryst	Jacobs et al., (2015)	Eastern DML
j1212-F1 granite gneiss	SHRIMP	547	5	cryst	Jacobs et al., (2015)	Eastern DML
sg25 metadiorite	SHRIMP	630	4	cryst	Jacobs et al., (2015)	Eastern DML
sg28 grey migmatite gneiss	SHRIMP	802	6	cryst	Jacobs et al., (2015)	Eastern DML
sg28 grey migmatite gneiss	SHRIMP	597	8	met	Jacobs et al., (2015)	Eastern DML
sg24 granodiorite	SHRIMP	503	5	cryst	Jacobs et al., (2015)	Eastern DML
sg27 granite	SHRIMP	532	5	cryst	Jacobs et al., (2015)	Eastern DML
sg29 grey migmatite gneiss	SHRIMP	559	4	met	Jacobs et al., (2015)	Eastern DML
sg29 grey migmatite gneiss	SHRIMP	632	5	met	Jacobs et al., (2015)	Eastern DML
j1214b granite	SHRIMP	557	2	cryst	Jacobs et al., (2015)	Eastern DML
j1216a granite	SHRIMP	534	4	cryst	Jacobs et al., (2015)	Eastern DML
j1216b monzogranite	SHRIMP	554	5	cryst	Jacobs et al., (2015)	Eastern DML
Zircon rim	LAICPMS	617	9	met	Higashino et al., (2015)	Sor Rondane
Sr180	SHRIMP	612	1	met	Grantham et al., (2013)	Sor Rondane
sr180	SHRIMP	579	1	met	Grantham et al., (2013)	Sor Rondane
sr180	SHRIMP	552	1	met	Grantham et al., (2013)	Sor Rondane
sr180	SHRIMP	561	1	met	Grantham et al., (2013)	Sor Rondane
sr161a	SHRIMP	556	1	met	Grantham et al., (2013)	Sor Rondane
sr161a	SHRIMP	537	1	met	Grantham et al., (2013)	Sor Rondane
SR161d	SHRIMP	531	1	met	Grantham et al., (2013)	Sor Rondane
Sr188a	SHRIMP	544	1	met	Grantham et al., (2013)	Sor Rondane
Sr188a	SHRIMP	610	1	met	Grantham et al., (2013)	Sor Rondane
Sr188a	SHRIMP	587	3	met	Grantham et al., (2013)	Sor Rondane
Sr188a	SHRIMP	559	1	met	Grantham et al., (2013)	Sor Rondane
Sr188a	SHRIMP	529	1	met	Grantham et al., (2013)	Sor Rondane

Table 6. Table of zircon ages used in figure 11 and their reference sources.

References.

Adachi T., Osanai Y., Hokada T., Nakano N., Baba S., Toyoshima T. (2013) Timing of metamorphism in the central Sør Rondane Mountains, eastern Dronning Maud Land, East Antarctica: Constrains from SHRIMP zircon and EPMA monazite dating. *Precambrian Research* 234, 136–160.

Baba,S., Horie,K., Hokada, T., Owada, M., Adachi, T. and Shiraishi, K. (2015) Multiple Collisions in the East African–Antarctica Orogen: Constraints from Timing of Metamorphism in the Filchnerfjella and Hochlinfjellet Terranes in Central Dronning Maud Land. *The Journal of Geology*, 123, p. 55–78.

Bisnath A., Frimmel H.E., Armstrong R.A. & Board W.S. (2006) Tectonothermal evolution of the Maud Belt: New Shrimp U-Pb zircon data from Gjelsvikfjella, Dronning Maud Land, East Antarctica. *Precambrian Research,* 150, 95-121.

Board W.S., Frimmel., H.E., & Armstrong R.A. (2005) Pan-African Tectonism in the western Maud Belt: P-T-t path for High-grade gneisses in the H.U. Sverdrupfjella, East Antarctica. *Journal of Petrology*, 46, 671-699.

Elburg,M., Andersen, T., Jacobs,J., Läufer, A. Ruppel, A., Krohne, N., and Damaske D. (2016) One Hundred Fifty Million Years of Intrusive Activity in the Sør Rondane Mountains (East Antarctica): Implications for Gondwana Assembly. *The Journal of Geology*, 124, p. 1–26.

Grantham, G.H., Armstrong. R.A. and Moyes, A.B. (2006). The age, chemistry and structure of mafic dykes at Roerkulten, H.U. Sverdrupfjella, western Dronning Maud Land, Antarctica. pp.213-224 in *Dyke Swarms - Time Markers of Crustal Evolution*. Hanski E., Mertanen S., Ramo T. and Vuollo J. (eds) Proceedings of the Fifth/Fourth International Dyke Conference (IDC5), Rovaniemi, Finland. A.A. Balkema Press.

Grantham, G.H., Manhica, A.D.S.T. Armstrong, R.A., Kruger, F.J. and Loubser, M. (2011) New SHRIMP, Rb/Sr and Sm/Nd isotope and whole rock chemical data from central Mozambique and western Dronning Maud Land, Antarctica: Implications for the nature of the eastern margin of the Kalahari Craton and the amalgamation of Gondwana. *Journal of African Earth Sciences*. 59, 74-100.

Grantham, G.H., Macey, P.H., Horie,K., Kawakami, T., Ishikawa, I., Satish-Kumar M., Tsuchiya N., Graser P. and Azevedo S. (2013) Comparison of the metamorphic history of the Monapo Complex, northern Mozambique and Balchenfjella and Austhameren areas, Sør Rondane, Antarctica: Implications for the Kuunga Orogeny and the amalgamation of N and S Gondwana *Precambrian Research,* 234 (2013) 85–135.

Harris P.D. (1999) *The Geological Evolution of Neumayerskarvet in the northern Kirwanveggen, western Dronning Maud Land, Antarctica*. Unpublished PhD Thesis Rand Afrikaans University, 251pp.

Higashino F., Kawakami T., Tsuchiya N., Satish-Kumar M., Ishikawa M., Grantham G.H., Hatori K., Hirata T. (2015) Geochemical behavior of zirconium during upper amphibolite facies metamorphism - a case study from Bratnipene, Sor Rondane Mountains, east Antarctica. *Journal of Mineralogical and Petrological Sciences*, 110, 166-178.

Hokada T., Grantham G.H., Arima M., Saito S., Shiraishi K., Armstrong R.A., Eglington B., Misawa K. and Kaiden H. (2019) Stenian A-type granitoids in the Namaqua-Natal Belt, southern Africa, Maud Belt, Antarctica and Nampula Terrane, Mozambique: Rodinia and Gondwana amalgamation implications. Geoscience Frontiers, https://doi.org/10.1016/j.gsf.2019.04.003.

Jackson C. (1999) Characterization of Mesoproterozoic to Paleozoic crustal evolution of western Dronning Maud land. Unpublished report to South African National Antarctic Programme. Study 3. 80.pps.

Jacobs, J. Bauer W. Fanning C.M. (2003a). New age constraints for Grenvillian age metamorphism in western central Dronning Maud land (East Antarctica) and implications for the paleogeography of Kalahari in Rodinia. *Geologische Rundschau*, 92, 301-315.

Jacobs, J. Bauer W. Fanning C.M. (2003c) Late Neoproterozoic/Early Paleozoic events in central Dronning Maud Land and significance for the southern extension of the East African Orogen into East Antarctica. *Precambrian Research* 126, 27-53.

Jacobs J., Elburg M., Laufer A., Kleinhannse I., Henjes-Kunst F., Estrada S., Ruppel A.S., Damaske D., Montero P., Bea F. (2015) Two distinct Late Mesoproterozoic/Early Neoproterozoic basement provinces in central/eastern Dronning Maud Land, East Antarctica: The missing link, 15.21.E *Precambrian Research*, 265, 249–272.

Jacobs, J. Fanning C.M., Henjes-Kunst F., Olesch M., and Paech H.J. (1998) Continuation of the Mozambique Belt into East Antarctica: Grenville age metamorphism and Polyphase Pan-African high grade events in Central Dronning Maud Land. *Journal of Geology*, 106, 385-406.

Jacobs, J. Klemd R., Fanning C.M. Bauer W. & Colombo F. (2003b) Extensional collapse of the late Neoproterozoic-early Paleozoic East African-Antarctic Orogen in Central Dronning Maud Land, East Antarctica. pp271-287 in *Proterozoic East Gondwana: Supercontinent Assembly and Breakup*. Yoshida M., Windley B.F. and Dasgupta S. (eds), Geol. Soc. Lond. Spec. Publ. 206.

Kamei A., Horie K., Owada M., Yuhara M., Nakano, N., Osanai Y., Adachi T., Hara Y., Terao M., Teuchi S, Shimura T., Tsukada K., Hokada T., Iwata C., Shiraishi K., IshizukaH., Takahashii Y., (2013) Late Proterozoic juvenile arc metatonalite and adakitic intrusions in the SørRondane Mountains, eastern Dronning Maud Land, Antarctica *Precambrian Research* 234, 47– 62.

Kazami S., Tsunogae T., Santosh M., Tsutsumi Y., Takamura Y. (2016) Petrology, geochemistry and zircon U-Pb geochronology of a layered igneous complex from Akarui Point in the Lützow-Holm Complex, East Antarctica: Implications for Antarctica-Sri Lanka correlation. *Journal of Asian Earth Sciences* 130, 206–222.

Krynauw, J.R. and Jackson C. (1996) Geological evolution of western Dronning Maud Land within a Gondwana framework. South African National Antarctic Programme Final Report 1991-1996. Geology Subsection , 1-48.

Moyes A.B. and Harris P.D. (1996) Geological evolution of western Dronning Maud Land within a Gondwana framework. South African National Antarctic Programme Final Report 1991-1996. Radiogenic Isotope Geology Project, 1-38.

Nakano N., Osanai Y., Kamei A., Satish-Kumar M., Adachi T., Hokada T., Baba S., Toyoshima T (2013) Multiple thermal events recorded in metamorphosed carbonate and associated rocks from the southern Austkampane region in the Sør Rondane Mountains, East Antarctica: A protracted Neoproterozoic history at the Gondwana suture zone. *Precambrian Research*, 234, 161–182.

Paulsson, O. and Austrheim H. (2003) A geochronological and geochemical study of rocks from Gjelsvikfjella, Dronning Maud Land, Antarctica—implications for Mesoproterozoic correlations and assembly of Gondwana. *Precambrian Research*, 125, 113-138.

Pauly J., Marschall H.R., Meyer H-P., Chatterjee, N. and Brian Monteleone B. (2016) Prolonged Ediacaran–Cambrian Metamorphic History and Short-lived High-pressure Granulite facies Metamorphism in the H.U. Sverdrupfjella, Dronning Maud Land (East Antarctica): Evidence for Continental Collision during Gondwana Assembly. *Journal of Petrology*, 57, 185–228.

Ravikant V., Buhn B. and Pimentel M. (2018) Zircon U-Pb age constraints for Tonian-early Cryogenian deposition of metasedimentary rocks from the Schirmacher Oasis, East Antarctica: Implications for correlations across the Mozambique Ocean. *Polar Science, 18, 39-47.*

Shiraishi, K., Dunkley D., Hokada T., Fanning, C.M., Kagami, H. and Hamamoto T. (2008) Geochronological constraints of the Late Proterozoic-Cambrian crustal evolution in eastern Dronning Maud Land, East Antarctica: a synthesis of SHRIMP U-Pb age and Nd model age data. *Geodynamic Evolution of East Antarctica : a Key to the East-West Gondwana Connection*. eds M Satish-Kumar, Y Motoyoshi, Y Osanai, Y Hiroi and K Shiraishi, Geol. Soc. of London Spec. Publ., 308, p. 21.67.

Tsunogae T., Dunkley D.J., Horie K., Endo T., Miyamoto T., Kato M. (2014) Petrology and SHRIMP zircon geochronology of granulites from Vesleknausen, Lützow-Holm Complex, East Antarctica: Neoarchean magmatism and Neoproterozoic high-grade metamorphism. *Geoscience Frontiers* 5, 167-182

Sverdrupfjella	Sample	Rb	Sr	$^{87}Rb/^{86}Sr$	$^{87}Sr/^{86}Sr$	Precision	Sm	Nd	$^{147}Sm/^{144}Nd$	$^{143}Nd/^{144}Nd$	Precision
Dalmatian Granite	dvg2	182.3	273.4	1.94	0.72942	0.00001	2.405	14.205	0.1023	0.51128	0.00003
Dalmatian Granite	dvg-dal	231.4	271.4	2.48	0.73173	0.00001	2.368	15.27	0.0937	0.51142	0.00003
Dalmatian Granite	kk7	202.8	389.4	1.51	0.72386	0.00001	3.406	23.352	0.0882	0.51140	0.00003
Dalmatian Granite	kk6	185.1	244.5	2.19	0.72718	0.00015	3.671	27.022	0.0821	0.51153	0.00002
Dalmatian Granite	kk5	208.9	249	2.44	0.7301	0.00001	4.58	24.481	0.1131	0.51153	0.00004
Dalmatian Granite	bk62	199.2	235.4	2.46	0.75331	0.00001	3.265	16.695	0.1182	0.51151	0.00003
Dalmatian Granite	bk59	214.1	196.4	3.17	0.7531	0.00001	1.874	9.464	0.1197	0.51153	0.00003
Dalmatian Granite	bk58	219.5	192.2	3.32	0.75908	0.00003	2.135	10.654	0.1211	0.51157	0.00002
Dalmatian Granite	bk4	198.4	233.2	2.47	0.75315	0.00001	1.375	6.768	0.1228	0.51155	0.00003
Salknappen Granite Gneiss	SA 10	107	293	1.0578	0.71969	0.00001	9.252	37.962	0.1473	0.51214	0.00002
Salknappen Granite Gneiss	SA 09	111	300	1.0718	0.71960	0.00003	6.243	25.523	0.1479	0.51222	0.00002
Salknappen Granite Gneiss	SA 08	108	274	1.1418	0.72003	0.00001	5.293	23.575	0.1357	0.51225	0.00002
Kirwanveggan											
Kvervelnatten Orthogneiss	93/29	50.01	895.8	0.1615	0.70573	0.00015	5.966	37.29	0.096708	0.51199	0.00003
Kvervelnatten Orthogneiss	93/36	59.41	748.7	0.2296	0.70753	0.00013	9.718	44.4	0.13231	0.51224	0.00001
Issfosnippa Granite Gneiss	92/81	111.2	491.8	0.6546	0.71349	0.0002	8.039	51.34	0.09465	0.51201	0.00002
Issfosnippa Granite Gneiss	92/86	144.7	238.4	1.7601	0.73076	0.0019	2.651	15.67	0.102264	0.51208	0.00001
Kirwanveggan Megacrystic Orthogneiss	92/14	76.08	363.2	0.6065	0.71448	0.00016	10.79	51.56	0.126503	0.51219	0.00006
Kirwanveggan Megacrystic Orthogneiss	92/17	84.56	395.3	0.6192	0.71206	0.00017	11.94	56.45	0.127858	0.51215	0.00002

Kirwanveggan Megacrystic Orthogneiss	92/18	95.19	307	0.8979	0.71712	0.00015	14.74	70.21	0.126911	0.51226	0.00001
Kirwanveggan Megacrystic Orthogneiss	92/19	101.6	310	0.9492	0.71765	0.00014	14.11	64.25	0.132754	0.51220	0.00004
Garnet Kyanite granite Neuemeyerskarvet	92/26	130.7	221.3	1.7132	0.73403	0.00017	6.356	24.71	0.155496	0.51235	0.00004
Garnet Kyanite granite Neuemeyerskarvet	92/33	129.7	270.3	1.3908	0.72615	0.00013	2.934	21.5	0.082487	0.51189	0.00002
Garnet Kyanite granite Neuemeyerskarvet	92/51	65.67	198.3	0.9597	0.72468	0.00035	4.582	21.48	0.128948	0.51220	0.00003
Garnet Kyanite granite Neuemeyerskarvet	92/53	137.1	238.3	1.6685	0.73186	0.0002	6.599	27.34	0.145911	0.51233	0.00003
Garnet Kyanite granite Neuemeyerskarvet	92/65	20.12	218.6	0.2665	0.71624	0.00015	0.9537	10.87	0.053033	0.51195	0.00004